EUROPEAN ORGANIZATION FOR NUCLEAR RESEARCH

CERN-EP/82-81
21 June 1982

THE DRELL-YAN PROCESS

I.R. Kenyon*)

CERN, Geneva, Switzerland

To be published in
Reports on Progress in Physics

*) Permanent address: Physics Dept., Univ. of Birmingham, England.

ABSTRACT

The Drell-Yan process is an electromagnetic effect in which a quark and antiquark from a pair of interacting hadrons annihilate to give a lepton pair. A brief description of hadron structure and the parton model is given to provide a necessary background. Then the general features of lepton pair production are described and the Drell-Yan formalism is set up. Experimental techniques are described next; these are rather simple since it is only necessary to detect the leptons emitted from hadron interactions. Predictions and tests of the basic model show that in general it works well. The anomalous features are the over-all cross-section level (high by a factor of 2) and the unexpectedly large mean transverse momenta. Quantum chromodynamics (QCD) offers the explanation of these anomalies, and measurements of dilepton production provide important quantitative tests of QCD. Such measurements have also been used to determine nucleon structure functions and, for the first time, meson structure functions.

CONTENTS

1. INTRODUCTION

In 1970 Christenson *et al* reported on the first study of the continuum of $\mu^+\mu^-$ pairs produced in hadron-hadron collisions. A more recent high-resolution spectrum obtained by Lederman and his colleagues (1982) using 400 GeV/c protons incident on a nuclear target is shown in figure 1. The ψ and T families of resonances discovered by Aubert *et al* (1974) and Augustin *et al* (1974), and by Herb *et al* (1977) and Innes *et al* (1977) are clearly evident. It is the underlying continuum that is of interest to us here, and we shall not discuss the resonances any further. The obvious feature of the continuum is the spectacular fall in cross-section with increasing dilepton mass which the experimenters have followed over 10 orders of magnitude. Drell and Yan (1970a, 1971) proposed that the continuum of opposite-sign dileptons were produced in hadron-hadron collisions by the process pictured in figure 2a. In a first step an antiquark from one hadron annihilates on a quark from the other hadron to give a virtual photon. Subsequently this photon converts to a pair of (opposite-sign) leptons: $\mu^+\mu^-$, e^+e^-, ... The process is electromagnetic and exactly calculable. The appearance of the propagator of the virtual photon in the amplitude leads to a factor M^{-4} in the cross-section and hence to the rapid fall of cross-section with increasing dilepton mass. In order to predict the differential cross-section for dilepton production in a reaction such as

$$A + B \rightarrow \mu^+ + \mu^- + \text{anything} ,$$

it is necessary to know the (longitudinal) momentum distributions of the quarks and antiquarks in the parent hadrons A and B. These quantities are the so-called structure functions of A and B and are of obvious importance in describing how hadrons are constructed. Experimentally the

situation is very simple for dimuon detection. The target is followed by a thick filter which absorbs all the secondary hadrons produced from the interaction of the beam on the target. Only muons emerge and these can be momentum-analysed in a magnetic spectrometer.

Predictions of the Drell-Yan model explain most features of the dilepton continuum produced in hadron-hadron collisions. The exceptions are the over-all rate which is underestimated by a factor of around 2, and the lack of any rationale for the large average transverse momenta of dileptons. Study of the modifications to the simple Drell-Yan process caused by gluon emission and absorption by the quark or antiquark have been made in quantum chromodynamics (QCD). At the current state-of-the-art of calculations a simple factor of 2 enhancement above the naïve Drell-Yan cross-section is predicted. Also, gluon emission and gluon scattering provide natural mechanisms for giving high transverse momentum kicks to the dileptons. These results are important in testing QCD because there are few processes in which first-order effects in QCD perturbation theory are so large and readily calculable.

Measurements of Drell-Yan production cross-sections allow the extraction of the structure functions of the beam hadron. The results for proton beams match the more extensive measurements made in deep-inelastic lepton scattering experiments. In the case of meson beams the method has provided the only measurements of meson structure functions.

Below we describe these features in more detail. The introductory section which follows immediately is designed to provide some necessary background information for the general reader. Other more general reviews by Stroynowski (1981) and Matthiae (1981) are also recommended.

2. THE STRUCTURE OF HADRONS AND THE PARTON MODEL

2.1 The partons

The strongly interacting particles (hadrons) such as π mesons and nucleons are not elementary. They are made up from simpler particles: quarks, antiquarks, and gluons, known collectively as partons. The quarks are point-like, spin $\frac{1}{2}$ fermions, properties they share with the other class of matter particles, the leptons. Quarks differ from leptons in that they interact strongly via gluon exchange, whilst leptons only feel the electroweak force. Evidence on the internal structure of the hadrons has come from deep inelastic lepton scattering off nucleons (Breidenbach *et al* 1969) and from the hadron spectrum (Gell-Mann 1964 and Zweig 1964).

The quarks group into doublets, and the doublets of most interest here are shown in table 1 with their charges in units of the electron charge. Antiquarks $\bar{u}$, $\bar{d}$, etc., have opposite values of charge etc. to the corresponding quarks. Table 2 exhibits the (valence) quark content of the hadrons of interest.

Quarks are extremely well bound in hadrons and there is no confirmed evidence that they can exist in a free state (see however Larue *et al* 1981).

2.2 Colour

Electroweak and gravitational forces are known to be gauge interactions transmitted by gauge fields. In the case of the electroweak interaction, the fields are quantized as spin 1 (vector) particles, namely the photons and intermediate vector bosons. It is expected that the quark-quark strong interaction is also a gauge force.

Greenberg (1964) deduced evidence for a new symmetry called colour, which turned out to be the gauge symmetry. He pointed out that if account is taken of spin, flavour, and relative motion, then the quarks inside baryons with spin parity $^3/_2{}^+$ are in a totally symmetric state. This contradicts the Pauli principle. In order to resolve the dilemma, Greenberg proposed that a further threefold symmetry existed, SU(3) of colour, with the quarks assigned to the fundamental three-representation (red, blue, and green). Then if the quarks in a baryon are arranged in an antisymmetric colour state with no net colour, the difficulty disappears. The solution is to have one red, one blue, and one green quark inside each; in the mesons a quark of one colour is paired with an antiquark of the same colour. The state of the π^+ meson in this scheme becomes

$$(1/\sqrt{3})\left[u(r)\bar{d}(r) + u(b)\bar{d}(b) + u(g)\bar{d}(g)\right] .$$

Paradoxically the unbroken nature of the colour symmetry makes it difficult to observe any direct physical effects of colour; the hadrons are all colour singlets (no net colour) so there is no spectroscopy of colour. Indirect evidence for colour comes from the cross-sections that depend on the matching of colour between a quark and antiquark when they couple to a photon. This matching is, of course, necessary in the Drell-Yan process.

Gross and Wilczek (1973) and Politzer (1973) developed the quantum field theory of colour, now called quantum chromodynamics. The massless vector field particles in this model are called gluons. The gluons possess colour, and this fact constitutes a striking difference when compared with the case of the chargeless photons of electromagnetism. Gluons can emit gluons, and this generates an amplification of the

colour force between quarks as their separation is increased. Quarks are thought to be unable to escape from hadrons precisely because of this increase of force with separation. Conversely as the separation decreases, or equivalently as the relative four-momentum squared of a pair of quarks increases, the colour force decreases monotonically. At high enough relative momenta this leads to the quarks behaving as if they were free (Asymptotic Freedom).

2.3 The parton model

The interactions of leptons with hadrons lend themselves to a treatment by an impulse approximation when the relative four-momentum squared $|q^2|$ is large. Figure 2 shows the form this takes for a) the Drell-Yan process, b) e^+e^- annihilation, and c) deep-inelastic lepton scattering. The lepton (line) is supposed to interact instantaneously with a single quark (line), and any parton-parton interactions are ignored. On a longer time-scale the partons interact to give the hadronic final state. This impulse approximation leads to simple electromagnetic calculations of the cross-sections. Bjorken originally proved the model for lepton scattering at large energies and introduced the Bjorken x-variable (1969); x is the fraction of longitudinal momentum of the hadron that is carried by a given parton, and must lie in the range 0 to 1. The asymptotic freedom limit gives a theoretic basis to the impulse approximation inside QCD. When the inelastic momentum transfer to a hadron is large enough, it will appear to be made up of quasi-free point-like partons.

2.4 Structure functions

The structure functions needed below are the covariant scalar quantities used to describe deep-inelastic lepton scattering from nucleons (Bjorken and Paschos 1969, 1970). Most determinations of the structure functions of nucleons have been made in deep-inelastic scattering experiments for the reactions:

$$\ell^- + \text{nucleon} \rightarrow \ell^- + \text{hadrons}$$

$$\nu + \text{nucleon} \rightarrow \ell^- + \text{hadrons}$$

and their analogues. Under the assumption that a single vector boson exchange dominates, the dynamics of the reaction is described by the three structure functions F_1, F_2, and F_3, which are in turn functions of just two covariant kinematic quantities,

$$x = -q^2/2p\cdot q \quad \text{and} \quad -q^2 \ ,$$

where q is the four momentum transfer between the lepton and target nucleon, and p is the incident nucleon four-momentum.

Of central interest to us here is the interpretation of x and the structure functions in the parton model; x is to be interpreted as the fraction of longitudinal momentum of the parent hadron (Bjorken x) that is carried by the active, struck quark in the over-all centre-of-mass frame. If n(x) dx is the number of quarks carrying longitudinal momentum fractions between x and x + dx, then

$$F_2^{\ell}(x) = \sum_i Q_i^2 x n_i(x) \qquad \text{(charged leptons)} \ ,$$

$$F_2^{\nu}(x) = \sum_i x n_i(x) \qquad \text{(neutrinos)} \ ,$$

where the sums are taken over all quark flavours. The difference between

charged lepton and neutrino scattering arises from the difference between the weak and electromagnetic forces at usual experimental energies. The electromagnetic coupling requires the appearance of the quark charge, namely Q in units of e. In addition, the model requires exact relationships to hold between the structure functions:

$$F_2^{\ell} = 2xF_1^{\ell} \quad \text{and} \quad F_2^{\nu} = \pm xF_3^{\nu} = 2xF_1^{\nu} ,$$

where the sign is positive for neutrino-quark and antineutrino-quark scattering and negative for the other choices. Bjorken (1969) argued that the structure functions at large q^2 and finite x are functions of x alone (Bjorken scaling).

Suppose a target is made of equal numbers of protons and neutrons, and ignoring the small contributions of c and s quarks:

$$F_2^{\ell}/x = (5/18)(q+\bar{q})$$
$$F_2^{\nu}/x = q + \bar{q}$$
$$F_3^{\nu} = q - \bar{q} ,$$

where u(x) dx is the number of u quarks with longitudinal momentum fraction between x and x + dx inside a proton and q is the sum u + d; $\bar{q}(x)$ dx is the corresponding number of antiquarks. The results shown schematically in figure 3 for the kinematic range $4 < -q^2 < 8$ $(GeV/c)^2$ are taken from experiments by de Groot *et al* (1979) using neutrinos and by Bodek *et al* (1980) using electrons. Together the quarks carry something like half the nucleon momentum:

$$\int (q+\bar{q})x \, dx \approx 0.49 .$$

The remainder of the momentum must be carried by partons that do not feel the electroweak force, namely the gluons. From the neutrino-antineutrino difference the net number of quarks has been obtained,

most recently by de Groot *et al* (1979):

$$\int (q-\bar{q})\ dx \approx 3.2 \pm 0.5 \ .$$

This agrees well with the number of quarks (3) which Gell-Mann (1964) and Zweig (1964) require in the nucleon. These are called the valence quarks. Any additional quarks come in pairs with antiquarks, and these are termed sea quarks and antiquarks. The quark momentum is shared by valence and sea quarks. de Groot *et al* (1979) give:

$$\int (q-\bar{q})x\ dx \approx 0.34 \ .$$

This is further illustrated by figure 3b, where it can be seen that the spectrum of sea quarks peaks as x tends to zero.

Feynman (1969) argued from the constancy of the high-energy hadronic cross-sections that there must be large numbers of low-momentum partons in each hadron, with a spectrum peaking at zero. QCD offers a detailed justification for the presence of the sea: each quark confined in a hadron radiates and absorbs gluons as it moves inside the confining potential of the hadron. The gluons, in turn, radiate quark-antiquark pairs, while pairs also coalesce to give back gluons. Because the QCD coupling strength increases as the emitted energy falls, these processes lead to peaking in the sea quark numbers as x tends to zero.

2.4.1 *Phenomenology of structure functions*

Theoretic input on the expected form of the structure functions is meagre. At present no way has been discovered of calculating these quantities from QCD because of the infrared difficulties on the theory. Once structure functions are determined at some value of q^2, QCD can be used to predict how the structure functions evolve as q^2 changes. We

will be returning to this subject later. For predictions of the structure functions, recourse must be made to purely phenomenological arguments.

Drell and Yan (1970b) and West (1970) have made use of the fact that, in the limit as x tends to unity, inelastic scattering merges into elastic scattering. The Drell-Yan-West relation links the x dependence of the structure functions as x tends to unity and the q^2 dependence of the electromagnetic form factor. If the form factor behaves at large q^2 like $(q^{-2})^k$, then the structure function should have the form $(1-x)^{2k-1}$ in the limit. The nucleon form factors behave like q^{-4}, so that

$$F_2 \sim (1-x)^3 \quad \text{for} \quad x \to 1 \ ,$$

which is consistent with the data (Yan 1976). A phase-space argument has been made by Brodsky and Farrar (1973) that when there are m spectator quarks plus antiquarks the electromagnetic form factor should behave like $(q^{-2})^m$. Then coupling this result to the Drell-Yan-West relation yields

$$F_2 \sim (1-x)^{2m-1} \quad \text{as} \quad x \to 1 \ .$$

Scattering from a valence quark in the nucleon leaves a minimum of two spectators, so that

$$F_{2v} \sim (1-x)^3 \quad \text{as} \quad x \to 1 \ .$$

Scattering from a sea quark in a nucleon leaves at least four spectators (three valence quarks plus a sea antiquark), so

$$F_{2s} \sim (1-x)^7 \quad \text{as} \quad x \to 1 \ .$$

Farrar in 1974 pointed out that Regge theory has implications for the form of the structure functions. In the limit as x tends to zero the nucleon plus virtual photon sub-energy becomes large and Regge forms can be obtained for the structure function. Specifically,

$$F_2 \sim a + b\sqrt{x} \ ,$$

where the first and second terms represent the contributions from Pomeron and isospin exchange, respectively. According to the parton model the two terms represent the sea and valence contributions. With this assignment the sea quark behaviour is

$$q_s \sim 1/x \quad \text{as} \quad x \to 0 \ ,$$

and for the valence quarks

$$q_v \sim 1/\sqrt{x} \quad \text{as} \quad x \to 0 \ .$$

These arguments suggest that for the nucleon the total form of the quark distributions are

$$q_v = A_v(1-x)^3/\sqrt{x} \tag{2.1}$$

$$q_s = A_s(1-x)^7/x \ . \tag{2.2}$$

Some refinement is necessary to account for what is known about the measured structure functions. Measurements of scattering from both hydrogen and deuterium allow the comparison of the neutron and proton structure functions. The results show that, as x tends to unity,

$$d(x)/u(x) \to 0 \ .$$

A simple way to take account of this result is to allow an extra factor (1-x) in the valence d-quark structure function. Then

$$u_v = A_u(1-x)^3/\sqrt{x} \ , \quad d_v = (1-x)u_v \tag{2.3}$$

are the final forms.

Extensive measurements by the CERN-Dortmund-Heidelberg-Saclay (CDHS) neutrino collaboration (de Groot *et al* 1979) have been fitted by expressions of the form suggested by Buras and Gaemers (1978):

$$xu_v(x) = A_u x^a (1-x)^b \tag{2.4}$$

$$xd_v(x) = A_d x^a (1-x)^{b+1} \tag{2.5}$$

$$xq_a(x) = A_s (1-x)^c \ . \tag{2.6}$$

The results are given in table 3. It can be seen that there is good agreement with the predictions for the powers a, b, and c. This makes it reasonable to try analogous forms as first estimates of the meson structure functions. Using the fact that each meson contains one valence quark and one valence antiquark, we obtain

$$q_v(x) = B_v (1-x)/\sqrt{x} \tag{2.7}$$

$$q_s(x) = B_s (1-x)^5/x \ . \tag{2.8}$$

2.4.2 *Scaling violations*

Refinements in the measurement of structure functions in deep-inelastic scattering experiments have revealed that Bjorken scaling is not perfect (see, for example, Bosetti *et al* 1978). At low values of x below ~ 0.2, the structure functions increase slowly with increasing q^2, whilst at larger x values there is a slow fall with increasing q^2. Using first-order QCD, Altarelli and Parisi (1977) have set up equations which can be used to show that the variations are logarithmic in q^2. We shall use here the conceptual presentation of Kogut and Susskind (1974) to make the result plausible. When a hadron is probed at a given q^2, structures of size $\sim 1/\sqrt{|q^2|}$ are seen and a certain number of quarks, antiquarks, and gluons are observed. If q^2 is increased, then the virtual

cloud of partons round each original parton is explored in finer spatial detail. Partons are seen to contain partons, which at larger q^2 are seen to contain partons, and so on. At each successive emission the value of x of the partons declines. Thus the structure function falls at large x and increases at small x.

3. THE DRELL-YAN PROCESS

3.1 Properties of the continuum

Figure 1 showed the rapid fall of cross-section with increasing $\mu^+\mu^-$ mass measured by the Columbia-Fermilab-Stony Brook (CFS) Collaboration (Lederman 1982). The dotted curve indicates the level of corresponding $\mu^+\mu^-$ and $\mu^-\mu^-$ cross-sections which arise from uncorrelated leptonic decays of two of the secondary hadrons in any interaction. Evidently the contributions of corresponding coincidences to the $\mu^+\mu^-$ distribution is small. As the mass increases, the background becomes relatively smaller. This is because it is necessary to have a high-momentum and a low-momentum meson (in the laboratory) to give a high-mass pair. As the momentum increases, the lifetime is increasingly dilated, and so the chance that the fast meson is absorbed before decaying is increased.

Figure 4 shows the variation of differential cross-section with mass for dimuons produced by π^- mesons and π^+ mesons, as well as the difference between these cross-sections. The data come from the Birmingham-CERN-Palaiseau (Ecole Polytechnique) Collaboration (Omega Collaboration) using 40 GeV/c beams on a tungsten target (Corden *et al* 1980a). If the continuum were due to the tails of low-mass vector bosons or massive, broad, vector bosons, then the production by π^+ and π^- mesons would be nearly equal, whereas in fact the cross-sections differ by a factor of between 2 and 4.

The longitudinal and transverse momentum distributions complete the production characteristics of dileptons. Longitudinal momentum p_ℓ (the component parallel to the beam) in the centre-of-mass frame is expressed in terms of the Feynman x-variable, x_F. This is the longitudinal momentum divided by the maximum possible longitudinal momentum at

the experimental c.m. energy squared, s. If the dilepton transverse momentum and the effective mass of the hadrons recoiling against the dilepton are small compared to $\sqrt{s}$, then

$$p_{\ell,max} = \sqrt{s}/2 \ (1-M^2/s) \ .$$

If M is also small compared to $\sqrt{s}$,

$$p_{\ell,max} = \sqrt{s}/2 \ .$$

Thus

$$x_F = 2p_\ell/\sqrt{s} \ , \qquad (3.1)$$

which has a kinematic range of -1 to +1 only. In some cases a variation on x_F is preferred that takes account of M^2/s being non-negligible:

$$x_{F'} = x_F/(1-M^2/s) \ . \qquad (3.2)$$

Another useful variable is the rapidity y:

$$y = 0.5 \ \ln \left[(E+p_\ell)/(E-p_\ell)\right] \ .$$

Figure 5 shows the dependence of the cross-section on x_F for dimuons, measured by Anderson *et al* (1979a) for incident π^- mesons and protons on a heavy target. The range in longitudinal momentum (x_F) is restricted experimentally to large values because the thick absorber stops the slow-moving muons. The most significant feature of the cross-sections is a rapid fall with the longitudinal momentum carried by the dilepton (x_F). Recall that x_F equal to unity corresponds to a momentum equal to the beam c.m. momentum. A large value of x_F requires that the active quark from the beam carries a large fraction of the beam hadron's momentum. As may be seen from figure 3 the probability for this falls off rapidly as this fraction increases towards unity. The experimental

cross-section falls off more rapidly with x_F for incident protons than for incident π^- mesons. For the moment we note that according to the Drell-Yan description this is also qualitatively reasonable: a proton's momentum is shared by three valence quarks, whereas a meson's momentum is only shared by two valence quarks. In order to pursue these points quantitatively, it will be needful to develop the formalism for the Drell-Yan process.

A typical set of transverse momentum distributions for dimuons obtained by the Omega Collaboration (Corden *et al* 1981), using 39.5 GeV/c π^- mesons incident on a tungsten target, are shown in figure 6. There is a rapid fall of differential cross-section with increasing transverse momentum squared, p_t^2. This can be fitted with an exponential form

$$d\sigma/dp_T^2 = A \exp(-Bp_T^2) ,$$

from which a mean p_t^2 can be extracted:

$$\langle p_t^2 \rangle = 1/B .$$

For the data exhibited, $\langle p_T^2 \rangle$ measured in $(GeV/c)^2$ increases monotonically with dilepton mass, from 0.76 ± 0.05 for the 2.0 to 2.3 GeV/c^2 mass interval to 1.76 ± 0.16 for the 4 to 5 GeV/c^2 mass interval. This is already a good deal larger than the values of $\langle p_T^2 \rangle$ measured by Albrow *et al* (1978) for single hadrons produced in high-energy hadron-hadron collisions. The Drell-Yan model in its original form has no explanation for this fundamental fact: the corrections arising in QCD are essential for an explanation. Another important dimensionless kinematic quantity can be constructed from the dilepton effective mass M, namely:

$$\tau = M^2/s , \qquad (3.3)$$

3.2 Backgrounds at low mass

There are several sources of background which come to dominate the dilepton continuum at low dilepton mass:

a) Dilepton decays of the closely spaced (neutral) vector mesons $\rho(770)$, $\omega(780)$, $\phi(1020)$, and $\rho'(1600)$, of which the ρ and ρ' have substantial width;

b) Dalitz decays of neutral mesons in general, including the $\eta(550)$, $\omega(783)$, and others;

c) Bethe-Heitler pairs;

d) Accidental coincidences of leptonic decays such as $\pi^+ \to \mu^+ + \nu_\mu$ between two hadrons produced in any hadronic interaction.

At low mass it is therefore difficult to extract the Drell-Yan signal from background. For this reason we will restrict discussion to data on dileptons with masses above 2 GeV/c^2.

3.3 The dynamics of the Drell-Yan process

Drell and Yan (1970a, 1971) proposed a simple electromagnetic process to account for the production of the continuum of dilepton pairs from hadron-hadron collisions:

$$A + B \to \ell^+ + \ell^- + \text{anything} .$$

The essential steps are the annihilation of a single antiquark from one hadron on a single quark from the other hadron to produce a virtual photon. Subsequently the virtual photon converts to a pair of leptons. If the mass M of the dilepton is large compared to the nucleon mass, then the Heisenberg Uncertainty Principle tells us that the time of interaction is short on the nuclear scale. There is thus no opportunity

for the annihilating quark-antiquark pair to interact with other components of the parent hadrons. The other partons can be treated purely as spectators. Subsequently, on a time-scale that is long compared to the annihilation, the spectators rearrange themselves into outgoing hadrons. Generally the leptons alone are detected and momentum-analysed. This procedure measures the inclusive cross-section for dilepton production and sums over all possible combinations of the final-state hadrons. Thus in the calculation of the cross-section the factor expressing the probability that the spectators convert to hadrons is simply unity.

The dilepton kinematic variables τ and x_F are directly related to the Bjorken x-values (longitudinal momenta) of the parent quark and antiquark. Suppose the active quark (antiquark) in the beam particle has a Bjorken x of x_1, and the active antiquark (quark) in the target has a Bjorken x of x_2. Then in the c.m. frame of beam plus target the annihilating pair have longitudinal momenta $x_1\sqrt{s}/2$ and $-x_2\sqrt{s}/2$, respectively. If the quarks are massless their energies are $x_1\sqrt{s}/2$ and $x_2\sqrt{s}/2$. Then equating the four-momentum of the annihilating pair to the dilepton four-momentum (E,p_ℓ) gives

$$E = (x_1+x_2)\sqrt{s}/2 \tag{3.4}$$

and

$$p_\ell = (x_1-x_2)\sqrt{s}/2 \ . \tag{3.5}$$

The dilepton mass squared is

$$M^2 = E^2 - p_\ell^2 = sx_1x_2 \ .$$

Two basic relations between the quark variables and the observables now emerge:

$$\tau = M^2/s = x_1x_2 \tag{3.6}$$

and $$x_F = 2p_\ell/\sqrt{s} = x_1 - x_2 \ . \qquad (3.7)$$

Figure 2 brings out the great similarity between the parton processes underlying e^+e^- annihilation, deep-inelastic lepton scattering, and the production of lepton pairs: in each case a virtual photon couples a lepton line to a quark line. These basic processes are thus described by a single amplitude in quantum electrodynamics. If the photon four-momentum is denoted by q, then in deep-inelastic lepton scattering q^2 is negative, whereas in the other pair of reactions q^2 is positive. We can speak of space-like photons in the first case and time-like photons in the second. According to the parton model the full calculation of cross-section for deep-inelastic lepton scattering and the Drell-Yan process makes use of the selfsame momentum distribution of the quarks and antiquarks in the hadron.

3.4 Drell-Yan formalism

The process underlying the production of the continuum of dileptons has been shown in figure 2a:

$$q + \bar{q} \rightarrow \mu^+ + \mu^- \ .$$

This is the annihilation of point fermions, and formally resembles the electron-positron annihilation to $\mu^+\mu^-$. Quantum electrodynamics yields the same cross-section (well above threshold):

$$\sigma = 4\pi\alpha^2Q^2/3q^2 \ ,$$

where α is the fine structure constant, Qe is the quark charge, and q^2 is the four-momentum of the virtual photon. The factor q^{-2} comes from the photon propagator term in the amplitude. Here q^2 is just the dilepton mass squared M^2, therefore

$$\sigma = 4\pi\alpha^2Q^2/3M^2 \ .$$

This expression has now to be multiplied by i) the probability $q_B(x_1)\,dx_1$ that a quark in the beam carries a momentum fraction x_1, and ii) the probability $\bar{q}_T(x_2)\,dx_2$ that an antiquark carries a fraction x_2 of the target momentum. Then

$$d^2\sigma = 4\pi\alpha^2 Q^2 q_B(x_1)\bar{q}_T(x_2)\,dx_1\,dx_2/3M^2 \ .$$

Equally the quark may originate in the target, which gives a second similar term in the cross-section with $\bar{q}_B(x_1)q_T(x_2)$ replacing $q_B(x_1)\bar{q}_T(x_2)$. Each quark flavour can contribute, so we sum over flavours. Finally, the quark and antiquark colour must match, which reduces the cross-section by a factor of 3. Putting in all these ingredients, the cross-section becomes

$$\frac{d^2\sigma}{dx_1dx_2} = \left(\frac{4\pi\alpha^2}{9M^2}\right) \sum Q^2 \left[q_B(x)\bar{q}_T(x_2) + \bar{q}_B(x_1)q_T(x_2)\right] . \qquad (3.8)$$

Re-expressing this in terms of the measurable dilepton parameters M and x_F gives:

$$\frac{d^2\sigma}{dM^2dx_F} = \left(\frac{4\pi\alpha^2}{9M^4}\right)\left(\frac{x_1x_2}{x_1+x_2}\right) \sum Q^2 \left[q_B(x_1)\bar{q}_T(x_2) + \bar{q}_B(x_1)q_T(x_2)\right] , \qquad (3.9)$$

where

$$x_1 = \frac{1}{2}\left[\sqrt{(x_F^2+4\tau)} + x_F\right] ,$$

$$x_2 = \frac{1}{2}\left[\sqrt{(x_F^2+4\tau)} - x_F\right] .$$

In terms of rapidity $dy = dp_L/E = dx_F/(x_1+x_2)$, thus:

$$\frac{d^2\sigma}{dMdy} = \left(\frac{8\pi\alpha^2}{9Ms}\right) \sum Q^2 \left[q_B(x_1)\bar{q}_T(x_2) + \bar{q}_B(x_1)q_T(x_2)\right] . \qquad (3.10)$$

When the dilepton has zero longitudinal momentum the kinematics simplifies considerably:

$$x_F = y = 0 \quad \text{and} \quad x_1 = x_2 = \sqrt{\tau} \ .$$

Then equations (3.9) and (3.10) give

$$\left.\frac{d^2\sigma}{dM^2 dx_F}\right|_{x_F=0} = \frac{2\pi\alpha^2\sqrt{\tau}}{9M^4} \sum Q^2 \left[q_B(\sqrt{\tau})\bar{q}_T(\sqrt{\tau}) + \bar{q}_B(\sqrt{\tau})q_T(\sqrt{\tau})\right] \tag{3.11}$$

$$\left.\frac{d^2\sigma}{dMdy}\right|_{y=0} = \frac{8\pi\alpha^2}{9Ms} \sum Q^2 \left[q_B(\sqrt{\tau})\bar{q}_T(\sqrt{\tau}) + \bar{q}_B(\sqrt{\tau})q_T(\sqrt{\tau})\right] . \tag{3.12}$$

3.5 Phase space

The kinematics of the Drell-Yan process (neglecting any transverse momentum) are summarized by the simple expressions (3.6), (3.7):

$$\tau = x_1 x_2$$

and

$$x_F = x_1 - x_2 .$$

According to the formulation of the quark model the Bjorken x is limited physically to the range 0 to 1. The available phase space for the Drell-Yan process is then a square on a plot of x_2 versus x_1. This is shown in the upper part of figure 7. Lines of constant dilepton mass and τ (= M^2/s) are rectangular hyperbolae, and lines of constant x_F are diagonals. The parameters x_F and τ define a unique point in phase space. If the data are recorded on such a plot then the density at (x_F, τ) is seen from expression (3.8) to be proportional to the number of quarks (antiquarks) in the beam hadron at Bjorken x equal to x_1 and to the number of antiquarks (quarks) in the target hadron at x_2. This is illustrated in the lower part of figure 7, where quark distributions are drawn appropriately for proton-proton collisions.

4. EXPERIMENTAL METHODS

4.1 General requirements

The simple Drell-Yan model makes statements about the lepton pairs produced in hadronic collisions and not about the accompanying hadrons, so it has been sufficient to detect solely leptons in order to make many tests of the model. Experiments have been performed with fixed targets; this allows the use of a range of beam particles ($\pi^{\pm}$, $K^{\pm}$, p, and $\bar{p}$) but with a limited range of c.m. energy, up to 28 GeV for a beam momentum of 400 GeV/c. At the CERN Intersecting Storage Rings (ISR) proton beams are brought into collision with momenta up to 30 GeV/c, which corresponds to a c.m. energy of near 60 GeV.

Detection of muons has been preferred to detection of electrons because of the relative simplicity. At current experimental energies the principal source of muon pairs is from decays of uncorrelated pairs of mesons, both π and K mesons. This gives a rate 10^4 times the Drell-Yan rate. By placing a wall of heavy material, several interaction lengths thick, immediately downstream of the target, the majority of π and K mesons can be caused to interact before decaying. Muons that emerge from the absorber can be detected by scintillator hodoscopes which form part of the trigger. A magnetic spectrometer downstream of the absorber is needed to measure the muon momenta.

Electron detection requires shower counters with good spatial and energy resolution over a wide area. These are expensive devices, more complicated to build and maintain than the scintillator hodoscopes needed for muon detection. Little material is situated between the target and detector. This has two advantages: first, there is no multiple

scattering so that the mass resolution is much improved over the dimuon case; secondly, it is possible to place a magnetic spectrometer between target and shower counters and study the associated hadrons. In practice, these advantages of electron detection have not yielded much additional information to date (see section 9).

Cross-sections for the Drell-Yan process at high masses are low, e.g. 10^{-38} cm^2 GeV^{-1}/nucleon at a mass of 10 GeV/c^2 with 400 GeV/c protons incident. Most experiments with fixed targets have therefore used heavy nuclear targets. Hydrogen is in principle preferable as the target material in order to eliminate nuclear effects. Fortunately it has proved possible to show that specifically nuclear effects are absent in high-mass dilepton production. In colliding beam experiments the data rate is lower owing to low luminosity and to the smaller cross-section at the higher c.m. energies.

Only the high-mass continuum is important for the study of the Drell-Yan process, but of course the cross-section falls with increasing mass. If the momenta of the leptons are p_+ and p_- and the opening angle is θ, then the mass squared is given approximately by

$$M = 2\sqrt{p_+ p_-}\ \theta \ . \qquad (4.1)$$

Simple selective triggers apply a cut on the opening angle, and more sophisticated triggers use a determination of bending in the spectrometer to estimate p_+ and p_- as well. The detector elements used in the trigger are fast scintillator and wire planes with some hard-wired matrix logic to select preferentially high-mass pairs. Then rejection at the level of 10^2 to 10^4 is feasible for the low-mass pairs.

Several experiments are now described in order to give an idea of the range of techniques applied. The Omega Collaboration experiment will be described first and in rather more detail. Table 4 summarizes many of the parameters of the experiments, and figure 8 shows the acceptances of several of them on the phase-space plot.

4.2 The CERN Omega spectrometer experiment

The apparatus has been described by Corden *et al* (1978, 1980b) and is shown in figure 9 in horizontal section. A set of four Čerenkov counters were used to identify each beam particle in the unseparated 40 GeV/c beam; H1 and H2 are crossed hodoscopes to provide time and position information on the beam particles. Two targets were used: 67 cm of hydrogen and 6 cm of tungsten, 93 cm apart. The tungsten target is followed by a 1.1 m thick copper absorber with a central conical plug of tungsten to absorb the most energetic secondary hadrons around the beam axis. Charged particles emerging from the absorber entered a magnetic spectrometer comprising optical spark chambers in the Omega dipole field of 1.8 T. The return yoke of the magnet provided a further 1.25 m of iron to stop residual hadrons that had penetrated the copper absorber.

Triggering was made with the two scintillator hodoscopes S6 and BH, each made of horizontal slabs. A logic matrix was used to impose correlations between the elements of S6 and BH in order to accept only particles whose trajectories pointed back within multiple scattering errors to the target. At least one such track was required above and below the median plane, and a minimum opening angle requirement was also imposed to suppress the acceptance of pairs of low effective mass. Information from counters and spark chambers was recorded on magnetic tape.

Subsequent analysis involved reconstructing the tracks in the spark chambers. Tracks were required to extrapolate so as to intersect active elements of each hodoscope in order to be validated as muons. Upstream they were also required to extrapolate to one or other target.

A total of 1.3 (0.9) million triggers were recorded with the negative (positive) beam. The beam fractions were 93.9% π^-, 3.4% K^-, and 2.7% $\bar{p}$; 74.6% π^+, 3.4% K^+, and 22.0% p. After analysis, 11,500 (5700) $\mu^+\mu^-$ pairs with effective mass above 2 GeV/c^2 remained (including ψ and ψ'), originating from the tungsten target. Physics results discussed below included information on continuum dilepton production cross-sections for all six beam types, and on transverse momentum distributions. Measurements of the K-factor and of the π-meson structure function were also made.

4.3 Review of fixed-target experiments

The Columbia-Fermilab-Stony Brook (CFS) Collaboration used a symmetric two-arm spectrometer to detect muon or electron pairs emitted at 90° in the c.m. frame (Ito *et al* 1981). Each arm covered only 0.2 sr, so the acceptance was small in phase space (figure 8). Proton beams of 200, 300, and 400 GeV/c were used: no beam identification was necessary and high fluxes could be used. In this way some 10^6 $\mu^+\mu^-$ pairs were detected with masses ranging up to 20 GeV/c^2. Physics results included the discovery of the T family of resonances (Herb *et al* 1977, Innes *et al* 1977).

A second experiment at Fermilab with a modest acceptance magnetic spectrometer was carried out by the Chicago-Illinois-Princeton (CIP) Collaboration (Anderson *et al* 1976a and Hogan *et al* 1979a). A 225 GeV/c beam was employed, and beam Čerenkovs allowed π^+/proton separation.

Multiwire proportional chambers (MWPCs) placed in front of and behind the spectrometer magnet determined track trajectories. Scintillator hodoscopes located upstream from the magnet and behind the final absorber were used for triggering. A hard-wired digital processor was selected on the basis of the opening angle between the tracks and on track stiffness. This gave a rejection factor for low-mass dimuons of $\sim 10^2$.

A more sophisticated magnetic spectrometer with larger acceptance has been built by Badier *et al* (1979a, 1980a). The NA3 Collaboration has made very high statistics studies of dimuons produced by 150, 200, and 280 GeV/c beams at the CERN Super Proton Synchrotron (SPS). Full beam identification was provided by beam Čerenkov counters, and both tungsten and hydrogen have been used as targets. The target was followed by 1.5 m of iron absorber with a central tungsten/uranium plug. Downstream, 31 planes of MWPCs measured track trajectories with bending provided by a 4 T·m dipole placed close to the target. Three scintillator hodoscopes were used in the trigger wired to a logic matrix to suppress low-mass pairs.

A rather different apparatus has been designed by the CEN Saclay-Imperial College-Southampton-Indiana Collaboration (Goliath). This was reported by Abolins *et al* (1979). It was the first fixed-target experiment to dispense with an absorber between target and spectrometer. Particle trajectories were measured by proportional chambers immersed in the 1.5 T field of the Goliath magnet. Lead/scintillator sandwich detectors identified and measured the energies of any electromagnetic showers produced by photons and electrons. Further downstream, 3 m of steel was used to absorb hadrons, and this was followed by a scintillator hodoscope to detect muons. Data were collected at 150 and

175 GeV/c beam momentum. Both the Goliath Collaboration and the CFS Collaboration have compared their $\mu^+\mu^-$ with their e^+e^- mass spectra and find excellent agreement.

Better mass resolution is possible with the so-called open spectrometer arrangement, which is very useful in the search for narrow resonances. This does not compensate for the low data-taking rate and the large background of dilepton pairs from uncorrelated meson decays when studying the Drell-Yan continuum. An experiment at low beam energies at Brookhaven (McCal *et al* 1979) is not reviewed here. The interpretation of the data in terms of the Drell-Yan mechanism is difficult because of the proximity of the kinematic threshold.

4.4 Review of ISR experiments

Three series of experiments have been carried out at the CERN Intersecting Storage Rings (ISR) over the last few years. These experiments are important in that they provide information at high centre-of-mass energies not available in fixed-target experiments. Their data samples are necessarily small both because cross-sections at a given value of τ drop as $1/s$ and because the luminosity available with colliding beams is small.

The CERN-Columbia-Oxford-Rockefeller (CCOR) Collaboration have performed experiments to detect dielectron pairs (Angelis *et al* 1979a). The momenta of particles emerging from the interaction region were measured with cylindrical drift chambers inside a solenoidal magnet. Electron identification was made with two arrays of lead-glass detectors. Most showers observed were the result of π^0 conversions. Only 174 opposite-sign dielectrons were detected compared to 52 like-sign pairs.

The Athens-Brookhaven-CERN-Syracuse (ABCS) Collaboration used argon calorimeters to detect electrons at the ISR (Cobb *et al* 1977, 1979). Track trajectories were measured with proportional chambers but without any magnetic field. Only a few hundred dielectron pairs have been obtained with a considerable background of uncorrelated decay pairs.

The third series of ISR experiments have detected dimuon pairs. These experiments have been carried out by the CERN-Harvard-Frascati-MIT-Naples-Pisa (CHFMNP) Collaboration and the apparatus has been described by Antreasyan *et al* (1980, 1981a). Seven magnetized iron toroids filter the muons and give magnetic momentum analysis. Drift chambers placed around the interaction point and between the toroids are used for track measurements. About 4000 $\mu^+\mu^-$ pairs with mass above 5 GeV/c^2 have been collected.

5. PREDICTIONS FOR THE DRELL-YAN PROCESS

5.1 Scaling

The expression for the Drell-Yan cross-section (equation 3.9) contains a factor M^{-4} that originates from the propagator of the intermediate photon in the diagram of figure 2a. It is this factor that is responsible for the rapid fall of cross-section with increasing mass seen in figures 1 and 4. Rearranging the cross-section,

$$M^3(d^2\sigma/dMdx_f) = \mathcal{F}_{BT}(x_1,x_2) \equiv F_{BT}(x_F,\tau) \ , \qquad (5.1)$$

where F_{BT} is a function that depends on the quark content of beam and target. Thus $M^3(d^2\sigma/dMdx_F)$ for a given combination of beam and target is predicted to be independent of beam energy, provided measurements are made at identical values of x_F and τ. This property of scaling with energy provides a test of the validity of the model even though the structure functions convoluted inside F_{BT} may be poorly known. In terms of the rapidity, $M^3(d^2\sigma/dMdy)$ should scale. There is some simplification when x_F is equal to zero:

$$M^3(d^2\sigma/dMdy)_{y=0} \equiv \tau^{3/2} \left(s \frac{d^2\sigma}{d\sqrt{\tau}dy} \right)_{y=0}$$

$$= \frac{8\pi\alpha^2}{9} \tau \sum Q^2 \left[q_B(\sqrt{\tau})\bar{q}_T(\sqrt{\tau}) + \bar{q}_B(\sqrt{\tau})q_T(\sqrt{\tau}) \right]$$

$$= F'_{BT}(\sqrt{\tau}) \ , \qquad (5.2)$$

where the function F'_{BT} depends only on the structure functions at a Bjorken x of $\sqrt{\tau}$. Total cross-sections at a given value of τ are also required to scale:

$$M^3(d\sigma/dM) = G_{BT}(\tau) \ . \qquad (5.3)$$

5.1.1 *Tests of scaling*

The CFS Collaboration (Yoh *et al* 1978 and Ito *et al* 1981) have made tests of scaling with proton beams at momenta of 200, 300, and 400 GeV/c. This covers a range of $\sqrt{s}$ from 20 to 28.2 GeV. The two-arm spectrometer used restricts the range of accessible y. Figure 10 shows the comparison of the cross-section $s(d^2\sigma/d\sqrt{\tau}dy)$ at y equal to 0.2 over the range in τ from 0.15 to 0.5. Agreement is strikingly good. It should be remembered that although $\sqrt{s}$ increases by a factor 1.4 the actual cross-sections compared differ by a factor of 10. Another recent and comparable test has been made with dimuon data taken at the CERN ISR (proton on proton) by Antreasyan *et al* (1981a). Figure 11 illustrates their results for the scaling function $M^3(d^2\sigma/dMdx_F)$ at x_F equal to zero and $\sqrt{s}$ values of 44 and 62 GeV. The corresponding cross-sections for 23.8 and 27.4 GeV have been added from the tables given by Ito *et al* (1981).

Within the indicated experimental errors there is good evidence for scaling over the whole range of 24 to 60 GeV. The full line is the result of a calculation using the Drell-Yan model.

The most complete test of scaling for the cross-section of dimuons produced by meson beams is provided by a comparison of results of the NA3 Collaboration (Lefrançois 1980) and the Omega Collaboration (Corden *et al* 1980a). Figure 12 compares the cross-section $M^3(d\sigma/dM)$ for x_F greater than zero. The data were taken at beam momenta ($\sqrt{s}$) over the range 40 GeV/c (8.9 GeV) to 280 GeV/c (29.2 GeV). Again the hypothesis of scaling seems to be satisfied to within the limits of experimental uncertainty. In summary, it can be said that scaling is valid, over the experimental range explored, to the level of a few percent.

Deep-inelastic scattering experiments have observed slow departures from Bjorken scaling of the nucleon structure functions [see the recent review by Drees (1981)]. These are logarithmic in q^2 and vanish around a Bjorken x of 0.2. This means that Drell-Yan cross-sections should be free of scaling violations for the kinematic region:

$$x_F = 0 \quad \text{and} \quad x_1 = x_2 = \sqrt{\tau} \approx 0.2 \ .$$

This is just the kinematic region for the comparison made between the proton production experiments shown in figure 11. In the case of the comparison made for π-meson production (figure 12), the scaling function $M^3(d\sigma/dM)$ should only fall by a few percent at a $\sqrt{\tau}$ of 0.5 over the range of $\sqrt{s}$ investigated. This is well within the experimental uncertainties.

5.2 The beam dependence of cross-sections

At this stage we will examine the ratio between cross-sections for Drell-Yan production rather than absolute cross-sections. This eliminates from the discussion the over-all enhancement of cross-section predicted by QCD. In taking a ratio, all that remains of consequence will be the terms $[q_B(x_1)\bar{q}_T(x_2) + \bar{q}_B(x_1)q_T(x_2)]$ or integrals over these; $q_B(x_1)$ is the quark distribution in the beam hadron and $q_T(x_2)$ is the same thing for the target hadron.

The lower portion of figure 7 illustrates the convolution of quark distributions for proton-proton interactions. In this case, the only anti-quarks are provided by the seas. It is clear from the figure that at any given fixed x_F (for example zero) the products $q_B\bar{q}_T$ and $\bar{q}_B q_T$ decline rapidly as τ increases, because the sea is concentrated close to Bjorken x equal to zero.

In table 2 the valence quark content of the relevant hadrons is given. Note that as well as the proton, the neutron and K^+ meson do not contain any valence $\bar{u}$ or $\bar{d}$ antiquarks that could annihilate on valence u or d quarks in target nucleons. Thus the convolution factor for all three types of beam must decline rapidly as τ increases. On the other hand, antiprotons, π^+ mesons, π^- mesons, and K^- mesons all contain valence $\bar{u}$ and/or $\bar{d}$ quarks. For these beam particles, both sea and valence quarks can contribute and the convolution factor will not decline so quickly as τ increases.

There are only two valence partons in mesons against three in the nucleons. Thus the valence $\bar{u}$ antiquark in the π^- meson is expected to have a larger $\langle x \rangle$ than the $\bar{u}$ (or $\bar{d}$) antiquark in the antiproton. Consequently it is reasonable to expect in the Drell-Yan model that, as τ increases, the convolution of quark distributions will fall less quickly for meson beams than for $\bar{p}$ beams.

To summarize, the model predicts that at intermediate values of τ, the K^-, π^+, and π^- mesons, and $\bar{p}$ beams, will all be more effective in producing Drell-Yan pairs than will K^+ meson or proton beams. This advantage will grow as τ tends to unity. In addition, the mesons will become more effective than the antiprotons as τ tends to unity. Notice that at very low values of τ the sea is the dominant contribution, and all beam types may be expected to be equally effective in giving Drell-Yan pairs.

Quantitatively, it is possible to predict the ratio of π^+-meson to π^--meson production cross-sections at large τ irrespective of any detailed knowledge of structure functions. At large τ, only the convolution involving the valence antiquark in the meson is of importance:

$$\lim_{\tau\to 1}\left[\sigma(\pi^+)/\sigma(\pi^-)\right] = \frac{\int (dx/x_1x_2)\bar{d}_+(x_1)d_T(x_2)Q_d^2}{\int (dx/x_1x_2)\bar{u}_-(x_1)u_T(x_2)Q_u^2} \ . \qquad (5.4)$$

If the target contains equal numbers of protons and neutrons (an 'isoscalar' target), then $u_T \equiv d_T$ and hence:

$$\lim_{\tau\to 1}\left[\sigma(\pi^+)/\sigma(\pi^-)\right] = Q_d^2/Q_u^2 = 0.25 \ . \qquad (5.5)$$

On the other hand, if the target is hydrogen, $u_T \approx 2d_T$ so that

$$\lim_{\tau\to 1}\left[\sigma(\pi^+)/\sigma(\pi^-)\right] = 0.125 \ . \qquad (5.6)$$

5.2.1 *Tests of beam dependence*

The production of dileptons by the full range of $\pi^{\pm}$, $K^{\pm}$, p, and $\bar{p}$ has been reported by the Omega Collaboration (Corden *et al* 1978, 1980a) and by the NA3 Collaboration (Lefrançois, 1980) at 40 GeV/c and 200 GeV/c beam momentum, respectively. Figure 13 obtained by Corden *et al* (1978) combined several measurements of proton-produced cross-sections with their own data on π^--produced cross-sections. At low τ, where annihilation is mostly of sea quarks, the cross-sections are not very different. As τ increases, the annihilation of the valence $\bar{u}$ antiquark in the π^- meson comes into play; this possibility is absent for the incident proton; hence by the time τ reaches 0.4, the relative proton-induced cross-section has fallen away spectacularly by 2 orders of magnitude relative to the π^--meson induced cross-section. This was confirmed by Hogan *et al* (1979b).

Production cross-sections relative to π^- production for dileptons are shown in figure 14 for all types of beam particles (Corden *et al* 1980a). There is rough equality for the beam particles that contain $\bar{u}$ or $\bar{d}$ valence antiquarks ($\bar{p}$, π^-, π^+, and K^-), whereas the K^+ and proton

have smaller cross-sections. Note also that there is some evidence that the $\bar{p}$-produced cross-section is falling relative to the π^-- and K^--produced cross-sections as τ increases. This is at least consistent with the naive expectation that the mean Bjorken x is relatively larger for the valence quarks in the mesons.

The π^+/π^- production ratio is the one best measured. Figure 15 shows measurements of the ratio plotted as a function of $\sqrt{\tau}$. The measurements on isoscalar targets were made by the CIP Collaboration (Anderson *et al* 1979a), the NA3 Collaboration (Lefrançois 1980), and the Omega Collaboration (Corden *et al* 1980a). At low $\sqrt{\tau}$ the sea-on-sea annihilations are expected to be important and the ratio is close to unity. It then declines steadily towards the expected asymptotic ratio of 0.25. The data taken with a hydrogen target by the NA3 Collaboration (Matthiae 1981) are also shown. In this case the π^+/π^- production ratio is evidently lower and is consistent with an asymptotic limit of 1/8.

All results are qualitatively and quantitatively consistent with the Drell-Yan model. The lines drawn in figure 14 exhibit the predictions of the model (Corden *et al* 1980a) for a single consistent set of structure functions.

5.3 A dependence of the cross-section

The quark-antiquark annihilation that produces dileptons is a point-like electromagnetic interaction; thus the cross-section on a nucleon is the incoherent sum of the cross-sections on its component quarks and antiquarks. It should be equally true that the cross-section on a nucleus is the incoherent sum of the cross-section on its component nucleons and will be proportional to A, the atomic number.

This contrasts markedly with the A dependence of hadronic cross-sections. The mean free path for hadronic interactions in nuclear matter is so short that the beam particles interact in the front face of the nucleus whilst the interior is shielded. The resulting cross-section is proportional to the nuclear surface area which varies as $A^{2/3}$. Observation of an A^1 dependence for the dilepton production cross-section is therefore a good check that the Drell-Yan process is indeed electromagnetic with no shielding.

Measurements of the cross-section for several nuclear targets are fitted by an expression of the form

$$\sigma(Z,A) = A^{\alpha}\sigma_0 \ , \qquad (5.7)$$

from which α is extracted. It should be appreciated right away that α can be determined very accurately if a wide range in A is made use of. The NA3 Collaboration used hydrogen and platinum (A = 195), so in principle an error of 50% in relative cross-sections translates into an error of less than 0.1 in α.

Most nuclei, and in particular hydrogen, are not isoscalar, and account must be taken of the factor of 4 difference between the u-quark and d-quark annihilation cross-sections. For π^- mesons incident at typical accelerator energies, the annihilation of the valence $\bar{u}$ antiquark on a valence u quark in the nucleons contributes most of the cross-section. Two thirds of the valence quarks in hydrogen are u quarks, against half in an isoscalar nucleus, so that an enhancement of about $^4/_3$ in cross-section is expected. In practice, account must also be taken of the explicit quark distributions and of sea quarks. The enhancement is then about 1.5 at 200 GeV/c beam momentum and is not very

sensitive to uncertainties in the structure functions (Badier *et al* 1981a). The previous expression generalizes to

$$\sigma(A,Z) = \sigma_0(A,Z)A^{\alpha'} \quad . \tag{5.8}$$

where $\sigma_0(A,Z)$ represents a cross-section corrected for departure from an isoscalar target. With this correction the prediction from the Drell-Yan model is that α' is identically unity.

To summarize, a test with targets that are close to isoscalar is not sensitive to details of the structure functions, whilst a test with hydrogen will reveal any unexpected nuclear effects and have the greatest intrinsic sensitivity.

5.3.1 Tests of the A dependence of cross-section

The A dependence of dimuon cross-section has been measured in some detail with proton and π^--meson beams. Figure 16a shows a compilation of α values taken from experiments by Branson *et al* (1977), Anderson *et al* (1979a) and Ito *et al* (1981) with proton beams. The targets employed, Be, C, Cu, Pt, and W, are reasonably close to isoscalar, so that α only differs from α' by approximately 0.03. It is apparent that α rises from around $^2/_3$ at low masses to plateau close to unity above 2 to 4 GeV/c^2. The Drell-Yan process only dominates at large masses, so the over-all behaviour seems well understood. Local dips in α near the ψ and Υ families of resonances may also be present; although the evidence is not compelling.

The data of the CFS Collaboration (Ito *et al* 1981) from 5 to 11 GeV/c^2 in mass, fix the plateau value of α' at $1.007 \pm 0.018 \pm 0.028$, where the errors are statistical and systematic respectively. This is a clear success for the Drell-Yan model. There is no marked dependence of α on the transverse momentum, see figure 16b.

Studies with π-meson beams show a similar rise of α with dilepton mass to a plateau close to unity above 2 to 3 GeV/c^2. Table 5 brings together measurements of the plateau value of α and α′. The measured values found with isoscalar targets are equal to unity within experimental errors, apart from the older CIP result (Anderson *et al* 1979a).

Results of the NA3 Collaboration comparing cross-sections measured with hydrogen and platinum have been reported by Badier *et al* (1980c and 1981b). The plateau values of α and α′ are also given in table 5. Notice that the difference $\pi^- - \pi^+$ should ideally remove any hadronic background.

Briefly we can say that all the measurements of α′ for proton- and π-meson produced dimuons with masses above 3 GeV/c^2 are in excellent agreement with the Drell-Yan prediction of unity. Below 2 GeV/c^2, α falls to the hadronic value of $^2/_3$. Thus the high-mass data are free from specifically nuclear effects that might have distorted the Drell-Yan process. Data taken with heavy targets are therefore equally valuable in studying the Drell-Yan process along with data from hydrogen target experiments. This conclusion is of great practical significance because the data-taking rate with heavy targets is much greater than with hydrogen, whilst the compactness of the heavy targets makes it easier to design selective hardware triggers based on identifying particle trajectories going back to the interaction point.

5.4 The decay angular distribution

The Drell-Yan model also leads to the prediction of a simple decay angular distribution of the leptons in the rest frame of the dilepton pair. In collinear collision the quark-antiquark annihilation produces

a photon with its spin aligned along the beam axis. The amplitude for the decay of the photon into a dilepton pair is then

$$A(\theta,\phi) = \uparrow\uparrow Y_0^1(\theta,\phi) + \uparrow\downarrow Y_1^1(\theta,\phi) \ ,$$

where the arrows indicate the spin alignments of the leptons (up being parallel to the beam) and the Y's are the spherical harmonic functions of the polar angles with respect to the beam axis. The angular distribution is

$$dN/d\Omega = |A(\theta,\phi)|^2$$

which, integrated over azimuth gives,

$$dN/d\theta = 1 + \cos^2 \theta \ . \qquad (5.9)$$

Experiments show that dilepton transverse momenta are of the order of 1 GeV/c or more. It is not clear, in any given event, how to apportion this transverse momentum between the parent quark and antiquark intrinsic transverse momenta, and the dynamics of the production process. In any event the alignment axis of the virtual photon becomes uncertain by an angle of order p_t/p_ℓ. Several choices of the reference axis in the rest frame of the dilepton pair have been employed in attempts to minimize this problem. These are the u-channel, the t-channel, and Collins-Soper (1977) choices. The u-channel choice has the polar axis pointing opposite to the incident target nucleon direction, and the t-channel choice has the polar axis along the incident beam particle direction. If the transverse momenta were all contributed by the beam (target) quark, then the u-channel (t-channel) choice would be appropriate. Collins and Soper take a direction midway in angle between the

u- and t-channel polar axes as the polar axis. Then if the two parent partons contribute equally, on the average, to the transverse momentum, the Collins-Soper choice would minimize the distortion of the decay angular distribution.

5.4.1 *Measurements of the decay angular distribution*

Several groups have measured the decay angular distribution for dileptons, and have fitted their data by an expression of the form:

$$dN/d\theta = 1 + \alpha \cos^2 \theta \ . \qquad (5.10)$$

Results from three experiments are given in figure 17 (Kourkoumelis *et al* 1980, Antreasyan *et al* 1980, and Badier *et al* 1980a). This illustrates the lack of data in the regions close to cos θ equal to + or -1, which are the regions most sensitive to variations in α. If cos θ is close to (±) unity in a fixed-target experiment, one or other of the leptons is travelling backward in the c.m. frame and hence is at low momentum in the laboratory. The slow muon stops in the thick absorber and the data are lost. At the CERN ISR, the beam pipe and equipment cut out some of the forward angular range.

Table 6 gives a summary of measurements of the parameter α, with an indication of the choice of reference axis in each case. Within the quite substantial errors, the global data are all consistent with the simple Drell-Yan prediction that α should equal unity.

5.5 Transverse momentum distributions

According to the Drell-Yan model, the transverse momentum of the dileptons should just be the vector sum of the intrinsic transverse momenta of the annihilating quark-antiquark pair. It should therefore be possible to estimate the magnitude from the transverse momentum of

hadrons produced in strong interactions. Secondary hadrons have transverse momentum distributions that are exponentially falling with increasing p_t and have mean values of around 0.35 GeV/c for c.m. energies up to 60 GeV (Albrow *et al* 1978). Intrinsic transverse momentum distributions can also be obtained by taking the Fourier transform of the charge distribution of hadrons measured in elastic scattering. This is in accord with a mean transverse momentum ($\langle p_t \rangle$) of 0.35 GeV/c for secondary hadrons.

Dilepton transverse momentum distributions do fall off exponentially with increasing p_t, as for example in figure 6. However, the mean is larger than expected and increases with dilepton mass in the data shown. Figure 18 shows a compilation of the variation of $\langle p_t \rangle$ with mass for a) proton-produced and b) π-meson produced dileptons at similar incident momenta. The measurements displayed come from experiments by the CFS Collaboration (Ito *et al* 1981) and the CIP Collaboration (Anderson *et al* 1979a) with protons, and by the NA3 Collaboration with π mesons. This figure shows two main features: i) that $\langle p_t \rangle$ value for π^--produced dileptons is consistently larger in the plateau region by about 0.2 GeV/c. It should be borne in mind that as $\sqrt{\tau}$ increases to the kinematic limit of unity, the value of $\langle p_t \rangle$ must ultimately decline from the plateau value to zero. As the c.m. energy increases so does the plateau value of $\langle p_t \rangle$. This is illustrated in figure 19, where measurements by the CFS Collaboration are compared with measurements at higher c.m. energies at the ISR presented by Angelis *et al* (1979b), Becker (1979), and Antreasyan *et al* (1981a).

The Omega Collaboration have presented plots of the variation of $\langle p_t \rangle$ with $\sqrt{s}$ (or s) at a fixed value of the scaling variable $\sqrt{\tau}$

(Corden *et al* 1981). Figure 20a shows the variation of $\langle p_t \rangle$ with $\sqrt{s}$ at $\sqrt{\tau}$ of 0.22 for proton-produced dileptons. The dependence is close to linear and has been fitted with the form:

$$\langle p_t \rangle = 0.45 + 0.025 \sqrt{s} \ . \tag{5.11}$$

A similar plot is shown in figure 20b for π^--meson production at $\sqrt{\tau}$ of 0.28. This plot shows the variation of $\langle p_t^2 \rangle$ against s to accommodate available data. A fit of a linear form gives the result:

$$\langle p_t^2 \rangle = 0.59 + 0.0029 \ s \ . \tag{5.12}$$

A similar fit to the $\langle p_t \rangle$ distribution gives

$$\langle p_t \rangle = 0.54 + 0.029 \sqrt{s} \ . \tag{5.13}$$

The fitted lines for π^--meson and proton production are nearly parallel with the proton line lying lower.

Transverse momentum distributions of dileptons are thus very much at odds with what is expected in the Drell-Yan model. Mean transverse momenta are altogether too large and increase linearly with c.m. energy. The value of $\langle p_t \rangle$ at low c.m. energies is compatible within errors with the intrinsic transverse momentum contributed by the quark-antiquark pair, namely $\sqrt{2} \times 0.35 \approx 0.49$ GeV/c.

5.6 Summary

The Drell-Yan process provides, in general, an adequate explanation of high-mass continuum lepton pair production by hadrons. The scaling of cross-sections, the linear A dependence of cross-sections, and the $(1 + \cos^2 \theta)$ decay angular distribution are all clearly confirmed. Cross-section dependence on the quark structure of the beam hadron has also been demonstrated, although at this point we have not considered

how experimentalists have extracted hadron structure functions. Where the model fails is in its inability to predict the observed large transverse momenta of dilepton pairs. This failure has a straightforward explanation when the necessary QCD corrections are made to the model. It is this topic that we consider next.

6. THE DRELL-YAN PROCESS IN QCD

6.1 The prediction of the total cross-section

The failure of the simple Drell-Yan model to predict the substantial transverse momenta of dileptons comes about because the model neglects the interaction between partons making up each hadron. Quantum chromodynamics has emerged as the only viable model for these interactions, and it is in the framework of QCD that the Drell-Yan model needs to be modified. The emission of a hard (large energy) gluon by a quark provides the immediate mechanism by which a quark can obtain a transverse momentum kick. We turn now to calculations in QCD of the Drell-Yan total cross-section and later to the differential cross-section in transverse momentum.

The calculations have been mainly confined to consideration of the first-order processes shown in figure 21, where there is at most one hard gluon involved. This amounts to taking the first term in the perturbation expansion. At large four-momentum squared this is justifiable because the quark-gluon coupling constant can be expressed as

$$\alpha_s(q^2) = 12\pi/\left[(33-2f)\ \ln\ (q^2/\Lambda^2)\right] ,$$

where f is the number of quark flavours and Λ ($\sim$ 200 MeV/c) sets the scale of the interactions. With $\sqrt{q^2}$ set to the value of typical dimuon masses, the value of α_s is small (of order 0.1) so that a perturbation expansion is not unreasonable.

The diagrams of figure 21 include the basic Drell-Yan diagram 21a and a vertex correction diagram 21b. Figures 21c and 21d involve gluon emission, and together with figure 21b are called annihilation diagrams. Figures 21e and 21f show a quark from one hadron scattering off a gluon

from the other hadron; these are the Compton diagrams, so named by analogy with the similar electromagnetic process. The amplitudes for the annihilation and Compton diagrams are copies of the QED amplitudes with colour factors added (Baer and Khoze 1965, Altarelli *et al* 1978). They suffer from two sorts of divergences, one of which is already met and solved in QED. This latter is the divergence in the cross-section when the photon energy falls to zero (soft photon). Bloch and Nordsieck (1937) solved the problem in electromagnetism by focusing attention on the physical indistinguishability of states with arbitrary numbers of soft photons that are undetected by the measuring apparatus. Cross-sections for physically indistinguishable states are finite, because the divergences arising from one or more soft photons in the final state cancel with divergences from having one or more soft photons exchanged as in figure 21b. A similar cancellation occurs in QCD. Beyond this there is a second type of divergence of importance in QCD related to the fact that both quark and gluon are massless. A single quark with energy E can be replaced by a quark plus collinear gluon with total energy E, and there an infinite number of such replacements. Cross-sections diverge when all equivalent collinear final states are summed over.

Politzer (1977) noted that the same collinear divergences are present in field theory calculations of deep-inelastic scattering and of lepton pair production. In each case the quarks interacting with the virtual photon can radiate soft and/or collinear gluons. He therefore proposed that the divergences could be safely absorbed into the structure functions. This idea was shown to work by Sachrajda (1978) in the so-called leading log approximation (LLA). A leading log approximation

for a hard process is made by writing amplitudes for emitting any number of collinear gluons and retaining only those pieces where each extra power of α_s for an additional gluon emission is accompanied by an extra logarithm $\log (q^2/\Lambda^2)$, arising from the divergence. Because of the way α_s depends on $\log (q^2/\Lambda^2)$, these selected terms are the dominant ones by a factor of at least α_s and would spoil the perturbation series if they were not taken account of completely.

According to this result the naïve Drell-Yan formula for cross-section should still apply, provided the quark distributions used have been measured at the corresponding value of $|q^2|$ in deep-inelastic lepton scattering. The only implication is the simple one that scaling violations discovered in the deep-inelastic scattering experiments should carry over into the Drell-Yan process. We should now replace the scaling formulae of subsection 5.1 by new expressions with explicit mass dependence; for example, equation (5.3) becomes

$$M^3(d\sigma/dM) = G(\tau, \ln M^2) \ . \tag{6.1}$$

Calculations in QCD for the Drell-Yan cross-section have been carried beyond the LLA by Altarelli, Ellis and Martinelli (1979) and by Kubar *et al* (1979). These authors made explicit calculations using the diagrams of figure 21, whilst allowing for the development of the parton distributions with q^2 according to the first-order Altarelli-Parisi equations. They found that the next-to-leading log correction was large. The inclusion of the first-order annihilation diagrams gives the major effect, which has the approximate form:

$$\sigma \approx \sigma_{\text{naïve}}\left[1 + (\alpha_s/2\pi)(4/3)(1 + 4\pi^2/3)\right] \ . \tag{6.2}$$

On the other hand, the Compton diagrams give a small negative correction. Over all, at current energies the prediction obtained is

$$\sigma \approx K \cdot \sigma_{naïve} \ , \tag{6.3}$$

where K is close to 2 and is constant over the kinematic range $0.02 < < \tau < 0.7$. This seems to show that the perturbation expansion fails. However examination shows that the main part of the difference comes from a change in available phase space for the vertex correction graph (figure 21b) between the positive q^2 (Drell-Yan) and negative q^2 (deep-inelastic scattering) cases. Recently, Khalafi (1982) has shown that this result is not sensitive to the choice of regularization scheme adopted. Higher-order corrections involve formidable calculations and have yet to be completed. By analogy with QED, Curci and Greco (1980) argue that the K factor ought to exponentiate when all orders are summed; that is to say,

$$K \to \exp\left[(\alpha_s/2\pi)(4\pi^2/3)\right] . \tag{6.4}$$

If this were to be the case then K is expected to change only very little from its current estimate. A very convenient summary of relevant formulae for QCD corrections to the Drell-Yan process has been collected by Ellis (1981), and the reader is referred to this article for further details.

6.2 The measurement of the K factor

The ideal test of the QCD prediction for the Drell-Yan cross-section is to study dilepton production in $\bar{p}p$ interactions. Then the structure functions are identical and have been measured in deep-inelastic lepton-proton scattering. What is more, the main contribution comes from annihilation of a valence quark in the proton on a valence

antiquark in the antiproton, and only requires knowledge of the well-measured valence structure function. Badier *et al* (1980b) have presented results based on 275 dileptons with masses greater than 4.1 GeV/c^2 produced by a 150 GeV/c $\bar{p}$ beam on a Pt target. Using 35 p events collected with comparable luminosity, the authors form the difference between the antiproton and proton cross-sections from which all sea-quark contributions cancel. This difference can be derived from equation (3.8) and including the K factor. To good precision:

$$d^2\sigma/dx_1dx_2(\bar{p}p) = (4\pi\alpha^2)/(81x_1x_2)Kf(x_1)g(x_2) \ . \qquad (6.5)$$

Here

$$f(x_1)/9 = (4/9)u(x_1) + (1/9)d(x_1)$$

is the antiproton valence-quark distribution weighted by the quark charges squared. The target Pt nucleus has Z/A of 0.4, and the valence distribution is:

$$g(x_2) = 0.4\ u(x_2) + 0.6\ d(x_2) \ .$$

Badier *et al* extracted $f(x_1)$ from their data by parametrizing $g(x_2)$ with the form obtained in deep-inelastic neutrino scattering by the CERN-Dortmund-Heidelberg-Saclay (CDHS) Collaboration (Turlay 1979). The result was then compared with the prediction of $f(x_1)$ expected from the CDHS parametrization. This comparison is shown in figure 22 with K equal to 2.3. By reversing the procedure and assuming $f(x_1)$, the parameter $g(x_2)$ was extracted and this gives similar good agreement to the CDHS parametrization for K equal to 2.3. Badier *et al* conclude that the simple Drell-Yan formula requires a normalization factor 2.3 ± 0.40 which is essentially constant over the kinematic range explored: $0.25 \leq x_1 \leq 1.0$ and $0.15 \leq x_2 \leq 0.45$.

Determinations of the K factor from data on dilepton production by proton beams alone have been performed by Badier *et al* (1979b), Ito *et al* (1981), and Smith *et al* (1981) in fixed-target experiments. Dilepton production in proton-nucleus collisions involves sea antiquarks annihilating on valence or sea quarks. Each of the three groups have extracted the sea-quark distribution from their data by using the valence-quark distribution for nucleons measured in deep-inelastic lepton scattering experiments. Their results are then compared to determinations of the sea-quark structure functions measured in deep-inelastic neutrino scattering experiments. Each group finds consistency in this comparison provided the Drell-Yan cross-section is raised by a factor of around 2. The comparison made by Ito *et al* (1981) for $\bar{u} + \bar{d} + 2\bar{s}$ is shown later in figure 26. The neutrino data come from de Groot *et al* (1979) and Benvenuti *et al* (1979). Antreasyan *et al* (1981b) have also measured the K factor for dilepton production at the CERN ISR in pp collisions at 44 and 62 GeV c.m. energy; they find $K = 1.6 \pm 0.2$ for the fit shown in figure 11.

The high statistics data on massive dilepton production by π-meson beams have been used by the NA3 (Badier *et al* 1979b) and Omega Collaborations (Corden *et al* 1980a) to test the normalization of the Drell-Yan cross-section. Because the π-meson structure functions have not been measured by any other method, the results are less secure. The NA3 Collaboration proceeded by making a fit to the measured differential cross-section $d^2\sigma/dMdx$, allowing the K factor and the meson and nucleon structure functions to vary. Normalization was imposed on the valence structure functions through the requirement that there are only two valence u quarks in the proton, and so on:

$$\int [u(x) - \bar{u}(x)]\, dx = 2 \quad \text{proton}$$
$$\int [u(x) - \bar{u}(x)]\, dx = 1 \quad \pi^+ \text{ meson}$$
$$\int [d(x) - \bar{d}(x)]\, dx = 1 \quad \text{proton}$$
$$\int [\bar{d}(x) - d(x)]\, dx = 1 \quad \pi^+ \text{ meson} .$$

There are corresponding isospin-rotated expressions for the neutron and π^- meson. Other constraints imposed were that around half the nucleon momentum be carried by the quarks (see section 2.4),

$$\int \sum [q(x) + \bar{q}(x)]x\, dx \simeq 0.50 ,$$

and that the strange sea be given by:

$$\bar{s} = 1/4(\bar{u} + \bar{d}) .$$

Within these general restrictions NA3 used parametrizations suggested by Buras and Gaemers (1978) for the quark distributions and described above in subsection 2.4.1. With data obtained with π^- and π^+ meson beams at 200 GeV/c, the nucleon structure functions are consistent with those measured in deep-inelastic lepton scattering, and the measured cross-section is found to be too large by a factor of around 2.4. The Omega Collaboration obtain a value for K close to 2.5. One refinement is to fit only the difference between π^-- and π^+-produced cross-sections so as to exclude any hadronic background. The Omega Collaboration find 2.22 ± 0.24 in this case for the K factor, giving the fits shown in figure 4. The NA3 Collaboration obtain a K factor of 2.4 ± 0.4 using the difference method. Further details about the meson structure functions extracted in these and other experiments are given in section 7.2.

The measurements of the factor by which the experimental dilepton cross-sections exceed the simple Drell-Yan formulae are summarized in

table 7. Agreement between experiments and with the K factor predicted in QCD by Altarelli *et al* (1979) and Kubar *et al* (1979) is very good. How far this agreement will be affected by calculations carried to higher orders remains to be seen. Curci and Greco (1980) point out that whilst the present calculation of the K factor shows little variation with τ in the kinematic region so far investigated, it is expected that above τ of 0.7 the K factor should rise rapidly. It would clearly be of major importance to investigate this region experimentally.

6.3 More on the transverse momentum distributions

The transverse momentum, p_t, distribution of dileptons is a first-order effect in QCD. There are few other places where such first-order effects are accessible, notably the broadening of jets in e^+e^- annihilations and in leptoproduction, or the study of high-p_t photons from hadron collisions. Measurements in the case of dilepton production are simpler and the interpretation is also simpler.

Some difficulties arise in QCD calculations of p_t distributions because of the existence of two energy variables, namely p_t and the dilepton mass M. Only when both are large compared with the QCD energy scale set by Λ is it reasonable to expect the simple perturbation expansion to apply. Calculations of this sort have been made by many authors (Altarelli *et al* 1978, Kajantie and Raitio 1978, Fritzsch and Minkowski 1978). They used the annihilation and Compton diagrams shown in figure 21.

Scott (1981) points out how the observed linear dependence of $\langle p_t^2 \rangle$ on s may be inferred for first-order QCD. The cross-sections for the annihilation and Compton diagrams at low p_t behave like

$$d\sigma/dp_t^2 \sim 1/p_t^2$$

and are proportional to α_s. To obtain $\langle p_t^2 \rangle$ the cross-section is weighted by p_t^2 and integrated over phase space. This gives (ignoring log s):

$$\langle p_t^2 \rangle \simeq \alpha_s(M^2)\, s\, f(\tau, \ln M^2) \ , \tag{6.6}$$

where f will depend on the parton densities. Dimensional arguments lead to the same expression for $\langle p_t^2 \rangle$. As p_t tends to zero, the cross-sections for the parton processes diverge as shown in figure 23 for example. This problem is compounded by not knowing the initial transverse momentum distribution of the quarks in hadrons. Altarelli *et al* (1978) invented a prescription to take these problems into account and give an acceptable cross-section. They define a regularized cross-section:

$$\sigma_R(M^2,\tau,p_t^2) = \sigma_0(M^2,\tau) f(p_t^2) + (1/\pi) \int d^2\vec{k}_t \sigma_{QCD}(M^2,\tau,2k_t/\sqrt{s}) \times \{f[(p_t-k_t)^2] - f(p_t^2)\} \ , \tag{6.7}$$

where σ_0 is the naïve Drell-Yan cross-section, and σ_{QCD} is the QCD differential cross-section valid at large p_t; $f(p_t^2)$ is a function chosen to reproduce the quark intrinsic transverse momentum distribution inside a hadron normalized to unity:

$$\int dp_t^2\, f(p_t^2) = 1 \ .$$

This prescription has two appropriate features: a) at large p_t the cross-section σ_R reduces to the QCD form σ_{QCD} and b) the cross-section integrated over p_t^2 gives back σ_0. For simplicity f was chosen to be a Gaussian:

$$f(p_t^2) = A \exp(-Ap_t^2) \ ,$$

so that

$$\langle p_t^2 \rangle = A^{-1} \ .$$

Fits to data obtained at the ISR by Antreasyan *et al* (1981b) are shown in figure 23. At large p_t the fit is testing QCD predictions in a favourable kinematic region and things appear to go well. The important process in this region is Compton scattering. At small p_t it is the intrinsic transverse momentum that is responsible for the fit. This is equivalent to absorbing the collinear soft divergences into the structure functions in a calculation of the total Drell-Yan cross-section. The intrinsic r.m.s. transverse momentum required by the fit is 0.48 GeV/c.

The procedure of Altarelli *et al* leads to the generalization of equation (6.6):

$$\langle p_t^2 \rangle = \alpha_s(M^2)\, s\, f(\tau, \ln M^2) + \langle k_t^2 \rangle \ . \qquad (6.8)$$

This then implies the linear dependence of $\langle p_t \rangle$ on $\sqrt{s}$ observed at constant τ and shown in figure 20a and b. The interpretation of the constant term as the contribution of intrinsic quark transverse momentum appears reasonable. The value of 0.48 GeV/c found by fitting the transverse momentum distribution for proton-produced dileptons at the ISR is remarkably close to the value obtained for the fit shown in figure 20a, whilst both values are compatible with the naïve estimate of $\sqrt{2} \times 0.35$ GeV/c.

One caveat that should be borne in mind about the quality of the QCD fits at large p_t is that there is an uncertainty as to whether p_t or M ought to be used in calculating α_s. With p_t of about 3 GeV/c and M of 6 GeV this leads to an uncertainty of 30% in normalization.

Calculations valid at intermediate values of p_t have been made by Dokshitzer *et al* (1978) using the LLA. Their results have been improved by Parisi and Petronzio (1979) by working in impact parameter space. Halzen and Scott (1980) have shown that the agreement with proton-produced data is good in the range of validity of the approximation ($\Lambda^2 << p_t^2 << M^2$).

The data on transverse-momentum distributions of π-meson-produced dileptons provide an important further test on QCD. In contrast with the case of production by protons, the hard annihilation diagrams of QCD are important at large p_t. Figure 20b shows that $\langle p_t^2 \rangle$ depends linearly on s for dileptons produced by π mesons, and the intrinsic $\langle k_t^2 \rangle$ is not very different from the value found for proton production. Different versions of the QCD calculation have varying degrees of success in fitting the p_t distributions at all energies.

Calculations following the prescription of Altarelli *et al* (1978) give cross-sections low by a factor of 2. The reason for this discrepancy seems to be that second-order corrections are important and of the right order to correct the disagreement (Ellis *et al* 1981). However, a rather large value [order 1 $(GeV/c)^2$] is found for the intrinsic $\langle k_t^2 \rangle$ due to the quarks so the matter is not fully resolved. An alternative approach has been made by Chiapetta and Greco (1981), who explicitly include the dominant contributions to the transverse momentum distribution: i) an intrinsic contribution due to motion of the parent quark and antiquark; ii) a contribution from hard first-order processes, and iii) a sum of contributions from soft-gluon emission made in a way similar to that of Petronzio and Parisi. It is also necessary for the authors to include an explicit K factor of 1.8, which is in substantial agreement with other determinations. Excellent fits are obtained to both transverse momentum

distributions and $\langle p_t^2 \rangle$ variation with s for both π-meson and proton-produced dileptons. Figures 24 and 25 show the fits to data from the NA3 Collaboration for π-meson-produced dileptons; $\langle k_t^2 \rangle$ is then found to have an acceptable small value, around 0.4 $(GeV/c)^2$.

Although good agreement is obtained with much data, the calculations of p_t distributions remain phenomenological. We might ask why this should be the case when calculations of the total cross-section permit a clear test of QCD. In both cases the same hard QCD processes are at work, giving rise to finite transverse momenta and boosting the total cross-section. The answer seems to lie in the concentration at low transverse momenta, dictated by the infrared divergences, which merges into the region of intrinsic k_t. Only when more detailed data become available at transverse momenta much larger than k_t will this situation improve.

6.4 *QCD effects on the decay angular distribution*

Lam and Tung (1978) have shown that if dileptons are produced via a single virtual photon then the general expression for the decay angular distribution has the general form:

$$dN/d\Omega = (3/16\pi)\left[(1 + \cos^2\theta)\, W_t + (1 - \cos^2\theta)\, W_\ell + W_\Delta \sin 2\theta \cos\phi + W_{\Delta\Delta} \sin^2\theta \cos 2\phi\right] . \qquad (6.9)$$

The W functions are analogous to structure functions measured in deep-inelastic scattering: they are not themselves invariants but are linear sums of products of invariant functions and kinematic factors. For this reason these helicity structure functions depend on the choice of axes made in the dilepton rest frame. W_t and W_ℓ are the structure functions for transverse and linearly polarized photons; W_Δ and $W_{\Delta\Delta}$ are the

structure functions for spin flip and double-spin flip. The kinematic factors determine that W_Δ and $W_{\Delta\Delta}$ vanish when the quark and antiquark momenta are collinear, whilst for small p_t

$$W_\Delta \sim p_t/M \tag{6.10}$$

and

$$W_{\Delta\Delta} \sim (p_t/M)^2 \ . \tag{6.11}$$

A more stringent requirement which only depends on the spin ½ nature of quarks and applies in all choices of frame is that

$$W_\ell = 2W_{\Delta\Delta} \ . \tag{6.12}$$

This relation is the equivalent of the Callan-Gross relation (Callan and Gross 1969) of deep-inelastic lepton scattering. Then at small enough p_t equation (6.9) reduces to

$$dN/d\Omega \sim (1 + \cos^2\theta) + A \sin^2\theta + B \sin 2\theta \cos\phi + C \sin^2\theta \cos 2\phi \ , \tag{6.13}$$

where

$$A/2 = C$$

and both B and C are functions of p_t/M only.

Collins (1979) considered the effect of QCD corrections on these general predictions. He showed that if gluon emission is the dominant correction in first order to the naïve Drell-Yan process, rather than gluon Compton scattering, then the relation between W_ℓ and $W_{\Delta\Delta}$ is not affected. This would be the case for π-meson- and $\bar{p}$-produced dileptons but not for proton production. His explicit calculation gives in this case:

$$C = (p_t^2/2)/(M^2 + p_t^2) \ .$$

Collins offers a mechanism to suppress Compton scattering contributions at large transverse momentum. There is a minimum centre-of-mass energy necessary for production of a dilepton of mass M and transverse momentum p_t, namely $p_t + \sqrt{(M^2 + p_t^2)}$. This implies that the Bjorken x-values of the partons involved must be relatively large. Collins argues that this inhibits Compton scattering because the gluons have x distributions falling more steeply with increasing x than have valence quarks. Lam and Tung (1978) reach a similar conclusion that the relation between W_ℓ and $W_{\Delta\Delta}$ is insensitive to first-order QCD corrections. It is important to realize that the change of rate by a factor of 2 does not lead to a significant change in the over-all angular distribution; when integrated over ϕ the angular distribution $(1 + \cos^2 \theta)$ of the naïve Drell-Yan process is recovered.

Recently, Michelini (1981) has reported on a detailed study of the angular distributions of π^--produced dileptons by the NA3 Collaboration. They have fitted their data using equation (6.13) in the u-channel, t-channel, and Collins-Soper frames. In the u-channel frame they find for the coefficients,

$$B \approx 0 , \quad C \approx 1.4 \, (p_t/M)^2$$
$$\text{or } C \approx 0.4 \, (p_t/M) ,$$

and consistency with $A \simeq 2C$. Within substantial errors the data are consistent with the expectation of QCD. The smallness of B in the u-channel frame argues that the nucleon direction is a good estimator of the quark-antiquark axis. Michelini points out that this would support the contention that most of the transverse momentum of the dilepton is associated with the quark (or antiquark) coming from the π meson.

Berger and Brodsky (1979) and Berger (1980) have made estimates of the effect of so-called higher-twist operators on the Drell-Yan process. The simplest of the higher-twist processes are those that involve a pair of partons from one parent hadron interacting with a single parton from the other hadron. Berger and Brodsky conclude that decay angular distributions would be sensitive to such processes and that there would be a strong dependence of such effects on the Bjorken x-values of the parent quarks and on p_t/M. Explicitly the angular distribution would be expected to have the form

$$dN/d\Omega \propto (1 - x_1)^2(1 + \cos^2\theta) + H(p_t/M)\sin 2\theta \cos\phi + H^2(p_t/M)\sin^2\theta \ . \qquad (6.14)$$

Anderson *et al* (1979b) reported evidence of a change in the decay angular distribution from $(1 + \cos^2\theta)$ at low x_1 to $(1 - \cos^2\theta)$ at x_1 close to unity for π-meson-produced dileptons. However, other experiments (Michelini 1981, Corden *et al* 1980a) see less evidence of any such effect. It remains true that the region close to unity in x_1 should be where the higher-twist effects can become significant.

6.5 Summary

The study of high-mass continuum dileptons offers fundamental tests of QCD. It is remarkable that such large first-order effects of QCD are manifest in this one process. Large transverse momenta are an immediate consequence of first-order QCD diagrams in which hard-gluon emission or Compton scattering occur. The observed linear dependence of $\langle p_t^2 \rangle$ on s is expected in QCD. In addition, the explicit QCD calculations of the transverse momentum distributions give agreement with experiment.

The predicted rescaling of the cross-section by a factor of 2 has been observed in a number of experiments now, and we await definitive word from the theorists that high-order corrections do not spoil this excellent agreement. Underlying this result is something very fundamental: that is, that factorization works even outside the range of negative q^2 where it can be proved using the Wilson operator product expansion. The implication is that factorization is likely to work elsewhere in hard processes calculable with QCD.

7. THE MEASUREMENT OF STRUCTURE FUNCTIONS

Expressions have been given in section 3.3 for the naïve Drell-Yan cross-section. It appears from what has been learnt about QCD corrections that these scale up cross-sections by a factor which is constant over the kinematic region explored experimentally. In this view it is possible to take the expressions of section 3.4 and use them to extract structure functions from measured differential cross-sections for dilepton production. Nucleon structure functions measured in deep-inelastic lepton scattering experiments provide both an input and a test for the Drell-Yan analysis.

7.1 The nucleon structure function

Mention has already been made in section 6.2 of the measurement of the nucleon valence-quark distribution by Badier *et al* (1980b). They made a subtraction of the proton from $\bar{p}$-produced dilepton differential cross-sections giving equation (6.5):

$$d^2\sigma/dx_1dx_2 = (4\pi\alpha^2/81x_1x_2s)Kf(x_1)g(x_2) \ ,$$

where $f(x_1)$ and $g(x_2)$ are the charge-weighted antiproton and target valence-quark distributions, respectively. By using the value of $f(x_1)$ measured in deep-inelastic lepton scattering, $g(x_2)$ can be extracted from the data and vice versa. Figure 22 shows the results, which compare well with the input forms found in deep-inelastic lepton scattering experiments.

The CFS Collaboration were able to extract information on the nucleon quark distributions from 300 and 400 GeV proton-produced data. Figure 8 shows the acceptance in phase space. Because of the rapid decline of the dilepton cross-section with increasing τ, the experiment

is sensitive mainly to the quark and antiquark distributions at low values of Bjorken x. Consequently attention is concentrated on measuring the antiquark (sea) distribution. Ito *et al* (1981) fitted their differential dimuon production cross-section with the equation (3.9). As input on the quark distribution, these authors used the q^2-dependent fit by Gordon *et al* (1979) to deep-inelastic scattering measurements of $F_2(x,q^2)$. In deep-inelastic lepton scattering q^2 has negative values so that it was necessary to take q^2 equal to $-M^2$, where M is the dilepton pair mass. Parametrizations of the sea quarks and antiquarks were chosen to be

$$x\bar{d}(x) = A(1-x)^b \qquad (7.1)$$

$$x\bar{u}(x) = A(1-x)^{b+d} \qquad (7.2)$$

$$x\bar{s}(x) = (\bar{u}+\bar{d})/4 \ . \qquad (7.3)$$

Field and Feynman (1977) have suggested that predominance of valence u quarks in the proton should lead to some suppression of u quarks in the sea through the action of the Pauli principle. The results of QCD calculations by Ross and Sachrajda (1979) support the idea.

The fits made by Ito *et al* (1981) are conspicuously better if d is allowed to vary. A χ^2 of 211 for 156 degrees of freedom was achieved in a fit with the final parameters:

$$A = 0.548 \pm 0.17 \ ,$$

$$b = 7.62 \pm 0.38 \ ,$$

and

$$d = 3.48 \pm 1.2 \ .$$

A further step was made in order to extract the sea-quark distributions in a manner less sensitive to the parametrization of equations (7.1) to

(7.3). Results of these two approaches are compared in figure 26 with results of neutrino scattering experiments (de Groot *et al* 1979, Benvenuti *et al* 1979) for the combination $x(\bar{u}+\bar{d}+2\bar{s})$. The solid curve corresponds to the parametrization fit result. In terms of shape, the quark distributions measured by the two types of experiment agree moderately well: there is also a factor of 2 difference in scale, which can be identified with the QCD enhancement of the Drell-Yan cross-section (K factor).

Another high-intensity proton beam experiment at FNAL (Smith *et al* 1981) has also determined the nucleon sea-quark distribution from dimuon differential production cross-sections. The mass acceptance of this experiment extends to 15 GeV/c^2, and the range of x explored is much larger (0.18 to 0.58) than for the CFS experiment. In a similar style of fit, they fix the parameter d to be 2.5 and have A, b, and the K factor as free parameters. Their fitted values are

$$A = 0.5 \pm 0.03 ,$$

$$b = 7.4 \pm 0.4$$

and

$$K = 1.6 \pm 0.3 .$$

These results agree substantially with the CFS determination of the nucleon sea.

The NA3 experiment has better acceptance in phase space, and has collected 960 dimuons with masses above 4.2 GeV/c^2 using a 200 GeV/c proton beam. These data were used to extract the valence-quark distribution (Badier *et al* 1979b). A fit was made to the differential cross-sections using equation (3.8). The parametrizations chosen for the

valence- and sea-quark distributions in the proton were:

$$xu_v(x) = A_u x^a (1-x)^b \tag{7.4}$$

$$xd_v(x) = A_d x^a (1-x)^{b+1} \tag{7.5}$$

$$xq_s(x) = A_s (1-x)^c \ , \tag{7.6}$$

with

$$q_s = u_s = \bar{u}_s = d_s = \bar{d}_s = 2s_s = 2\bar{s}_s \ .$$

Normalization of the valence-quark distributions was fixed by the requirement that the proton contains one valence d-quark and two valence u-quarks. Normalization of the sea-quark distribution was chosen to make the integral momentum carried by all quarks equal to half the proton momentum. Fits to the data made with naïve Drell-Yan formula and a free K factor give the results listed in table 3. For comparison, corresponding results from the neutrino scattering experiment of de Groot *et al* (1979) are also given in table 3. There is over-all good agreement between the results of the two methods and the expectations based on the quark counting rules of subsection 2.4.1.

Judged against deep-inelastic scattering results, the determination of nucleon quark and antiquark distributions from continuum dilepton production data seems quite reliable. This observation is the basis for confidence that the same technique should be able to extract quark distributions for mesons when applied to data on dilepton production by meson beams.

7.2 The meson structure functions

A lot of data are available on dilepton production by π^- mesons; because, firstly, negative secondary beams consist mostly of π^- mesons, and secondly the π^- meson contains a valence $\bar{u}$-quark available for

annihilation on the valence u-quarks in nucleons. The Drell-Yan formula involves, in this case, the convolution of meson and nucleon structure functions, so that by making use of measured values of the latter it is possible to extract the former from experimental data. This kind of analysis has provided almost all the information we possess on the meson structure function. It is not too much to say that the measurement of massive dilepton production cross-sections is the unique, reliable experimental means for studying the internal structure of the mesons.

Figure 5 shows that the dileptons produced by π mesons have a harder spectrum than those produced by protons. This confirms our prejudice that the valence quark and antiquark in the π^- meson should each carry more momentum than their counterparts in a nucleon. The data taken by the CIP Collaboration with 225 GeV/c π^- mesons incident on a tungsten target were used by them (Newman *et al* 1979) to make a first determination of a meson structure function. The parameter x_F is limited to positive values by the acceptance of the apparatus, which means that only those meson quarks with Bjorken x-values above 0.25 contribute. Effectively the meson sea-quarks are excluded so that the Drell-Yan formula (3.8) reduces to

$$d^2\sigma/dx_1dx_2 = (4\pi\alpha^2/9x_1x_2s) \times \left[(4/9)v_\pi(x_1)g_n(x_2) + (1/9)s_\pi(x_1)h_n(x_2)\right] . \qquad (7.7)$$

Here v_π and s_π specify the valence- and sea-quark distributions in the π meson, respectively; g_n and h_n are the appropriate combinations of sea- and valence-quark distributions for the nucleon. The authors simplified this to

$$d^2\sigma/dx_1dx_2 = (4\pi\alpha^2/9x_1x_2s)v_\pi(x_1)g_n(x_2) \ . \qquad (7.8)$$

A fit was made to the data with v_π of the form:

$$xv_\pi(x) = A\sqrt{x}\ (1-x)^b \ ,$$

and the results are given in table 8. The parameter b has the value 1.27 ± 0.06, quite close to the value (1) given in equation (2.7) by the quark counting rules. The fraction of the meson momentum carried by the valence quarks is 0.4 ± 0.1, which is not dissimilar to the baryon case.

Refinements of this early measurement of the π-meson structure function have been made by experiments with wider acceptance and larger data samples. The experiments of the NA3 and Omega Collaborations have good acceptance down to x_F of -0.3 and -0.5, respectively, so that Bjorken x-values down to zero come into play for the meson quark. With their improved sensitivity these groups can determine both the powers of x and 1-x in the valence-quark distribution. Having more data the NA3 Collaboration (Badier *et al* 1980c) were also able to make an estimate of the meson sea. Both groups made simultaneous fits to dilepton production cross-sections for π^- and π^+ mesons. As input the nucleon quark distributions measured in deep-inelastic neutrino scattering (de Groot *et al* 1979) were employed. The forms fitted to the meson quark distributions were:

$$xv_\pi(x) = Ax^a(1-x)^b$$
$$xs_\pi(x) = B(1-x)^c \ .$$

Table 8 presents the results found for the fitted parameters by the two experiments. Also included for completeness are results obtained by Barate *et al* (1979) from a smaller event sample from an experiment

using the Goliath spectrometer at CERN. There is good general agreement between the experiments.

Badier *et al* also extracted the meson structure function by a projection method. Expression (7.7) can be integrated over x_2 and rearranged to give

$$F_\pi(x_1) \equiv dN/dx_1/\left[(4\pi\alpha^2/9s)(L/x_1^2)I(x_1)\right]$$
$$= K\left[v_\pi(x_1) + J(x_1)s_\pi(x_1)/I(x_1)\right] x_1 \ . \qquad (7.9)$$

In the equation, I and J are integrals over G and H folded with the experimental acceptance $A(x_1,x_2)$:

$$I(x_1) = \int g(x_2)A(x_1,x_2)\ dx_2/x_2 \ ,$$
$$J(x_1) = \int h(x_2)A(x_1,x_2)\ dx_2/x_2 \ .$$

The target was platinum with Z/A equal to 0.4, so that for $\bar{\pi}$-meson beams

$$g = (1/9)(1.6u + 2.4d + 5s_n) \ ,$$

while

$$h = (1/9)(2.2u + 2.8d + 11s_n) \ .$$

Finally, L is the integrated luminosity of the exposure and K is the QCD K factor. The structure function $F_\pi(x_1)$ was projected out from the cross-section $d\sigma/dx_1$ using the integral $I(x_1)$ evaluated with the nucleon quark distributions found in deep-inelastic lepton scattering (de Groot *et al* 1979). The curves in figure 27 indicate the quantity $F_\pi(x_1)$ evaluated from the results of the fits.

Referring back to table 3, we see that the pion valence- and sea-quark distributions are much flatter than for the nucleons. This reflects the fact that there are few valence quarks in mesons. The

powers of x and (1-x) correspond very well to the values suggested from quark counting rules [equations (2.7) and (2.8)]. It appears that the fraction of meson momentum carried by all quarks plus antiquarks is around 60%, which is similar to the case for nucleons.

A small number of dimuon pairs produced by K^- mesons have been collected by the Omega and NA3 Collaborations using unseparated beams with individual beam particle identification. In an early publication (Corden *et al* 1978) the Omega Collaboration showed that the rate for dilepton production by K^- mesons was similar to that for π^- mesons. This argues that the structure functions of the two species are quite similar. More recently the NA3 Collaboration collected 700 dimuon pairs with masses above 4 GeV/c^2 produced by 150 GeV/c K^- mesons (Badier *et al* 1980d). These authors compare K^--induced cross-sections and π^--induced cross-sections to yield the ratio

$$R(x) = \bar{u}_k(x)/\bar{u}_\pi(x) \ .$$

The ratio R is fitted well by the form

$$R(x) = (1-x)^{0.18\pm0.07} \ ,$$

which indicates that the valence-quark distributions in K^- and π^- mesons are very similar. If confirmed, the more rapid fall of $\bar{u}_k(x)$ with x would be readily comprehensible. The $\bar{u}$-antiquark in the K meson is lighter than the s-quark so that it would carry a lower momentum, and hence a lower momentum than the $\bar{u}$-antiquark in the π^- meson.

8. STUDIES OF HADRONS ACCOMPANYING DILEPTON PRODUCTION

Limited studies of hadrons accompanying dilepton production have been made by Antreasyan *et al* (1981c) working at the CERN ISR and by the Goliath Collaboration (Pietrzyk 1981, Pietrzyk *et al* 1982). For such studies an open spectrometer arrangement is essential. Antreasyan *et al* find the multiplicity of associated hadrons is large for the available energy compared to typical hadronic events but similar to that seen in e^+e^- annihilations. This indicates that dilepton production is highly inelastic, as expected in the Drell-Yan model. The multiplicity also appears to increase slowly with the dilepton transverse momentum.

Data from the Goliath Collaboration are less easy to interpret because it involves π^--meson interactions on a nuclear target. In order to eliminate nuclear effects amongst the hadrons, only particles emerging in the forward hemisphere were retained for analysis. Viewed simplistically these forward hadrons are decay products of the initial d-quark from the incident π^- meson. The integrated charge of the forward hadrons is found to be -0.32 for Drell-Yan events, -0.52 for ψ production and -0.62 in standard hadronic events. These results are quite consistent with the charge flows expected in these different types of reaction.

9. SUMMARY AND CONCLUSIONS

The experimental study of the continuum high-mass dilepton production from hadron-hadron collisions reveals substantial agreement with the model of Drell and Yan (1970a, 1971), with certain significant exceptions. First, the model accounts for the extremely rapid fall of the cross-section with increasing dilepton mass and predicts constancy of such quantities as $M^3 d\sigma/dM$ at fixed τ. This scaling property has been confirmed for proton-produced dimuons by Yoh *et al* (1978) and Antreasyan *et al* (1981a), and for π-meson produced dimuons by Badier *et al* (1980a) and by Corden *et al* (1980a). A near-linear dependence of the cross-section on the target atomic number has been demonstrated by Ito *et al* (1981), Badier *et al* (1981a) and by Falciano *et al* (1981). This confirms the electromagnetic nature of the process. Also, the decay angular distribution fits the $1 + \cos^2 \theta$ form expected for a virtual photon decay [Hogan *et al* (1979b), Badier *et al* (1979d), and Kourkoumelis *et al* (1980)]. Finally, the very large differences between the production cross-sections for different beam species have been observed in several experiments [Branson *et al* (1977), Corden *et al* (1978 and 1980a), and Hogan *et al* (1979b)].

The simple Drell-Yan model gives no explanation for the large transverse momenta of the dileptons. According to the model, the dilepton transverse momentum should be the vector sum of the transverse momenta of the annihilating quark and antiquark. This is expected to be of the same order as the transverse momenta of secondary hadrons produced in hadron-hadron collision or 350 MeV/c. In fact the transverse momenta measured, for example, by Yoh *et al* (1978) and Branson *et al* (1977) are considerably larger. Angelis *et al* (1979a), Becker

et al (1979), and Antreasyan *et al* (1981a) have shown that the mean transverse momentum increases rapidly with c.m. energy.

Quantum chromodynamics appears to explain these large transverse momenta. Emission of a hard gluon, and hard-gluon Compton scattering shown in figure 21, are first-order processes which occur at a rate down by only a factor α_s relative to the simple Drell-Yan process. These processes were shown by Altarelli *et al* (1978), by Dokshitzer *et al* (1978), and by others, to provide an acceptable mean transverse momentum distribution.

A second significant departure of the data from the simple Drell-Yan model prediction concerns the cross-section. This anomaly, too, receives an explanation in QCD. Careful measurements by Badier *et al* (1980a) and by Corden *et al* (1980a) showed that the cross-section for dilepton production by proton-antiproton or π-meson beams was a factor of 2 higher than expected. The explanation is connected with the inclusion of the QCD diagrams of figure 21 in the calculation of cross-section, and with the question of factorization. Calculations by Altarelli *et al* (1979) and by Kubar *et al* (1979) show that the cross-section is increased by a factor (K factor) close to 2 compared with the simple Drell-Yan prediction over most of the kinematic range. If higher-order corrections do not upset this agreement, then again QCD has scored a striking success.

Measurements of the dilepton production with proton and antiproton beams have been analysed to determine the nucleon structure functions. Excellent agreement was obtained with previous determinations made in deep-inelastic lepton scattering experiments [Ito *et al* (1981) and Badier *et al* (1979b)]. Using data on dilepton production by π- and

K-meson beams, it was possible to determine the π- and K-meson structure functions for the first time. Deep-inelastic scattering of leptons from unstable mesons is, of course, not feasible. Determinations of the π-meson structure function have been made by Newman *et al* (1979), Badier *et al* (1980c), Corden *et al* (1980a), and Barate *et al* (1979), while comparisons between the π-meson and K-meson structure functions have been initiated by Badier *et al* (1980c) and by Corden *et al* (1980a). The structure functions for mesons seem to be very close to the simple quark counting-rule estimates.

The Drell-Yan process by its conceptual and experimental simplicity has proved to be an ideal area for testing and applying the ideas of the parton model and of QCD. In the K factor and the transverse momentum distributions we have two simple, large, quantitative effects by which QCD predictions differ from the parton model. If the higher-order corrections to the QCD predictions do not significantly mar the present accord between theory and experiment in this area, then the Drell-Yan process will have provided fundamental tests of QCD. This result would have the added bonus that it implies that factorization should work as well in other hard QCD processes. Beyond this the Drell-Yan process has provided, for the first time, a way to determine the meson structure functions. For the moment it remains the only direct means.

Acknowledgements

I would like to thank my colleagues at Birmingham for the stimulation they have provided, and particularly Professor J.D. Dowell and Dr. M.J. Corden who read and commented on the final draft. My thanks also go to Dr. R.K. Ellis for his generous guidance over the delicate area of the QCD calculations. Finally, I should like to thank the extremely efficient staff of the Scientific Reports Typing Service and Drawing Offices at CERN for their cheerful help.

APPENDIX ON FUTURE PROSPECTS

In view of the importance of the K factor, it is desirable that higher-order calculations be completed and that the crucial $\bar{p}p$ production be measured at high statistics. It will also be important to measure the K factor into the region above τ of 0.7, where it is expected to rise quickly. An FNAL experiment (ES37) is planned, which will study this (Cox 1981) with a novel negative beam at 125 GeV/c with 25% antiproton content. It will be interesting to look for scaling violations but the prospective range of q^2 is not large. This is because the Drell-Yan cross-section is expected to be swamped by background processes from heavy-flavour decays at high energies (Strauss 1981, Pakvasa *et al* 1979). At high energies, too, the production of dileptons via photon-photon interactions will become significant (Moore 1980). Progress is to be expected in the refinement of measurement of meson structure functions in the high-intensity experiments at CERN (NA10) and FNAL (E326). In the E615 experiment it is also planned to explore production close to x_F of 1 (Peoples 1981). This will be valuable in searching for any higher-twist effects (Berger and Brodsky 1979, Berger 1980).

Single direct photon production can occur via the QCD processes drawn in figures 21c to f. At very high energies their study is not sensitive to the backgrounds mentioned for the Drell-Yan process. There are different experimental problems so we may expect complementary results from studying the two mechanisms.

REFERENCES

Abolins M A *et al* 1979 *Phys. Lett.* 82B 145

Albrow M G *et al* 1978 *Nucl. Phys.* B135 461

Altarelli G and Parisi G 1977 *Nucl. Phys.* B126 298

Altarelli G, Parisi G and Petronzio R 1978 *Phys. Lett.* 76B 351 and 356

Altarelli G, Ellis R K and Martinelli G 1979 *Nucl. Phys.* B157 461

Anderson K J *et al* 1976a *Phys. Rev. Lett.* 36 237

——————— 1976b *Phys. Rev. Lett.* 37 799

——————— 1979a *Phys. Rev. Lett.* 42 944

——————— 1979b *Phys. Rev. Lett.* 43 1219

Angelis A L S *et al* 1979a *Phys. Lett.* 87B 398

——————— 1979b Paper contributed to the Int. Symp. on Lepton and Photon Interactions at High Energies, Batavia, Illinois

Antreasyan D *et al* 1980 *Phys. Rev. Lett.* 45 863

——————— 1981a *Phys. Rev. Lett.* 47 12

——————— 1981b MTI Lab. for Nucl. Sci. Tech. Report 119

——————— 1981c CERN-EP/81-116

Aubert J J *et al* 1974 *Phys. Rev. Lett.* 33 1404

Augustin J-E *et al* 1974 *Phys. Rev. Lett.* 33 1406

Badier *et al* 1979a *Phys. Lett.* 86B 98

——————— 1979b *Phys. Lett.* 89B 145

——————— 1979c preprint CERN-EP/79-67

——————— 1979d preprint CERN-EP/79-68

——————— 1980a preprint CERN-EP/80-36

——————— 1980b preprint CERN-EP/80-147

——————— 1980c preprint CERN-EP/80-148

——————— 1980d *Phys. Lett.* 93B 354

Badier *et al* 1981a preprint CERN-EP/81-63

———————— 1981b *Phys. Lett.* 104B 335

Baer V N and Khoze V A 1965 *Sov. Phys.-JETP* 21 629

Barate R *et al* 1979 *Phys. Rev. Lett.* 43 1541

Becker U *et al* 1979 *Proc. EPS Int. Conf. on High-Energy Physics*, Geneva, vol 2 (Geneva: CERN) p 779

Benvenuti A *et al* 1979 *Phys. Rev. Lett.* 42 1317

Berger E 1980 *Z. Phys.* C4 289

Berger E and Brodsky S J 1979 *Phys. Rev. Lett.* 42 440

Bjorken D J 1969 *Phys. Rev.* 179 1547

Bjorken D J and Paschos E A 1969 *Phys. Rev.* 185 1975

———————————— 1970 *Phys. Rev. D* 1 3151

Bloch F and Nordsieck A 1937 *Phys. Rev.* 52 54

Bodek A *et al* 1980 *Phys. Rev. D* 20 1471

Bosetti P C *et al* 1978 *Nucl. Phys.* B142 1

Branson J G *et al* 1977 *Phys. Rev. Lett.* 38 457, 580, 1330 and 1334

Breidenbach M *et al* 1969 *Phys. Rev. Lett.* 23 930

Brodsky S J and Farrar G R 1973 *Phys. Rev. Lett.* 31 1153

Buras A J and Gaemers K J F 1978 *Nucl. Phys.* B132 249

Callan G and Gross D J 1969 *Phys. Rev. Lett.* 22 156

Chiapetta P and Greco M 1981 CNRS report CPT 81/P.1307 (Marseille)

Christenson *et al* 1970 *Phys. Rev. Lett.* 25 1523

Cobb J H *et al* 1977 *Nucl. Instrum. Methods* 140 413

———————— 1979 *Nucl. Instrum. Methods* 158 93

Collins J C 1979 *Phys. Rev. Lett.* 42 291

Collins J C and Soper D E 1977 *Phys. Rev. D* 16 2219

Corden M J *et al* 1978 *Phys. Lett.* 76B 226

Corden M J *et al* 1980a *Phys. Lett.* 96B 417

———————— 1980b *Phys. Lett.* 96B 411

———————— 1981 *Proc. EPS Int. Conf. on High-Energy Physics*, Lisbon (in preparation)

Cox B 1981 Private communication

Curci G and Greco M 1980 *Phys. Lett.* 92B 175

de Groot J G H *et al* 1979 *Z. Phys.* C1 143

Dokshitzer Y L, D'yakonov D I and Troyan S I 1978 *Phys. Lett.* 79B 269

Drell S and Yan T M 1970a *Phys. Rev. Lett.* 25 316

———————— 1970b *Phys. Rev. Lett.* 24 181

———————— 1971 *Ann. Phys. (USA)* 66 578

Drees J 1981 *Proc. Int. Symp. on Lepton and Photon Interactions at High Energies*, Bonn (Bonn, the University), p 474

Ellis R K 1981 *Proc. Moriond Workshop on Lepton Pair Production*, Les Arcs (Dreux, France: Editions Frontières), vol 2, p 19

Ellis R K, Martinelli G and Petronzio R 1981 CERN report TH.3079

Falciano S *et al* 1981 preprint CERN-EP/81-52

Farrar G R 1974 *Nucl. Phys.* B77 429

Feynman R P 1969 *Phys. Rev. Lett.* 23 1415

Field R D and Feynman R P 1977 *Phys. Rev. D* 15 2590

Freudenreich K 1981 *Proc. Moriond Workshop on Lepton Pair Production*, Les Arcs (Dreux, France: Editions Frontières), vol 2, p 206

Fritzsch H and Minkowski P 1978 *Phys. Lett.* 73B 80

Frisch N J *et al* 1982 Fermilab/Chicago/Princeton preprint DOE-ER/03072-2

Gell-Mann M 1964 *Phys. Lett.* 8 214

Gordon B A *et al* 1979 *Phys. Rev. D* 20 2645

Greenberg O W 1964 *Phys. Rev. Lett.* 13 598

Gross D J and Wilczek 1973 *Phys. Rev. Lett.* 30 1343

Halzen F and Scott D M 1980 *Phys. Rev. D* 21 131

Herb S W *et al* 1977 *Phys. Rev. Lett.* 39 252

Hogan G E *et al* 1979a *Nucl. Instrum. Methods* 165 7

——————— 1979b *Phys. Rev. Lett.* 42 948

Innes W R *et al* 1977 *Phys. Rev. Lett.* 39 1240

Ito A S *et al* 1981 *Phys. Rev. D* 23 604

Kajantie K and Raitio R 1978 *Nucl. Phys.* B139 72

Khalafi F 1982 University of Cambridge report DAMTP 82/2

Kogut J and Susskind L 1974 *Phys. Rev. D* 9 697

Kourkoumelis C *et al* 1980 *Phys. Lett.* 91B 475

Kubar J, Le Bellac M, Meunier J L and Plaut G 1979 *Nucl. Phys.* B175 251

Lam C S and Tung W-K 1978 *Phys. Rev. D* 21 2712

Larue G S, Phillips J D and Fairbank W M 1981 *Phys. Rev. Lett.* 46 967

Lederman L 1982 Private communication

Lefrançois L 1980 *Proc. Int. Conf. on High-Energy Physics*, Madison (New York: AIP Conf. Proc. No. 68) p 1319

Matthiae G 1981 *Riv. del Nuovo Cim.* vol 4 No 3

McCal D *et al* 1979 *Phys. Lett.* 85B 432

Michelini A 1981 preprint CERN-EP/81-128

Moore R 1980 *Z. Phys.* C5 351

Newman C B *et al* 1979 *Phys. Rev. Lett.* 42 951

Pakvasa S, Dechantsreiter M, Halzen F and Scott D M 1979 *Phys. Rev. D* 20 2862

Parisi G and Petronzio R 1979 *Nucl. Phys.* B154 427

Peoples J 1981 Private communication

Pietrzyk B 1981 *Proc. Moriond Workshop on Lepton Pair Production*, Les Arcs (Dreux, France: Editions Frontières) vol 2, p 149

Pietrzyk B *et al* 1982 preprint CERN-EP/82-19

Politzer H D 1973 *Phys. Rev. Lett.* 30 1346

———————— 1977 *Nucl. Phys.* B129 301

Ross D A and Sachrajda C T 1979 *Nucl. Phys.* B149 497

Sachrajda C T 1978 *Phys. Lett.* 73B 185

Scott D M 1981 *Proc. Moriond Workshop on Lepton Pair Production*, Les Arcs (Dreux, France: Editions Frontières) vol 2, p 148

Smith S R *et al* 1981 *Phys. Rev. Lett.* 46 1607

Strauss J 1981 *Proc. Moriond Workshop on Lepton Pair Production*, Les Arcs (Dreux, France: Editions Frontières) vol 2, p 211

Stroynowski R 1981 *Phys. Reports* 71 1

Turlay R 1979 *Proc. EPS Int. Conf. on High-Energy Physics*, Geneva, vol 1 (Geneva: CERN) p 50

West G B 1970 *Phys. Rev. Lett.* 24 1206

Yan T M 1976 *Annu. Rev. Nucl. Sci.* 26 199

Yoh J K *et al* 1978 *Phys. Rev. Lett.* 41 684

Zweig G 1964 CERN report 8419/TH.412

Table 1

Charge +2e/3	u quark	c quark
Charge -e/3	d quark	s quark

Table 2

Proton	uud	antiproton	$\bar{u}\bar{u}\bar{d}$
Neutron	udd		
π^+ meson	$u\bar{d}$	π^- meson	$\bar{u}d$
K^+ meson	$u\bar{s}$	K^- meson	$\bar{u}s$

Table 3

	CDHS neutrino scattering data	NA3 dilepton data	Quark counting rule
a	0.51 ± 0.02	0.5 ± 0.2	0.5
b	2.8 ± 0.1	3.2 ± 0.4	3
c	8.1 ± 0.7	9.4 ± 1.0	7
As	0.27	0.37	
⟨valence⟩	0.34	0.3	
⟨sea⟩	0.15	0.2	

Table 4

Collaboration	Beam (GeV/c)	Mass range (GeV/c^2)	$\sqrt{\tau}$ range	Mass resolution (%)	x_F range
CFS[1]	p: 200, 300, 400	4-18	0.15-0.65	2	-0.1 to +0.4
CIP[2]	$\pi^{\pm}$, p: 150, 225	1.5-8	0.07-0.38	3	> 0.0
NA3[3]	$\pi^{\pm}$, $K^{\pm}$, p, $\bar{p}$: 150, 200, 280	4-8.5	0.20-0.42	4.5	> -0.3
Goliath[4]	π^-: 150, 175	3.8-8.5	0.22-0.5	1.5	> -0.2
Omega[5]	$\pi^{\pm}$, $K^{\pm}$, p, $\bar{p}$: 40	2-5	0.22-0.55	6	> -0.5
NA10[6]	π^-: 280, 200	2-12	0.20-0.5	3	
MNTW[7]	p: 400	1.5-15	0.18-0.58	7.5	$x_F' > 0.2$
ISR experiments	$\sqrt{s}$				
CCOR[8]	62	> 6.5	0.1-0.25	4	-0.2 to 0.2
CHFMNP[9]	44, 62	5-20	0.08-0.32	10	-0.1 to 0.5
ABCS[10]	53, 63	4.5-18	0.07-0.29	4	-0.2 to 0.2

1) Ito *et al* (1981).
2) Anderson *et al* (1976a,b), Hogan *et al* (1979a).
3) Badier *et al* (1979a, 1980a).
4) Abolins *et al* (1979).
5) Corden *et al* (1978, 1980a).
6) Falciano *et al* (1981), Freudenreich (1981).
7) Smith *et al* [Michigan-Northeastern-Tufts-Washington (MNTW) Collab.] (1981).
8) Angelis *et al* (1979a).
9) Antreasyan *et al* (1980, 1981a).
10) Cobb *et al* (1977, 1979), Kourkoumelis *et al* (1980).

Table 4 (contd.)

Collaboration	Targets	Lepton type	Acceptance (%)	Like-sign background (%)	Approximate event sample
CFS	Pt, Cu	μμ, ee	0.5	< 1 (M > 6)	$\sim 10^6$
CIP	Be, Cu, W	μμ	6-30	3	$\sim 2 \times 10^4$
NA3	Pt, H_2	μμ	10-30	< 1 (M > 4)	$\sim 10^5$
Goliath	Be	μμ, ee	-	< 17 (M = 4)	$\sim 4 \times 10^3$
Omega	Cu, W	μμ	1.5-30	< 1 (M > 3)	$\sim 4 \times 10^3$
NA10	C, Cu, W	μμ	-	-	$\sim 10^4$
MNTW	W	μμ	5	< 0.5 (M > 6)	2.5×10^5
CCOR	p	ee	9	20	200
CHFMNP	p	μμ	5	small (M > 8)	4×10^3
ABCS	p	ee	8 (M = 16)	6 (M > 8)	200

Table 5

Group	Beam	Momentum (GeV/c)	Targets	Mass (GeV/c^2)	α	α'
CFS (Ito *et al* 1981)	p	400	Be, Pt	5-11		$1.007 \pm 0.018 \pm 0.028$
CIP (Anderson *et al* 1979a)	π^-	225	C, Cu, W	4-9	1.12 ± 0.05	-
NA3 (Michelini 1981)		280	C, Pt	4-9	-	0.97 ± 0.05
NA10 (Falciano *et al* 1981)		280	C, Cu, W	4-8.4	0.94 ± 0.02	$0.97 \pm 0.02 \pm 0.02$
Frisch *et al* 1982		225	Be, Cu, Sn, W	4-8.5	0.98 ± 0.04	-
NA3 (Michelini 1981)	π^-	200	H_2, Pt	4-9	1.35 ± 0.13	1.02 ± 0.03
	π^+	200			1.13 ± 0.19	0.95 ± 0.04
	$\pi^- - \pi^+$	200			1.60 ± 0.34	1.03 ± 0.05
	π^-	150			1.47 ± 0.07	1.00 ± 0.02
	π^-	280			1.40 ± 0.07	1.00 ± 0.02

Table 6

Group	Beam (GeV/c)	Mass range (GeV/c^2)	p_t range (GeV/c)	Axis	α
CIP (Hogan *et al* 1979b)	π^-: 225	2-2.6	all	c-s	1.14 ± 0.17
	π^-: 225	> 3.5	all	c-s	1.30 ± 0.23
NA3 (Badier *et al* 1980a)	π^-: 200	3.5-9	all	c-s	0.85 ± 0.17
	π^-: 200	3.5-9	all	t	0.80 ± 0.17
ABCS (Kourkoumelis *et al* 1980)	pp: $\sqrt{s}$ = 53, 63	3.5-9	all	u	1.15 ± 0.34
CHFMNP (Antreasyan *et al* 1980)	pp: $\sqrt{s}$ = 63	3.5-9	all	c-s	1.6 ± 0.7
Omega (Corden *et al* 1980a)	$\pi^\pm$: 40	4-5	all	t	0.44 ± 0.48
Goliath (Abolins *et al* 1979)	π^-: 150, 175	3.5-9	all	t	0.52 ± 0.46

Table 7

Group	Beam and target	Momentum/$\sqrt{s}$ (GeV/c)/(GeV)	Measured cross-section / Naïve Drell-Yan prediction
NA3 Badier *et al* 1980b	$(\bar{p}$-p): Pt	150	2.3 ± 0.4
NA3 Badier *et al* 1979b	p: Pt	200	2.2 ± 0.4
CFS Ito *et al* 1981	p: Pt	300/400	$1.7\ ^{+\ 0.73}_{-\ 0.58}$
CHFMNP Antreasyan *et al* 1981b	pp	44, 63	1.6 ± 0.2
MNTW Smith *et al* 1981	p: W	400	1.6 ± 0.3
NA3 Lefrançois 1980	π^-: Pt	200	2.2 ± 0.3
NA3 Lefrançois 1980	π^+: Pt	200	2.4 ± 0.4
NA3 Lefrançois 1980	$(\pi^-$-$\pi^+)$: Pt	200	2.4 ± 0.4
Omega Corden *et al* 1980a	π^-: W	40	2.45 ± 0.42
Omega Corden *et al* 1980a	π^+: W	40	2.52 ± 0.49
Omega Corden *et al* 1980a	$(\pi^-$-$\pi^+)$: W	40	2.22 ± 0.41

Table 8

	CIP (Newman *et al* 1979)	Omega (Corden *et al* 1980a)	Goliath (Barate *et al* 1979)	NA3 (Badier *et al* 1980c)
Momentum (GeV/c)	225 π^-	40 $\pi^\pm$	150, 175 π^-	200 $\pi^\pm$
a	½ (input)	0.44 ± 0.12	½ (input)	0.45 ± 0.1
b	1.27 ± 0.06	0.98 ± 0.15	1.57 ± 0.18	1.04 ± 0.1
b_s	-	-	-	5.4 ± 2.0
⟨valence⟩	0.4 ± 0.1		0.4-0.5	0.35 ± 0.05
⟨sea⟩	-	-	-	0.23 ± 0.15

Figure captions

Fig. 1 : Dimuon spectra for 400 GeV/c protons incident on a Pt target. The solid histogram is the $\mu^+\mu^-$ spectrum; the dotted line shows the like-sign spectrum $\mu^+\mu^+ + \mu^-\mu^-$ (Ito *et al* 1981, Lederman 1982).

Fig. 2 : Feynman diagrams for three processes with a single intermediate photon: a) the Drell-Yan process, b) e^+e^- annihilation to hadrons, and c) deep-inelastic lepton scattering.

Fig. 3 : Schematic plots of the nucleon structure functions obtained from deep-inelastic lepton scattering experiments (de Groot *et al* 1979 and Bodek *et al* 1980): a) the measured structure functions $F_2(x)$ and $xF_3(x)$; b) the separated quark and antiquark structure functions.

Fig. 4 : The differential cross-sections $d\sigma/dM$ versus dimuon mass for $x_F > 0$; a) π^- produced, b) π^+ produced, and c) $(\pi^- - \pi^+)$ difference (Corden *et al* 1980b). The solid curves are calculated for the Drell-Yan process using the structure functions given by Badier *et al* (1980d).

Fig. 5 : The differential cross-sections $E(d\sigma/dx_F)$ (GeV•pb/nucleon) versus x_F: a) π^- produced and b) proton produced. The broken curves show fits made over the region $0.2 < x_F < 1$ and also reflected about $x_F = 0.2$ for (a). Data from Anderson *et al* (1979 a,b) using 225 GeV/c beams on heavy nuclear targets.

Fig. 6 : The differential event distributions dN/dp_t^2 versus p_t^2 for various dimuon mass intervals. Data obtained with 39.5 GeV/c π^- mesons incident on tungsten (Corden *et al* 1981).

Fig. 7 : The upper plot shows the available phase space for the Drell-Yan process: x_1 and x_2 are the Bjorken x-values for the parent quark and antiquark. The lower plot shows how the quark and antiquark distributions in beam and target influence the Drell-Yan cross-section. For the point chosen, x_F is 0.0 and τ is 0.1. $B = xq_B$ and $T = xq_T$.

Fig. 8 : The acceptance of several experiments: a) the Omega Collaboration experiment at CERN using 39.5 GeV/c beams; b) the NA3 experiment at CERN for 200 GeV/c beam energy; c) the CERN ISR experiment of the CHFMNP Collaboration at $\sqrt{s}$ of 62 GeV; and d) the CFS experiment using a two-arm spectrometer at FNAL. For case (d) the acceptance is shown for two of the three beam momenta employed, 200 GeV/c and 400 GeV/c.

Fig. 9 : A horizontal cut of the CERN Omega spectrometer experiment used to study dimuon production with 39.5 GeV/c beams (Corden *et al* 1980b).

Fig. 10 : A scaling test comparing the differential cross-section $s(d^2\sigma/d\sqrt{\tau}\, dy)$ ($y = 0.2$) measured with proton beams of 200, 300, and 400 GeV/c momentum (Yoh *et al* 1978).

Fig. 11 : A scaling test for proton-produced dimuons. The plot compares measurements of the cross-section $M^3(d^2\sigma/dMdx_F)$ ($x_F = 0$) made by Antreasyan *et al* (1981b) at a $\sqrt{s}$ of 44 and 62 GeV with measurements made at $\sqrt{s}$ of 23.8 and 27.4 GeV by the CFS Collaboration (Ito *et al* 1981), plotted as a function of $\sqrt{\tau}$.

Fig. 12 : A scaling test for π^--produced dimuons; $M^3(d\sigma/dM)$ is plotted versus $\sqrt{\tau}$. Data shown were obtained by Corden *et al* (1980a) at 40 GeV/c beam momentum and at 200 and 280 GeV/c by the NA3 Collaboration (Lefrançois 1980).

Fig. 13 : The comparison between the scaling cross-sections $M^3(d\sigma/dM)$ as a function of τ for π^-- and proton-produced dimuons (Corden *et al* 1978). The solid line indicates the results of the CFS Collaboration with 400 GeV/c proton beams.

Fig. 14 : Ratio between a) the π^+-produced and π^--produced dimuon cross-sections versus dimuon mass for $x_F > 0$; b) *idem* for $\bar{p}/\pi^-$; c) *idem* for p/π^-; d) *idem* for K^-/π^-; and e) *idem* for K^+/π^-. The solid curves are the predictions from the naïve Drell-Yan model using structure functions due to Badier *et al* (1979c). The data and curves were given by Corden *et al* (1980a).

Fig. 15 : Measurements of the ratio between π^+- and π^--produced dimuon cross-sections plotted as a function of $\sqrt{\tau}$. Data on heavy nuclear targets come from Hogan *et al* (1979b), Corden *et al* (1980a), and the NA3 Collaboration (Matthiae 1981). Data taken with a hydrogen target by the latter group are

also shown. The asymptotic limits of the ratio are predicted by the simple Drell-Yan model to be 1/4 for an isoscalar target and 1/8 for a hydrogen target.

Fig. 16 : a) The variation of the exponent α for the A dependence of dimuon production by protons plotted versus dimuon mass. The data come from Branson *et al* (1977), Anderson *et al* (1979 a,b), and Ito *et al* (1981).

b) The variation of α with transverse momentum for data obtained by the CFS Collaboration (Ito *et al* 1981).

Fig. 17 : Measurements of the decay angular distribution of lepton pairs by Kourkoumelis *et al* (1980), Antreasyan *et al* (1980) and by Badier *et al* (1980a). Fits to the form $1 + \alpha \cos^2 \theta$ are shown as solid curves and are discussed in the text.

Fig. 18 : The variation of the mean transverse momentum $\langle p_t \rangle$ versus mass for a) proton-produced dimuons and b) π^--produced dimuons. Data come from the CFS Collaboration (Ito *et al* 1981), the CIP Collaboration (Anderson *et al* 1979 a,b), and the NA3 Collaboration (Matthiae 1981). Beam energies are indicated.

Fig. 19 : The variation of mean transverse momentum $\langle p_t \rangle$ versus mass for proton-produced dileptons. Data come from the CFS Collaboration (Ito *et al* 1981) and several ISR experiments at much larger c.m. energy (Angelis *et al* 1979b, Becker *et al* 1979, and Antreasyan *et al* 1981a).

Fig. 20 : a) The variation of mean transverse momentum $\langle p_t \rangle$ for dimuons versus c.m. energy $\sqrt{s}$ at a fixed value of the scaling variable $\sqrt{\tau}$ (0.22). This is a compilation for dimuons produced by proton beams (Corden *et al* 1981) with additional data from Antreasyan *et al* (1981b). A linear least squares fit to the data is shown.

b) The variation of mean transverse momentum squared $\langle p_t^2 \rangle$ for dimuons versus c.m. energy squared s at a fixed values of $\sqrt{\tau}$ (0.28). This compilation was made by Corden *et al* (1981). A linear least squares fit to the data is shown.

Fig. 21 : The Feynman diagram for the naïve Drell-Yan process a) and additional first-order diagrams in QCD: b) the vertex correction diagram; c) and d) involve gluon emission in the final state; e) and f) are 'Compton' diagrams. The legend below each figure gives the interpretation for each line type.

Fig. 22 : The valence structure function $F(x_1)$ for the antiproton beam plotted versus the Bjorken x-value x_1 (Badier *et al* 1980b). The data points are obtained from experiment as described in the text, and the curve shows the corresponding values inferred from deep-inelastic scattering experiments.

Fig. 23 : The differential cross-section $d\sigma/dp_t^2$ is plotted versus the transverse momentum p_t for dimuons with masses in the range 5 to 8 GeV/c^2. The data come from an ISR experiment at c.m. energy 62 GeV (Antreasyan *et al* 1981b). The curves are discussed in the text.

Fig. 24 : Data on the transverse momentum distributions of π^--produced dimuons compared with QCD fits made by Chiapetta and Greco (1981). The differential cross-section $(1/p_t)$ $d^2\sigma/dp_t dM$ versus p_t for various dimuon mass intervals with a 150 GeV/c π^- beam.

Fig. 25 : The variation of mean transverse momentum squared for π^--produced dimuons versus the scaling variable $\sqrt{\tau}$ for π^- beam momenta of 150, 200, and 280 GeV/c. The curves are calculations in QCD made by Chiapetta and Greco (1981).

Fig. 26 : The sea structure function for the nucleon. Measurements made in a dimuon production experiment (Ito *et al* 1981) are shown together with measurements made in two deep-inelastic neutrino scattering experiments.

Fig. 27 : The π^--meson structure function as measured by Badier *et al* (1980c). The full curves show fits discussed in the text, and the broken curves show the valence contribution alone in these fits.

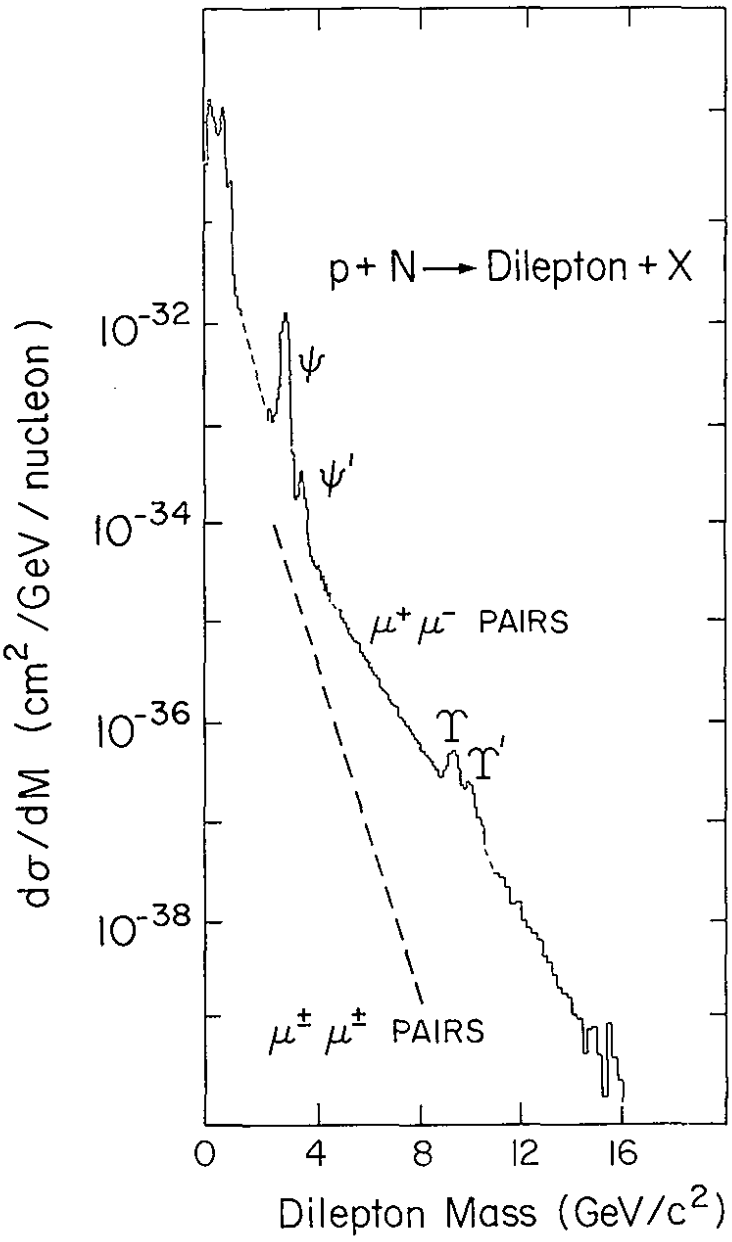
p + N → Dilepton + X
10^{-32}
10^{-34}
10^{-36}
10^{-38}
ψ
ψ'
$\mu^+\mu^-$ PAIRS
Υ
Υ'
$\mu^\pm\mu^\pm$ PAIRS
0
4
8
12
16
dσ/dM (cm²/GeV/nucleon)
Dilepton Mass (GeV/c²)

Fig. 1

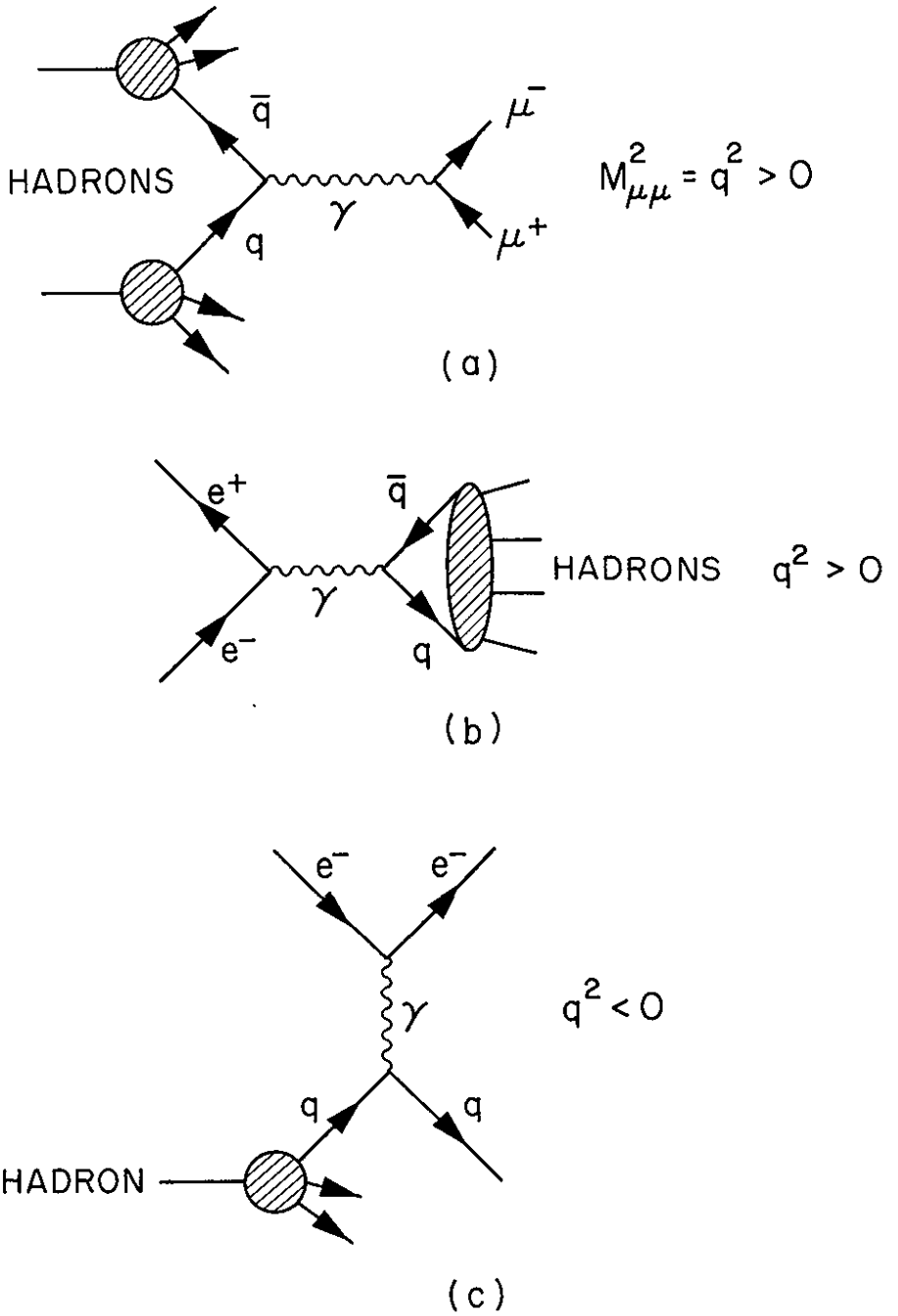
HADRONS
$\bar{q}$
q
γ
μ^-
μ^+
$M^2_{\mu\mu} = q^2 > 0$
(a)
e^+
e^-
$\bar{q}$
q
γ
HADRONS
$q^2 > 0$
(b)
e^-
e^-
γ
q
q
HADRON
$q^2 < 0$
(c)

Fig. 2

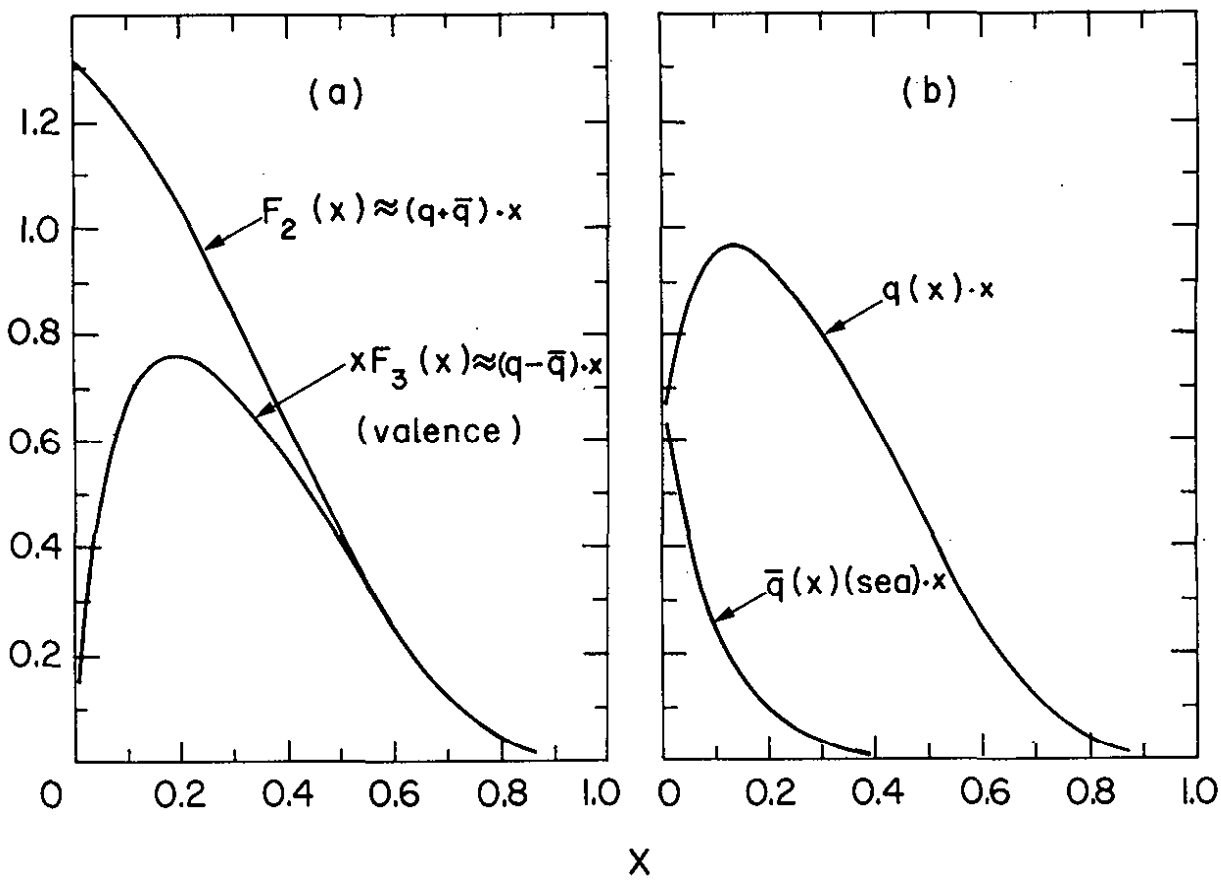
(a)
(b)
$F_2(x) \approx (q+\bar{q})\cdot x$
$xF_3(x) \approx (q-\bar{q})\cdot x$
(valence)
$q(x)\cdot x$
$\bar{q}(x)$(sea)$\cdot x$
1.2
1.0
0.8
0.6
0.4
0.2
0
0.2
0.4
0.6
0.8
1.0
X

Fig. 3

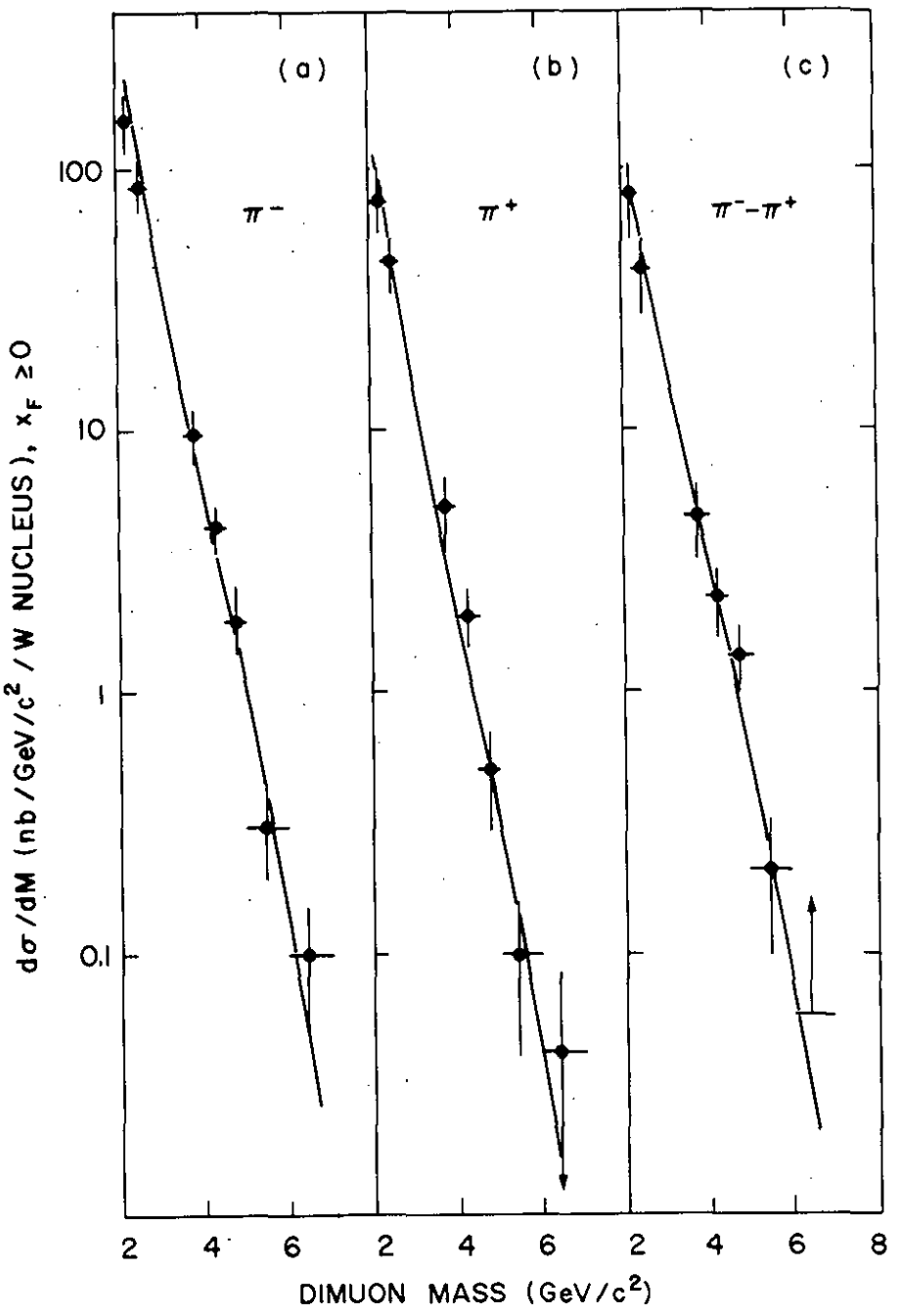
(a)
(b)
(c)
π^-
π^+
$\pi^- - \pi^+$
100
10
1
0.1
$d\sigma/dM$ (nb/GeV/c^2/W NUCLEUS), $x_F \geq 0$
2
4
6
2
4
6
2
4
6
8
DIMUON MASS (GeV/c^2)

Fig. 4

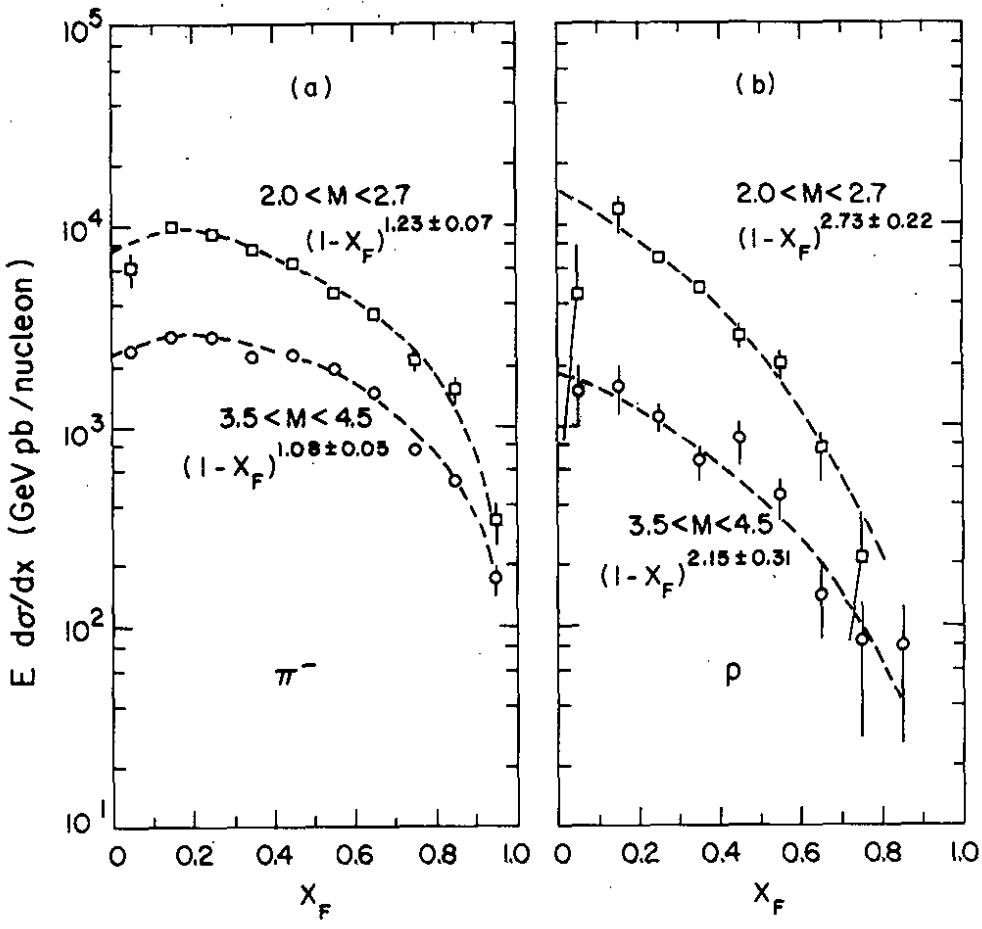
(a)
(b)
2.0 < M < 2.7
$(1-X_F)^{1.23\pm0.07}$
3.5 < M < 4.5
$(1-X_F)^{1.08\pm0.05}$
π^-
2.0 < M < 2.7
$(1-X_F)^{2.73\pm0.22}$
3.5 < M < 4.5
$(1-X_F)^{2.15\pm0.31}$
p
E dσ/dx (GeV pb/nucleon)
X_F
X_F

Fig. 5

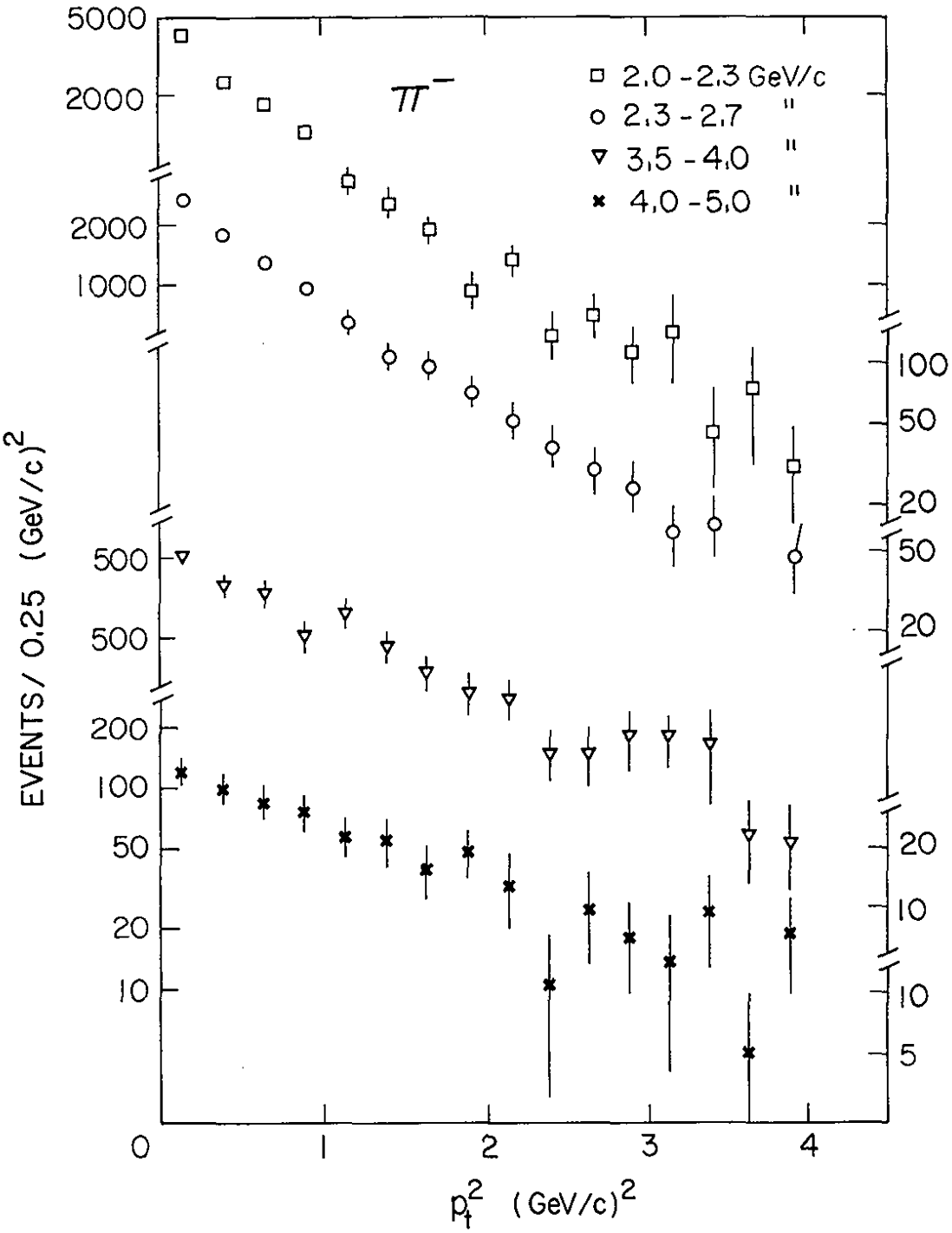
5000
2000
2000
1000
500
500
200
100
50
20
10
0
1
2
3
4
100
50
20
50
20
20
10
10
5
π^-
2.0 - 2.3 GeV/c
2.3 - 2.7 "
3.5 - 4.0 "
4.0 - 5.0 "
EVENTS/ 0.25 (GeV/c)^2
p_t^2 (GeV/c)^2

Fig. 6

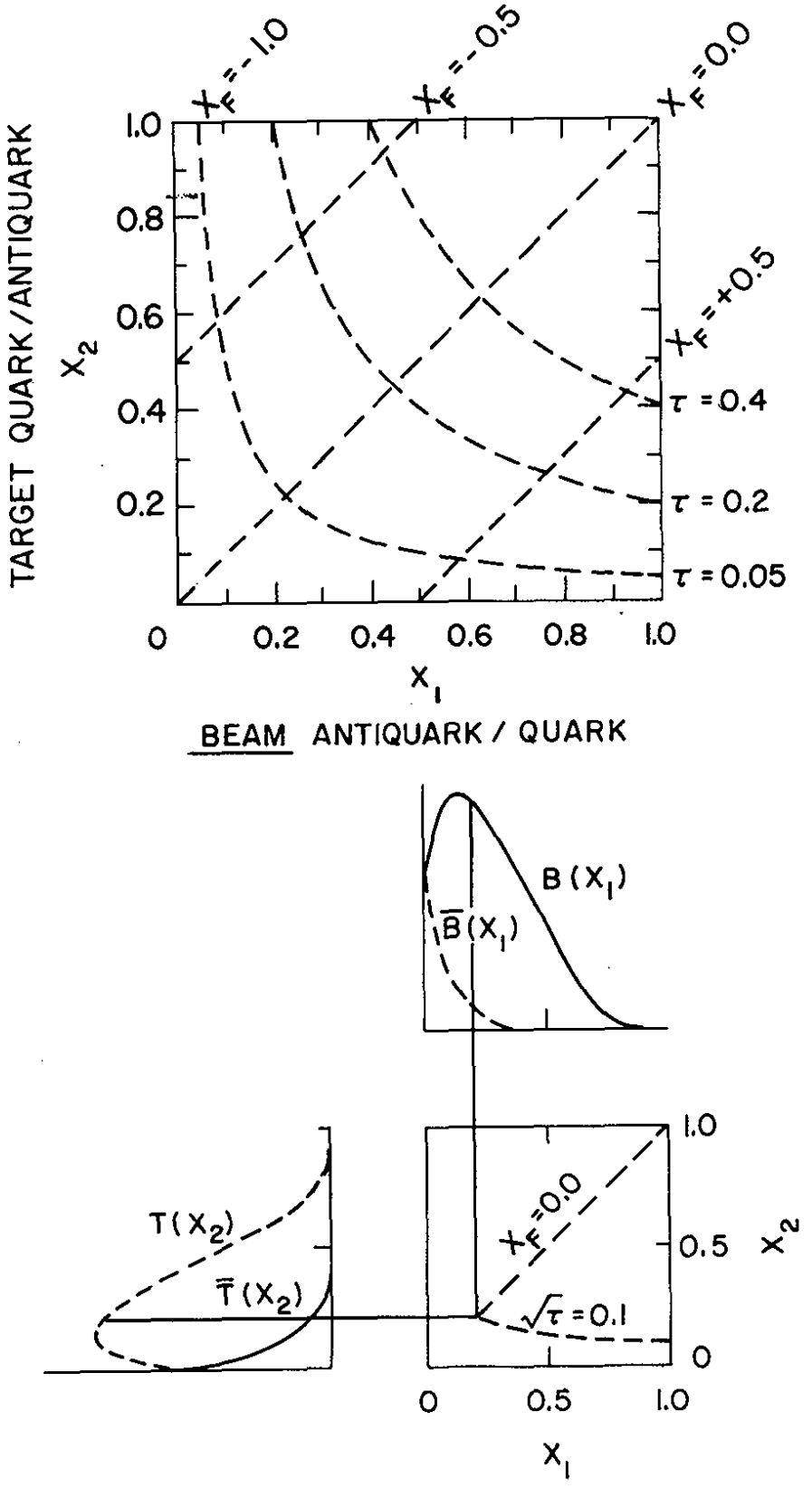
$x_F = -1.0$
$x_F = -0.5$
$x_F = 0.0$
$x_F = +0.5$
$\tau = 0.4$
$\tau = 0.2$
$\tau = 0.05$
TARGET QUARK / ANTIQUARK
x_2
1.0
0.8
0.6
0.4
0.2
0
0.2
0.4
0.6
0.8
1.0
x_1
BEAM ANTIQUARK / QUARK
$B(x_1)$
$\bar{B}(x_1)$
$T(x_2)$
$\bar{T}(x_2)$
$x_F = 0.0$
$\sqrt{\tau} = 0.1$
0.5
0
x_2
x_1

Fig. 7

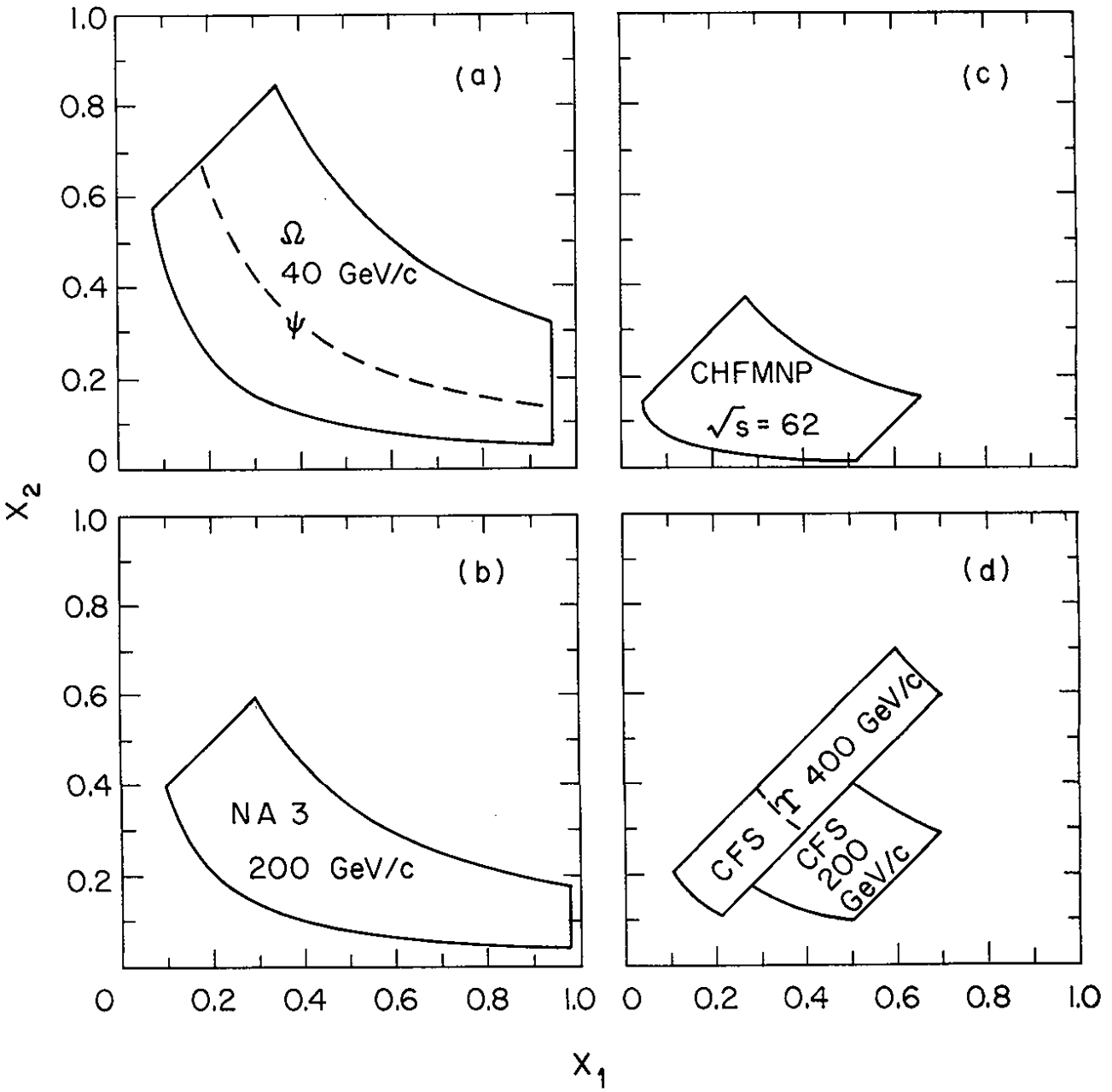
(a)
Ω
40 GeV/c
ψ
(c)
CHFMNP
√s = 62
(b)
NA 3
200 GeV/c
(d)
CFS π 400 GeV/c
CFS 200 GeV/c
X2
X1
0
0.2
0.4
0.6
0.8
1.0

Fig. 8

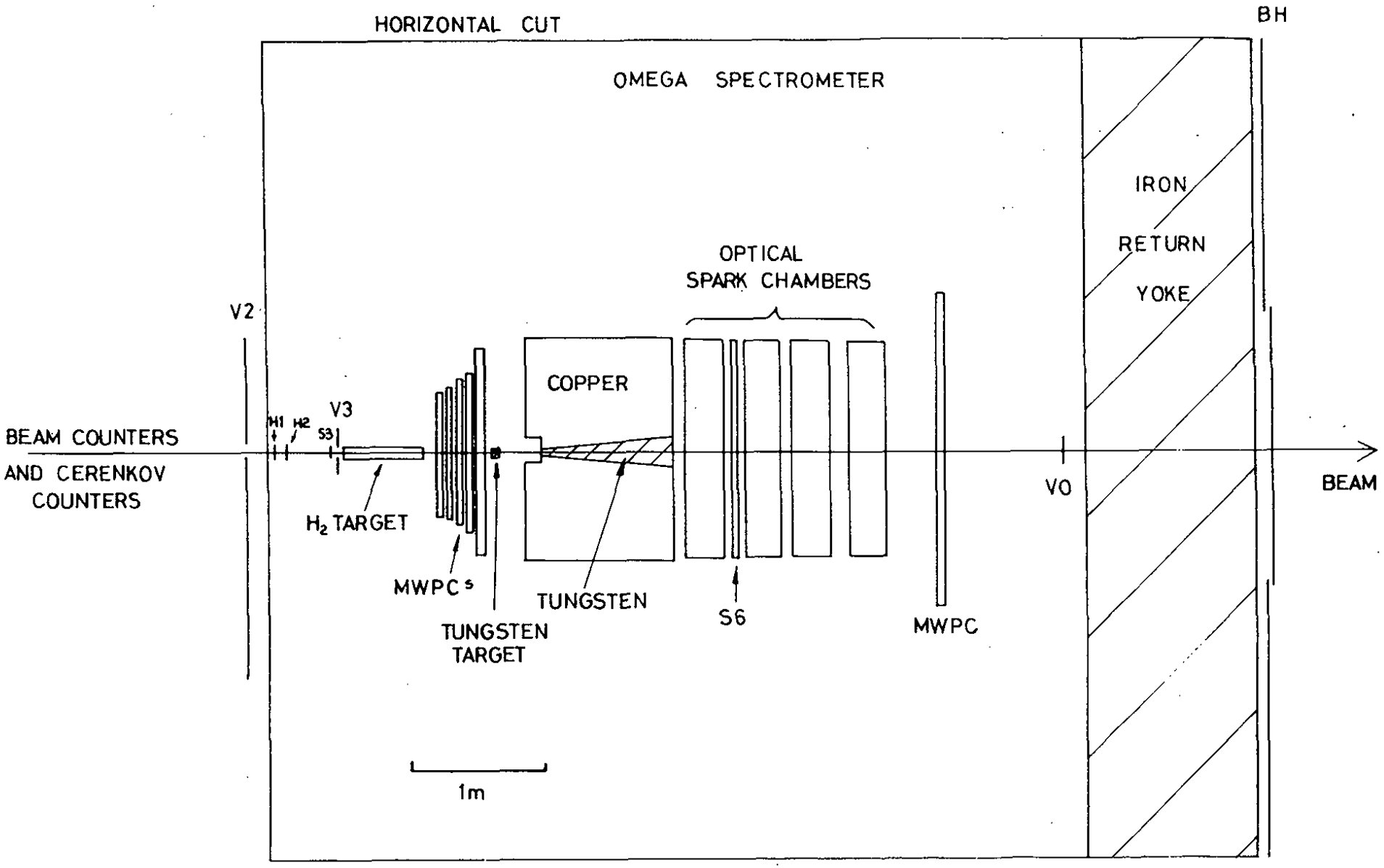
HORIZONTAL CUT
BH
OMEGA SPECTROMETER
IRON
RETURN
YOKE
OPTICAL
SPARK CHAMBERS
V2
COPPER
V3
H1
H2
S3
BEAM COUNTERS
AND CERENKOV
COUNTERS
H_2 TARGET
MWPC s
TUNGSTEN
TUNGSTEN
TARGET
S6
MWPC
V0
BEAM
1m

Fig. 9

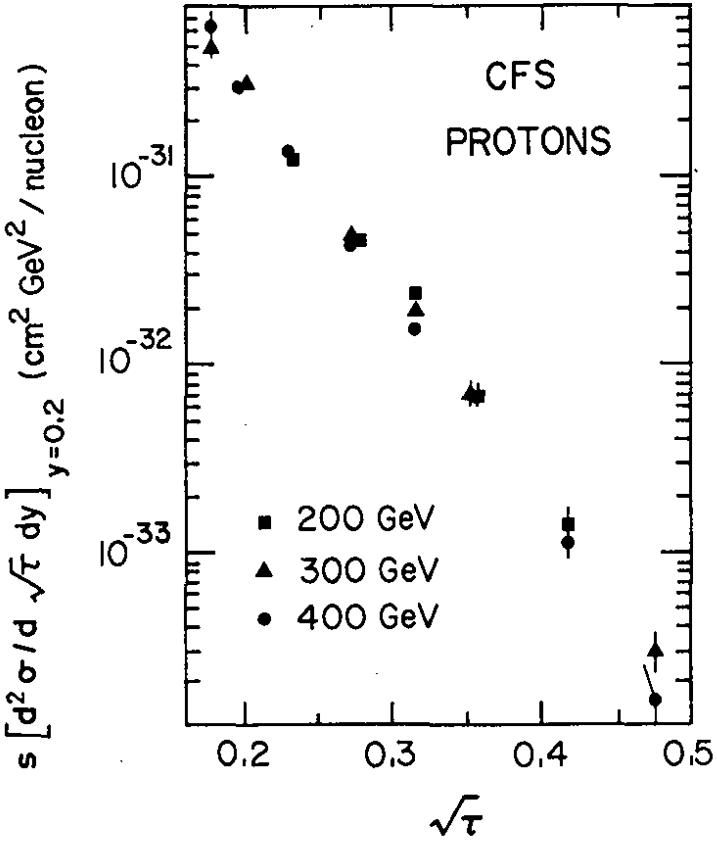
CFS
PROTONS
200 GeV
300 GeV
400 GeV
10^{-31}
10^{-32}
10^{-33}
0.2
0.3
0.4
0.5
$\sqrt{\tau}$
$s\left[d^2\sigma/d\sqrt{\tau}\,dy\right]_{y=0.2}$ (cm^2 GeV^2 / nucleon)

Fig. 10

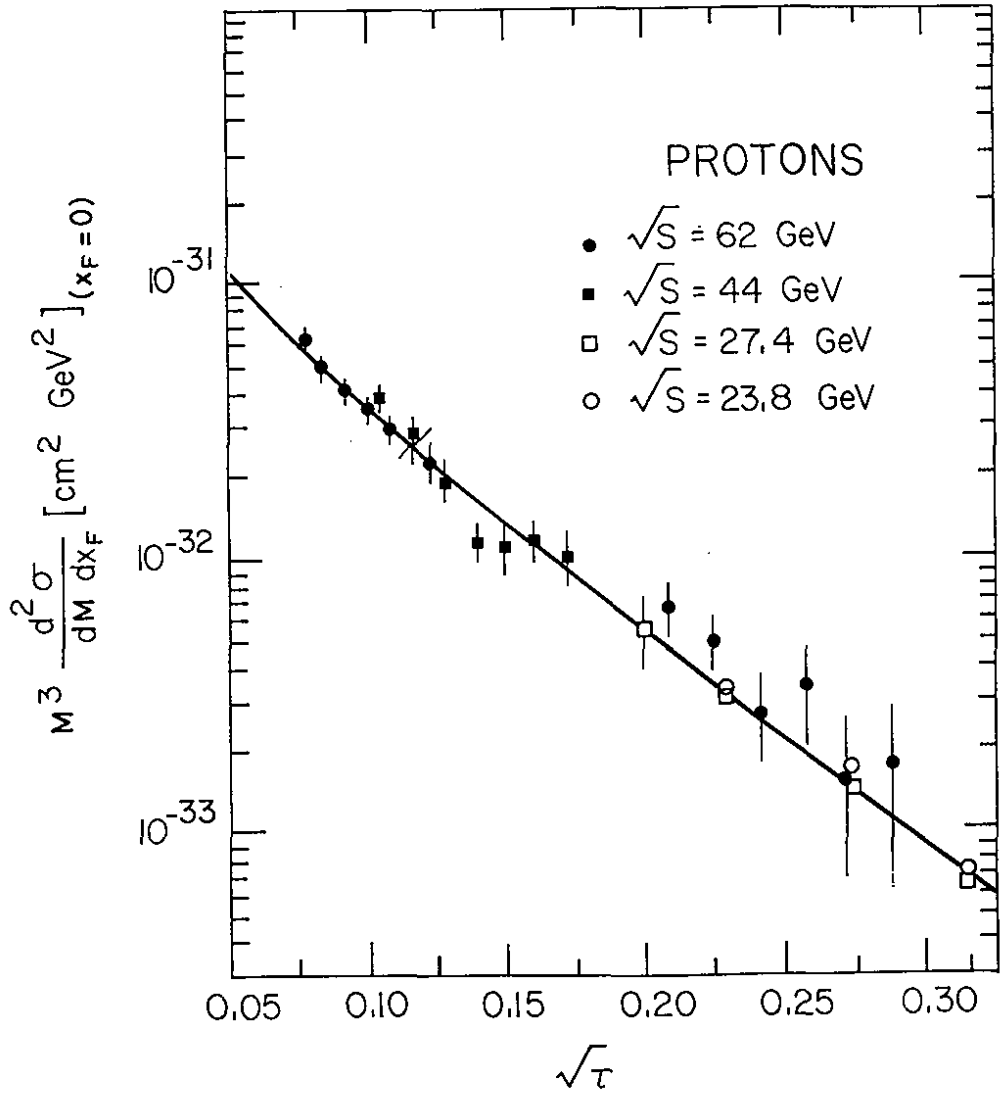
PROTONS
$\sqrt{s}$ = 62 GeV
$\sqrt{s}$ = 44 GeV
$\sqrt{s}$ = 27.4 GeV
$\sqrt{s}$ = 23.8 GeV
10^{-31}
10^{-32}
10^{-33}
0.05
0.10
0.15
0.20
0.25
0.30
$\sqrt{\tau}$
$M^3 \frac{d^2\sigma}{dM\,dx_F}$ [cm^2 GeV^2]$_{(x_F=0)}$

Fig. 11

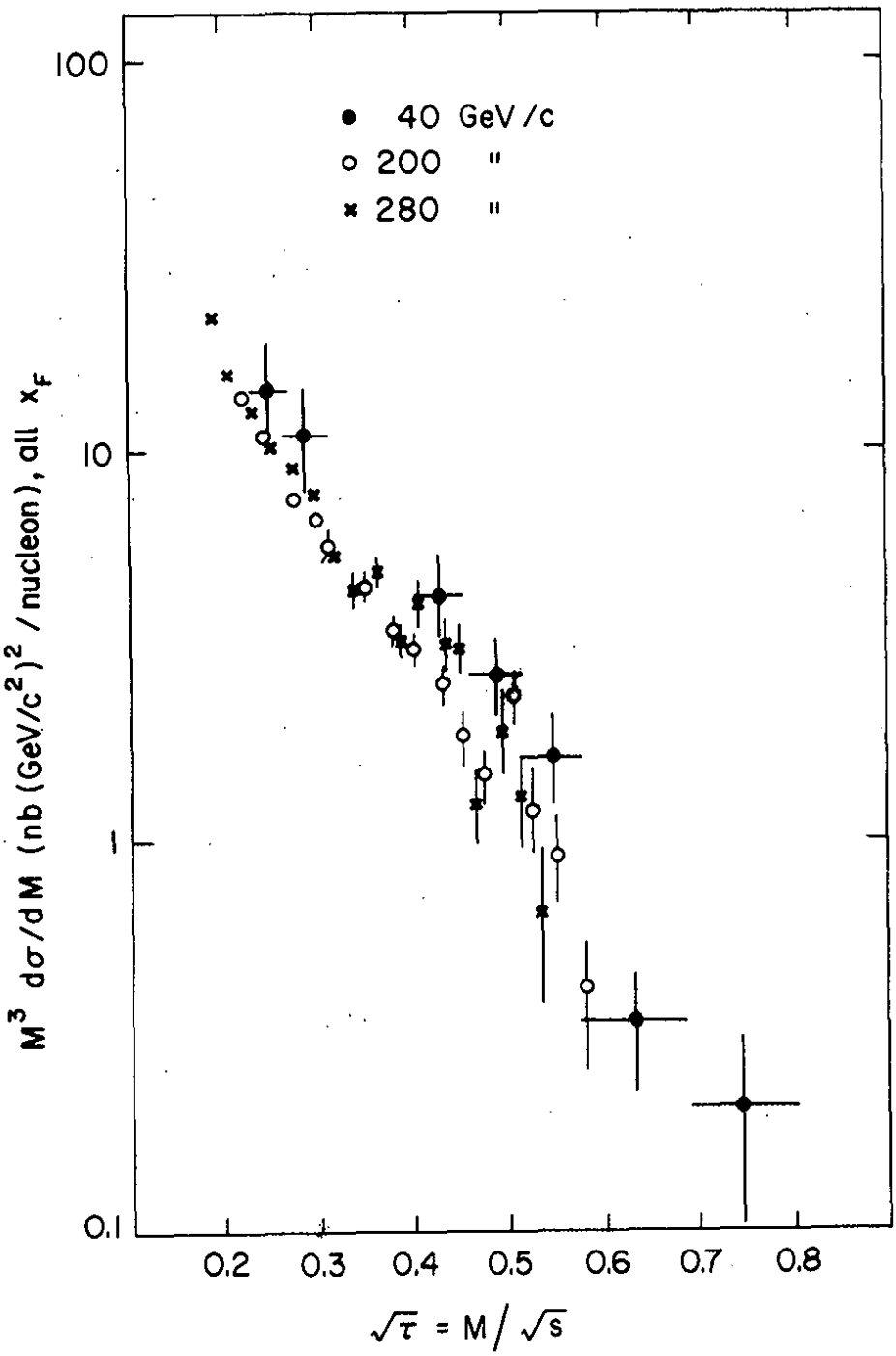
100
10
1
0.1
● 40 GeV/c
○ 200 "
× 280 "
$M^3\ d\sigma/dM$ (nb (GeV/c^2)^2 / nucleon), all x_F
0.2
0.3
0.4
0.5
0.6
0.7
0.8
$\sqrt{\tau} = M/\sqrt{s}$

Fig. 12

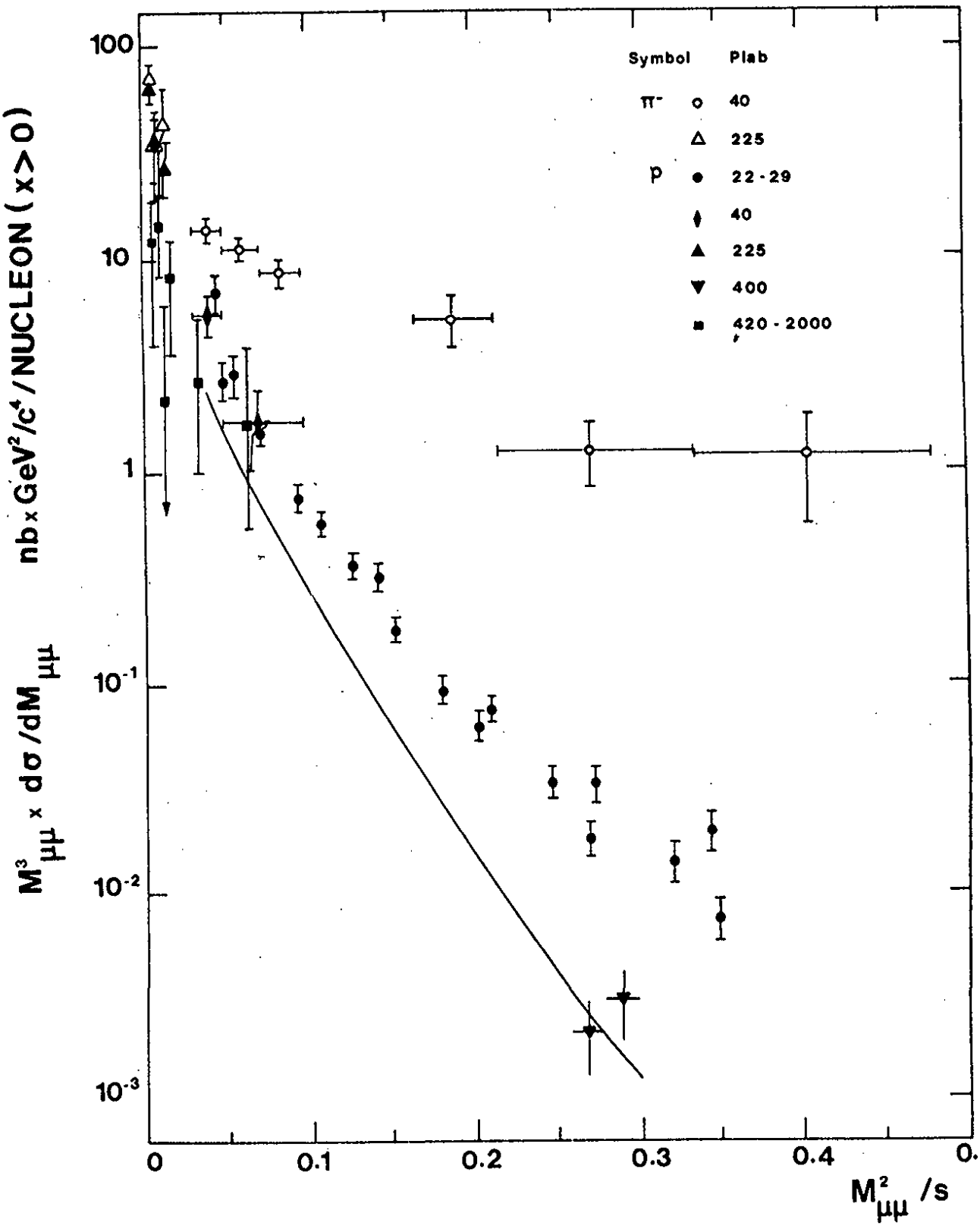
Symbol
Plab
π⁻
40
225
p
22 - 29
40
225
400
420 - 2000
100
10
1
10⁻¹
10⁻²
10⁻³
0
0.1
0.2
0.3
0.4
0.5
M²μμ /s
M³μμ x dσ /dMμμ
nb x GeV²/c⁴ / NUCLEON (x>0)

Fig. 13

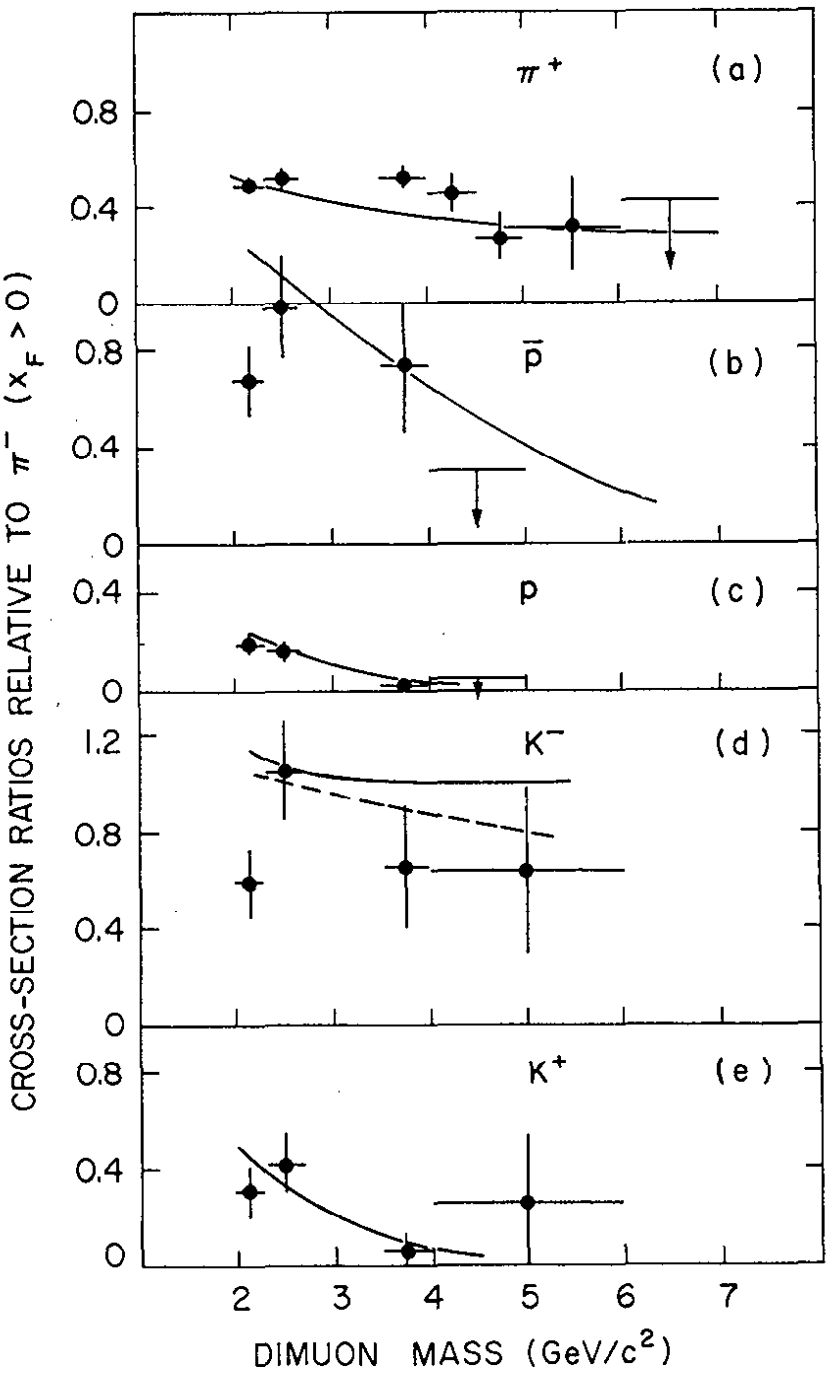
π^+ (a)
$\bar{p}$ (b)
p (c)
K^- (d)
K^+ (e)
0.8
0.4
0
1.2
2
3
4
5
6
7
CROSS-SECTION RATIOS RELATIVE TO π^- ($x_F > 0$)
DIMUON MASS (GeV/c^2)

Fig. 14

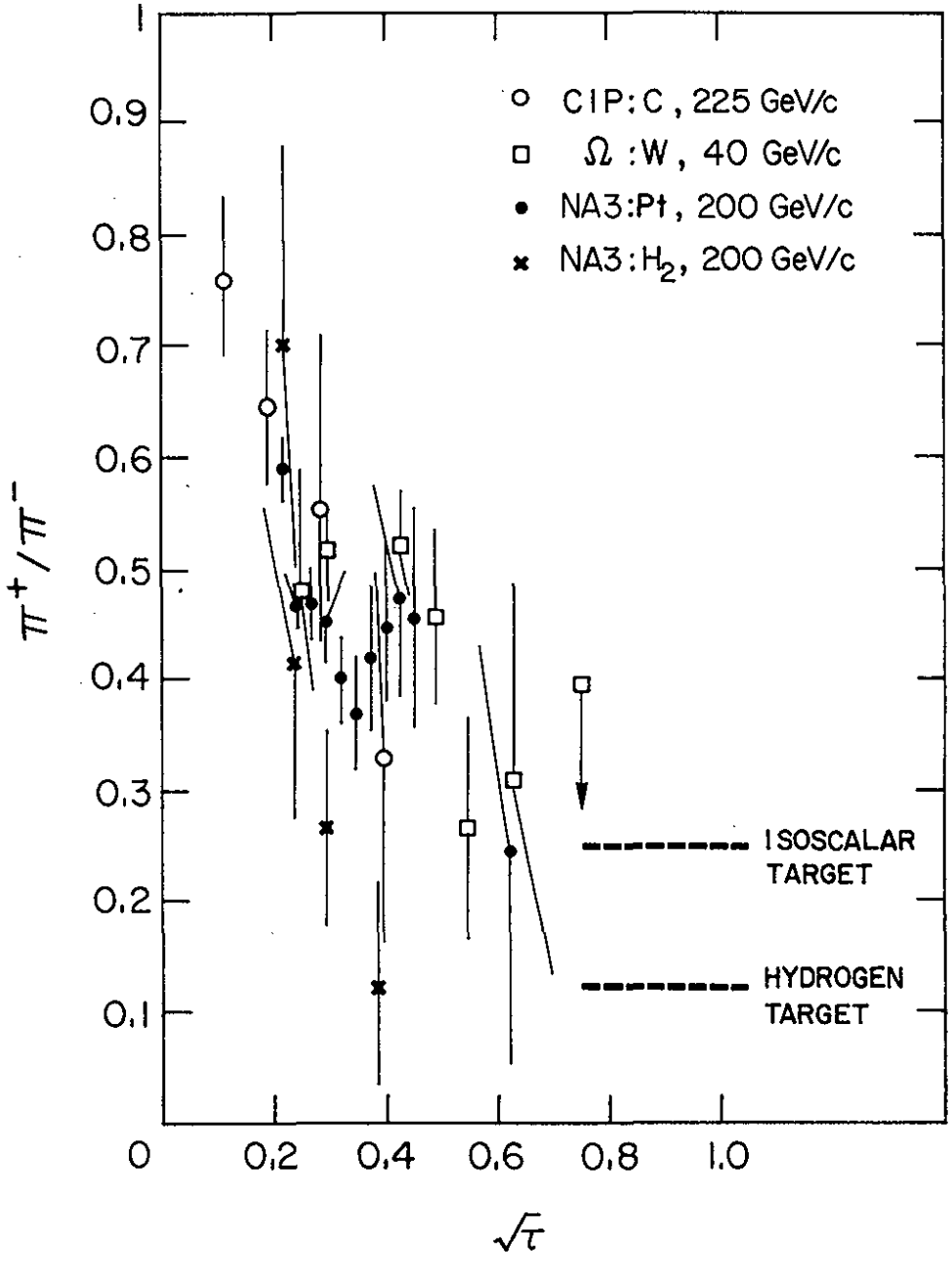
CIP: C , 225 GeV/c
Ω : W , 40 GeV/c
NA3: Pt , 200 GeV/c
NA3: H_2, 200 GeV/c
ISOSCALAR TARGET
HYDROGEN TARGET
π^+/π^-
$\sqrt{\tau}$
0
0.1
0.2
0.3
0.4
0.5
0.6
0.7
0.8
0.9
1
0.2
0.4
0.6
0.8
1.0

Fig. 15

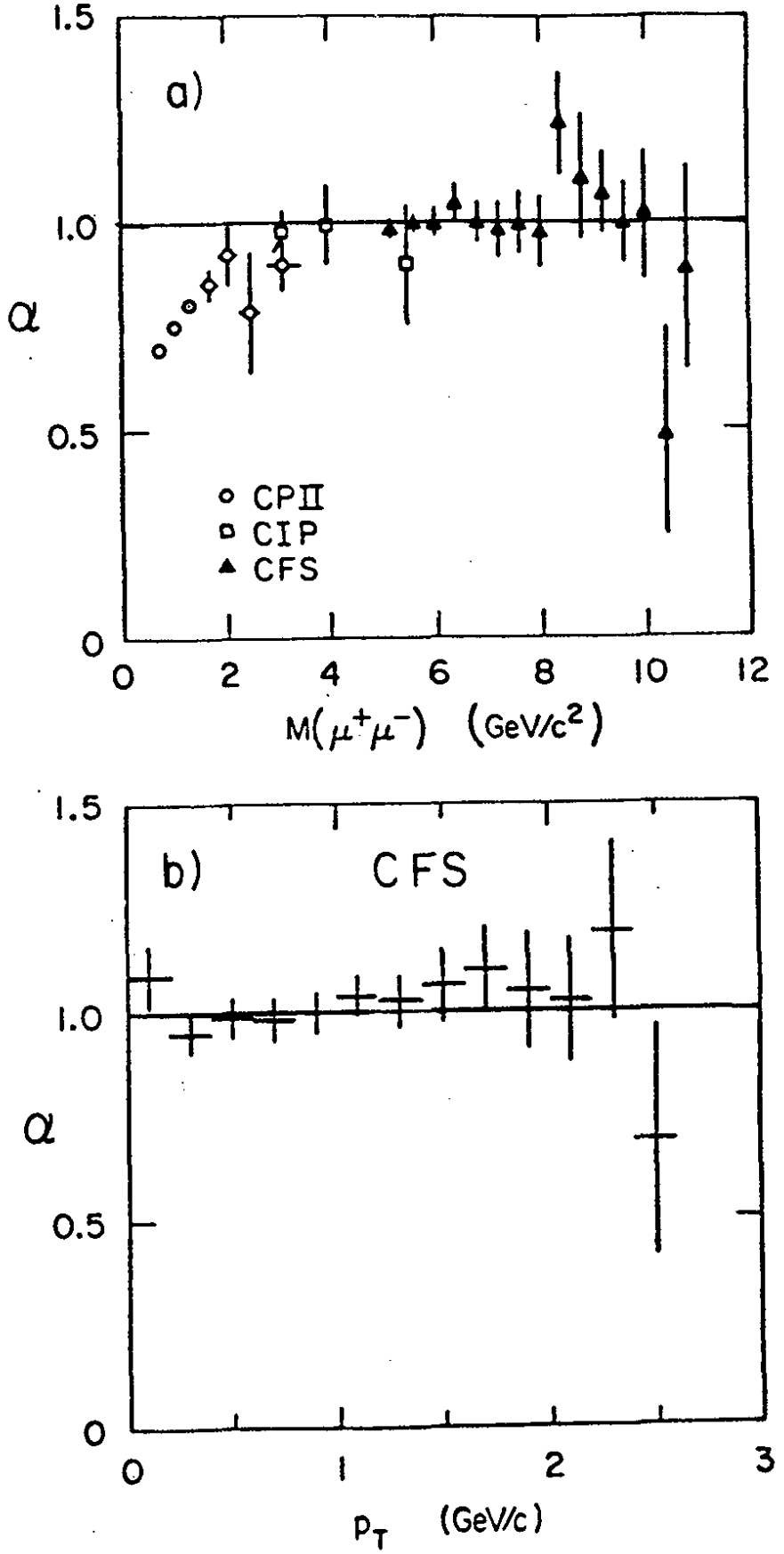
a)
1.5
1.0
0.5
0
α
CPII
CIP
CFS
0
2
4
6
8
10
12
M(μ⁺μ⁻) (GeV/c²)
b)
CFS
1.5
1.0
0.5
0
α
0
1
2
3
p_T (GeV/c)

Fig. 16

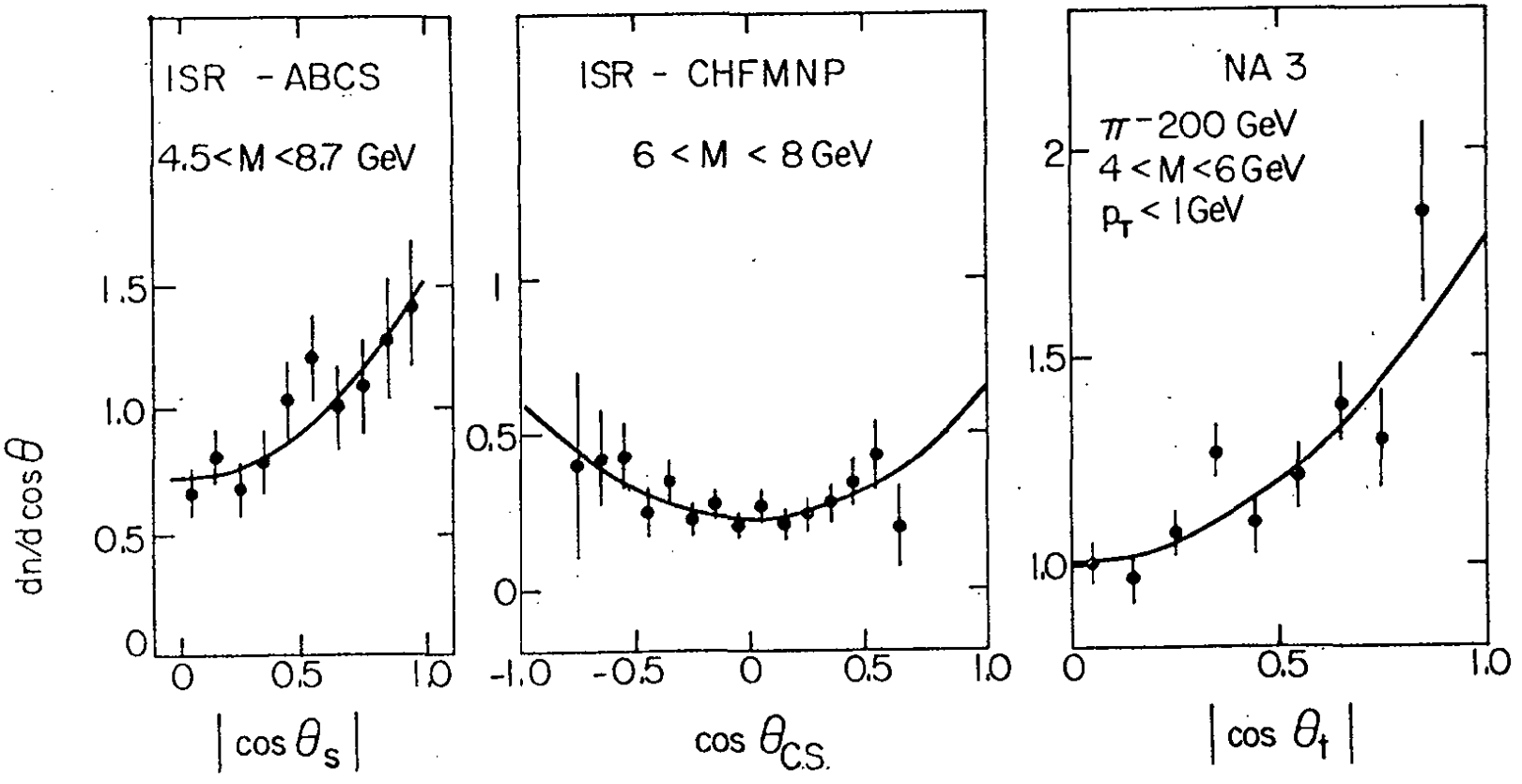
ISR - ABCS
4.5<M<8.7 GeV
ISR - CHFMNP
6 < M < 8 GeV
NA 3
π⁻ 200 GeV
4 < M < 6 GeV
p_T < 1 GeV
dn/d cos θ
| cos θ_s |
cos θ_CS
| cos θ_t |

Fig. 17

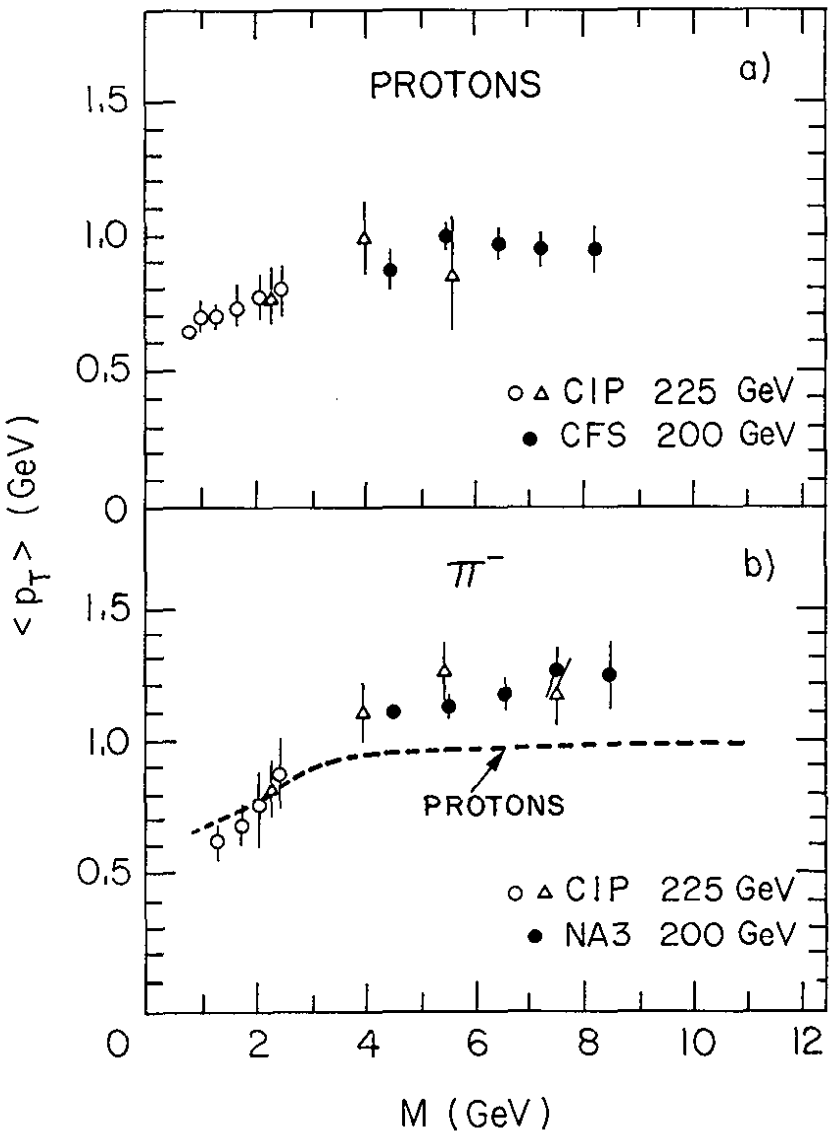
PROTONS
a)
1.5
1.0
0.5
0
CIP 225 GeV
CFS 200 GeV
π^-
b)
PROTONS
CIP 225 GeV
NA3 200 GeV
$\langle p_T \rangle$ (GeV)
0
2
4
6
8
10
12
M (GeV)

Fig. 18

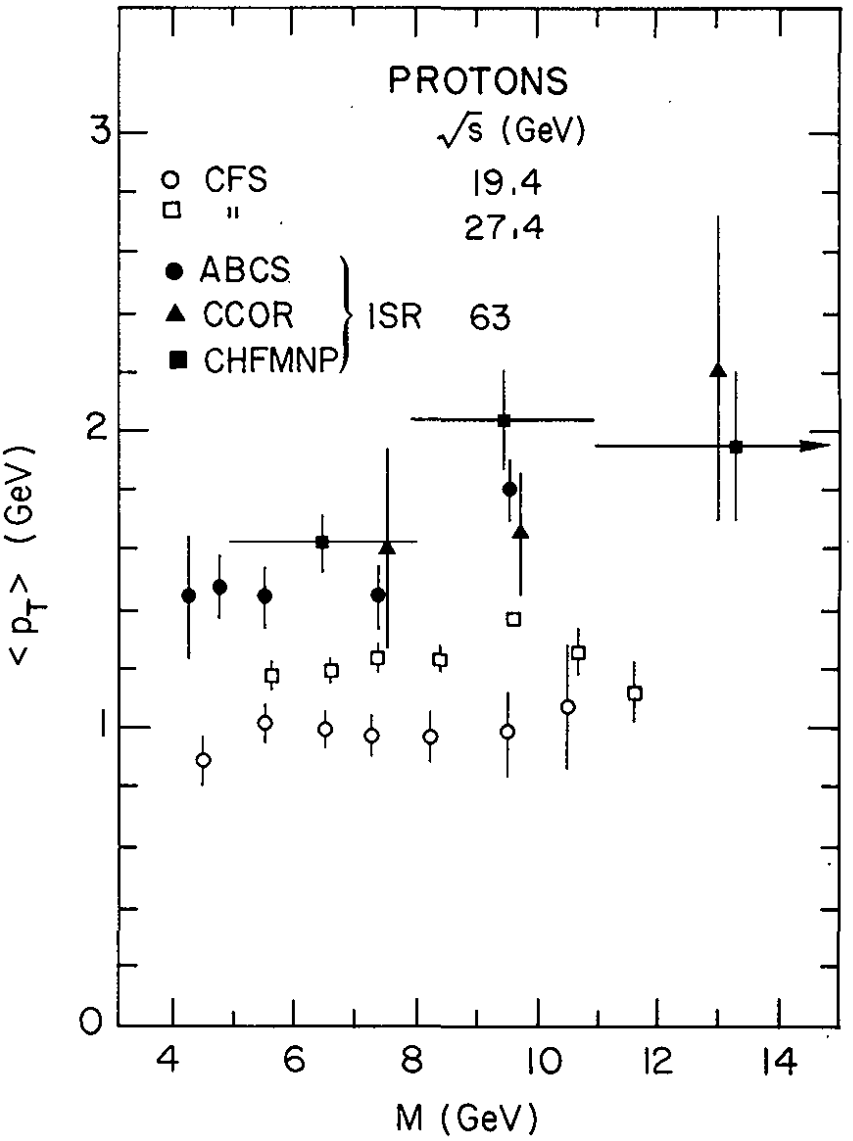
PROTONS
√s (GeV)
CFS
19.4
"
27.4
ABCS
CCOR
CHFMNP
ISR 63
< p_T > (GeV)
M (GeV)
0
1
2
3
4
6
8
10
12
14

Fig. 19

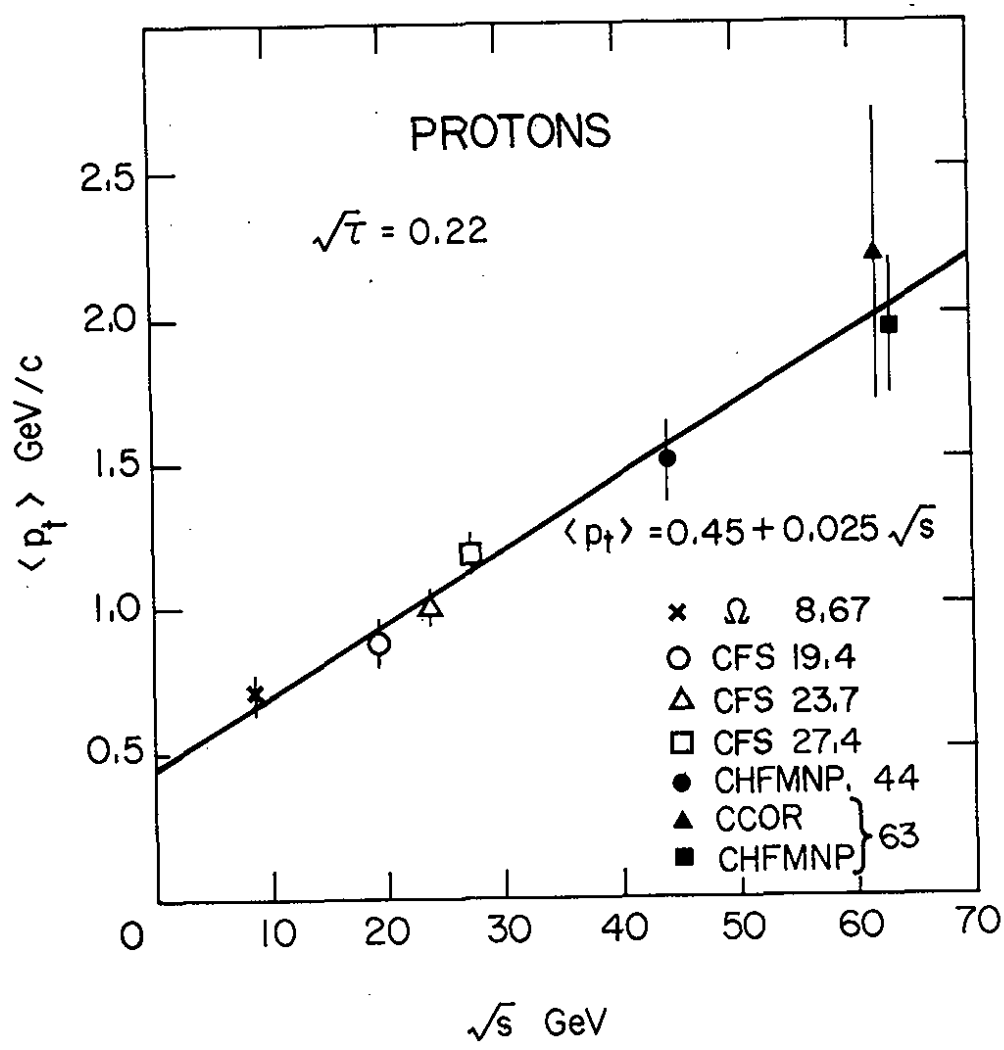
PROTONS
$\sqrt{\tau}$ = 0.22
$\langle p_t \rangle$ =0.45 + 0.025 $\sqrt{s}$
× Ω 8.67
○ CFS 19.4
△ CFS 23.7
□ CFS 27.4
● CHFMNP, 44
▲ CCOR
■ CHFMNP
63
$\langle p_t \rangle$ GeV/c
$\sqrt{s}$ GeV
0
0.5
1.0
1.5
2.0
2.5
10
20
30
40
50
60
70

Fig. 20a

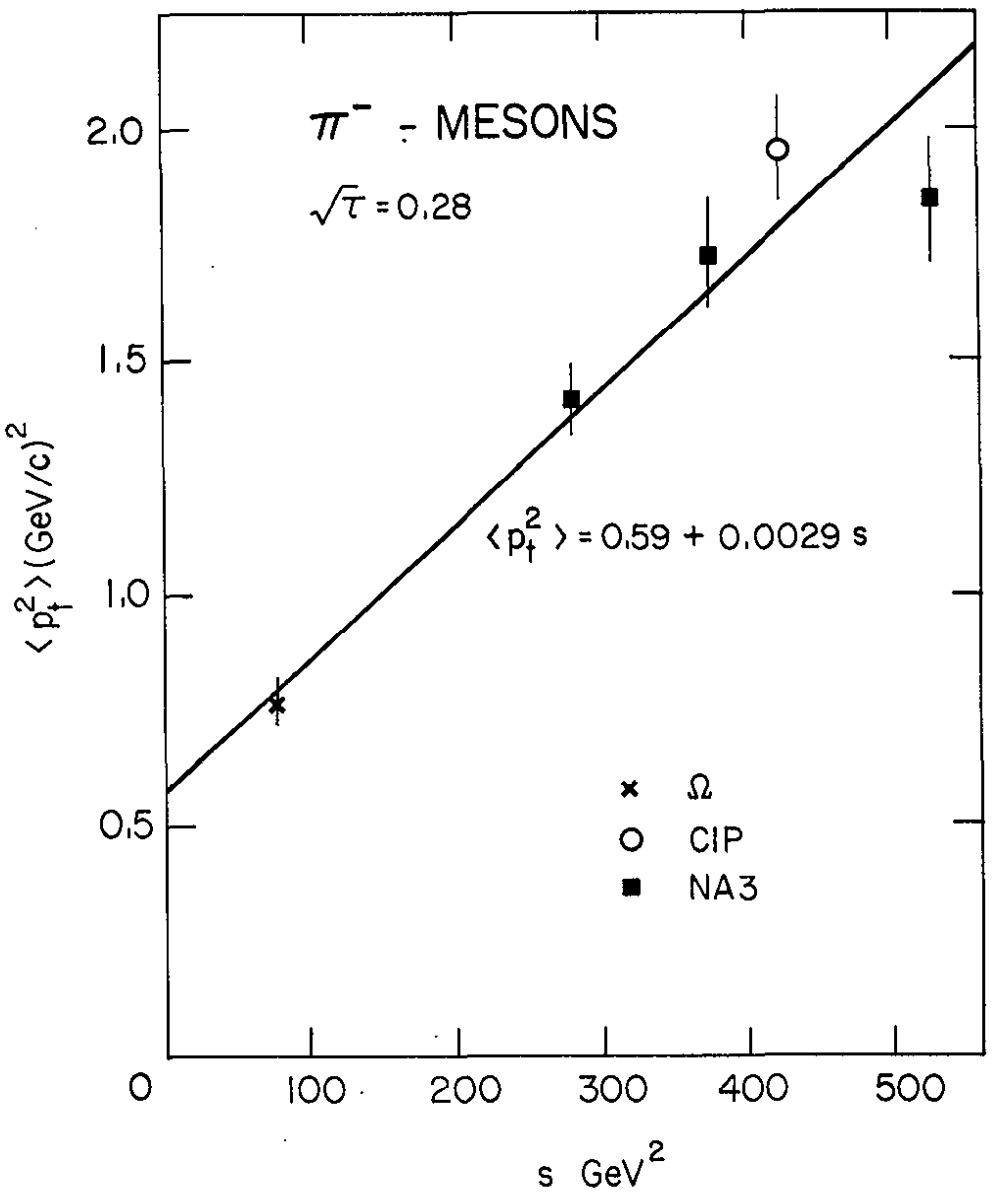
π^- - MESONS
$\sqrt{\tau} = 0.28$
$\langle p_t^2 \rangle = 0.59 + 0.0029\ s$
Ω
CIP
NA3
$\langle p_t^2 \rangle$ (GeV/c)^2
s GeV^2
0
0.5
1.0
1.5
2.0
100
200
300
400
500

Fig. 20b

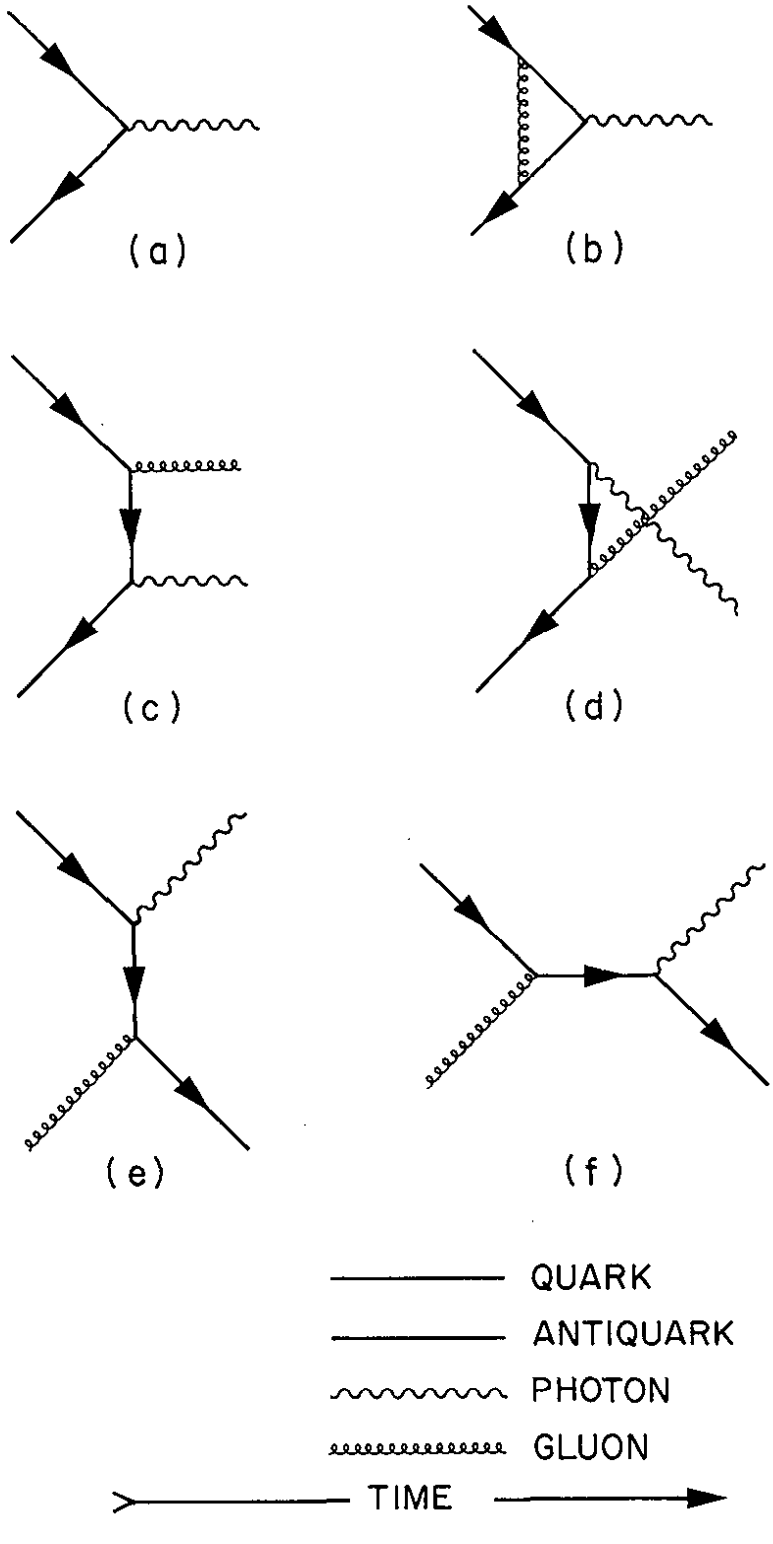

Fig. 21

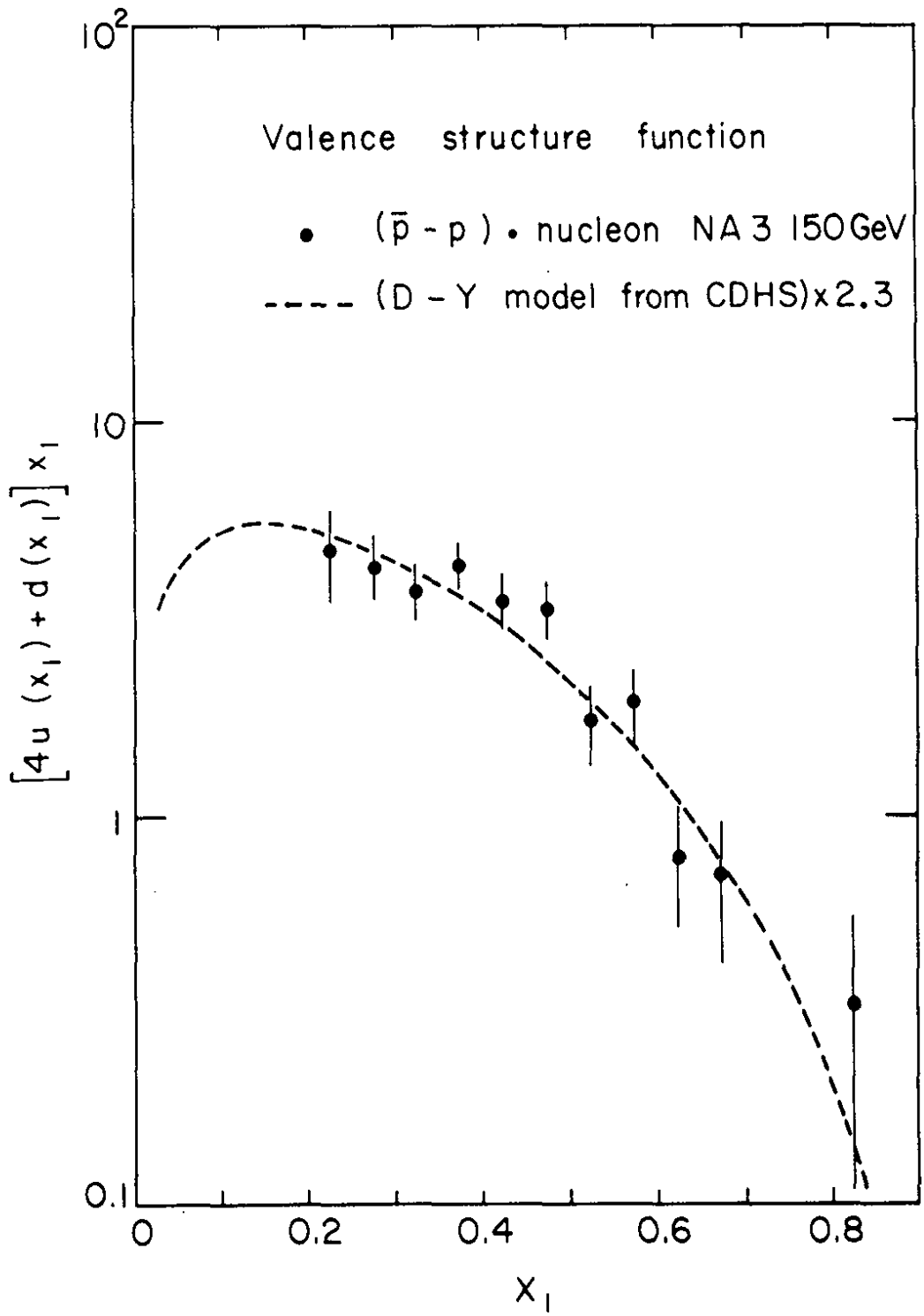
Valence structure function
(p̄ - p) • nucleon NA 3 150GeV
---- (D - Y model from CDHS)x2.3
$[4u(x_1) + d(x_1)]x_1$
10^2
10
1
0.1
0
0.2
0.4
0.6
0.8
X_1

Fig. 22

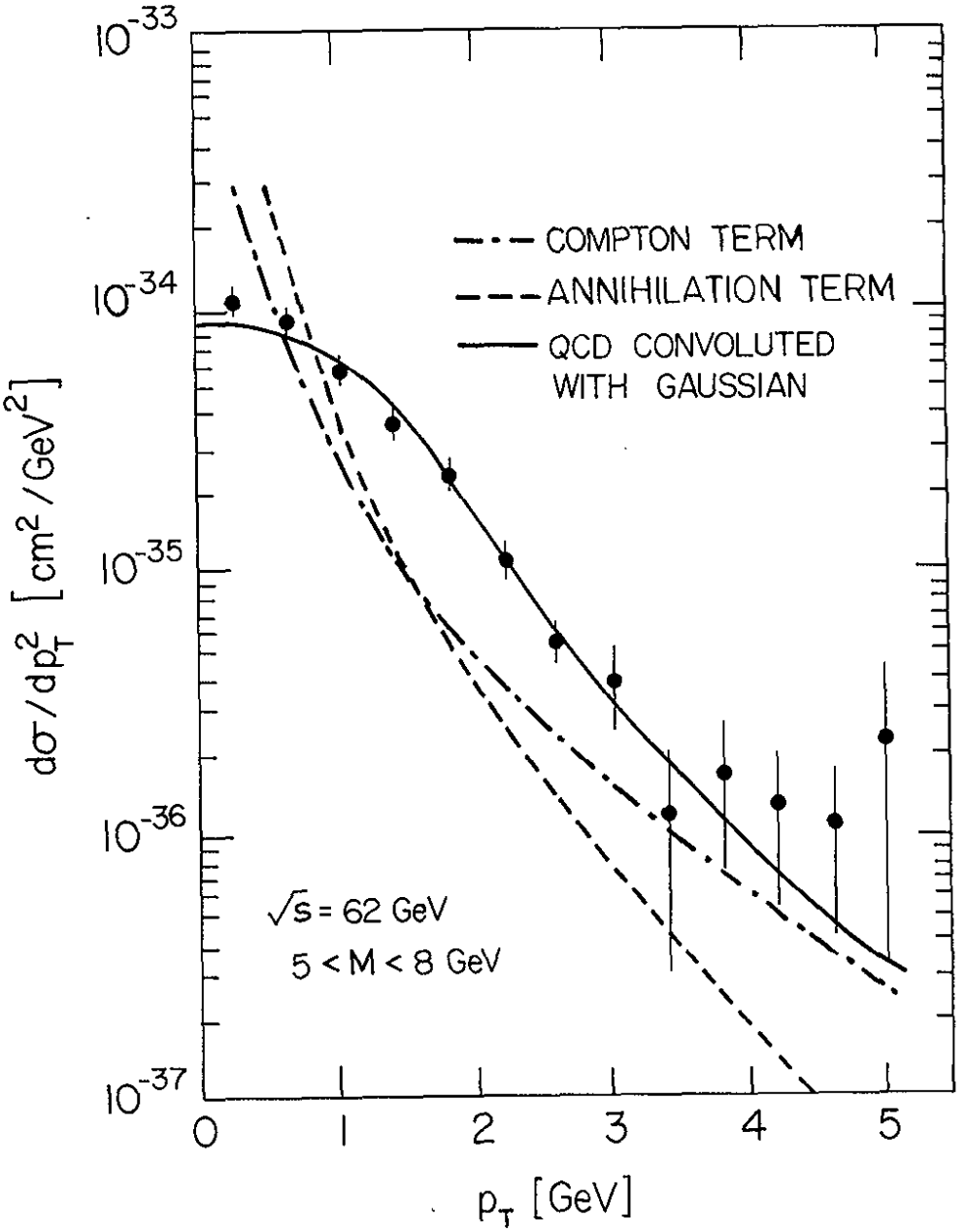
10^{-33}
10^{-34}
10^{-35}
10^{-36}
10^{-37}
$d\sigma/dp_T^2$ [cm^2/GeV^2]
COMPTON TERM
ANNIHILATION TERM
QCD CONVOLUTED WITH GAUSSIAN
$\sqrt{s}$ = 62 GeV
5 < M < 8 GeV
0
1
2
3
4
5
p_T [GeV]

Fig. 23

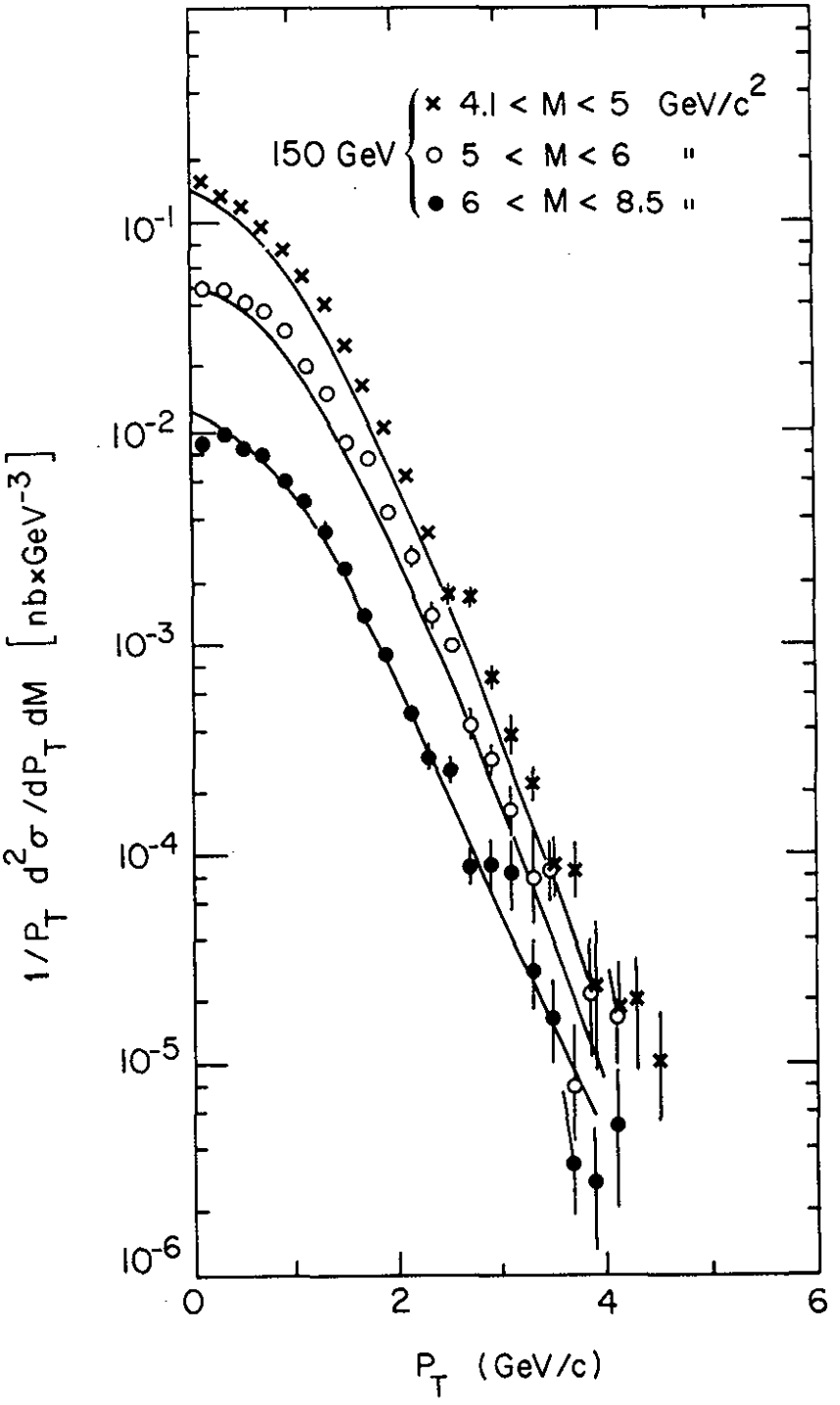
150 GeV
× 4.1 < M < 5 GeV/c²
○ 5 < M < 6 "
● 6 < M < 8.5 "
1/P_T d²σ/dP_T dM [nb×GeV⁻³]
10⁻¹
10⁻²
10⁻³
10⁻⁴
10⁻⁵
10⁻⁶
0
2
4
6
P_T (GeV/c)

Fig. 24

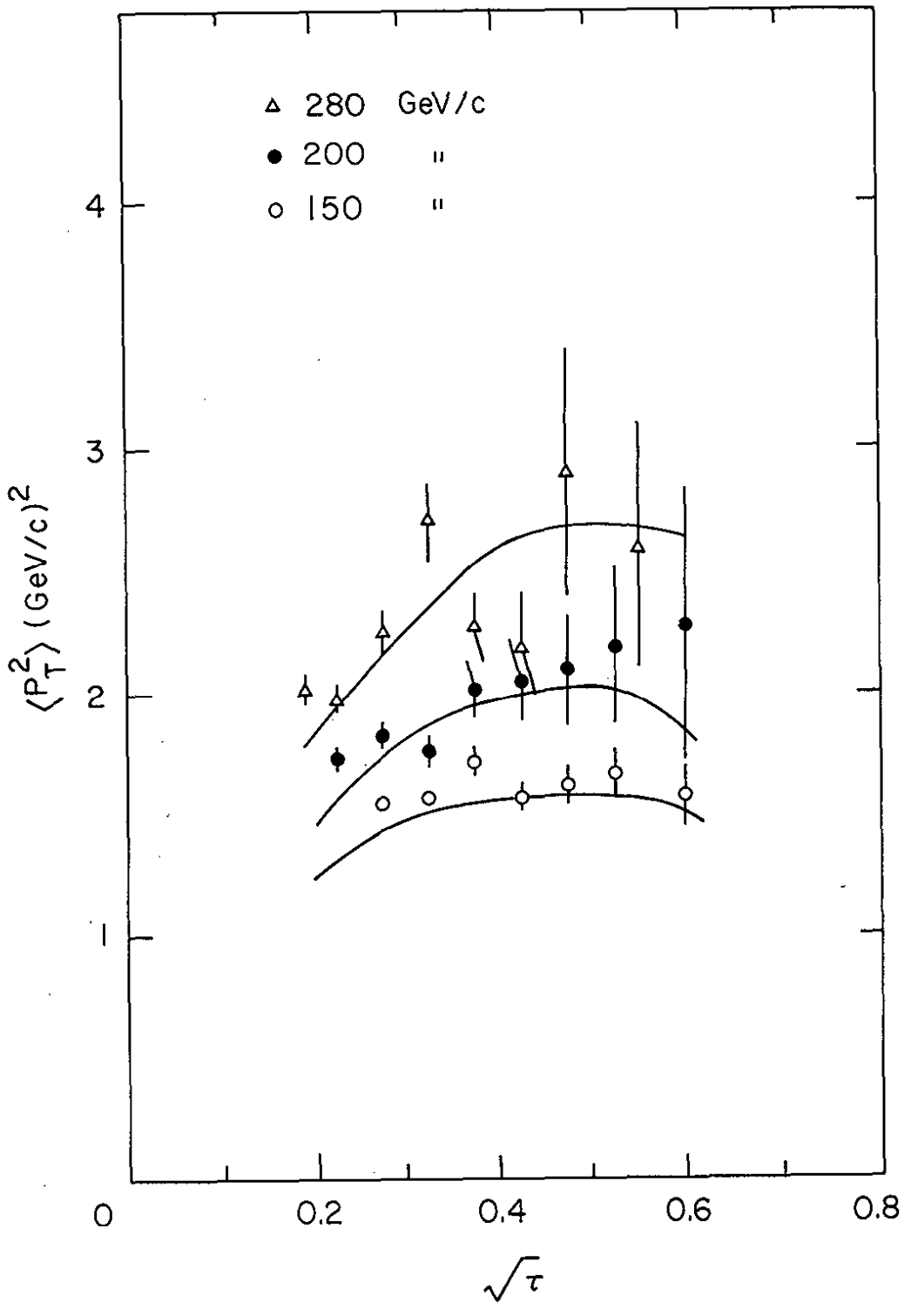
△ 280 GeV/c
● 200 "
○ 150 "
4
3
2
1
0
0.2
0.4
0.6
0.8
$\langle P_T^2 \rangle$ (GeV/c)^2
$\sqrt{\tau}$

Fig. 25

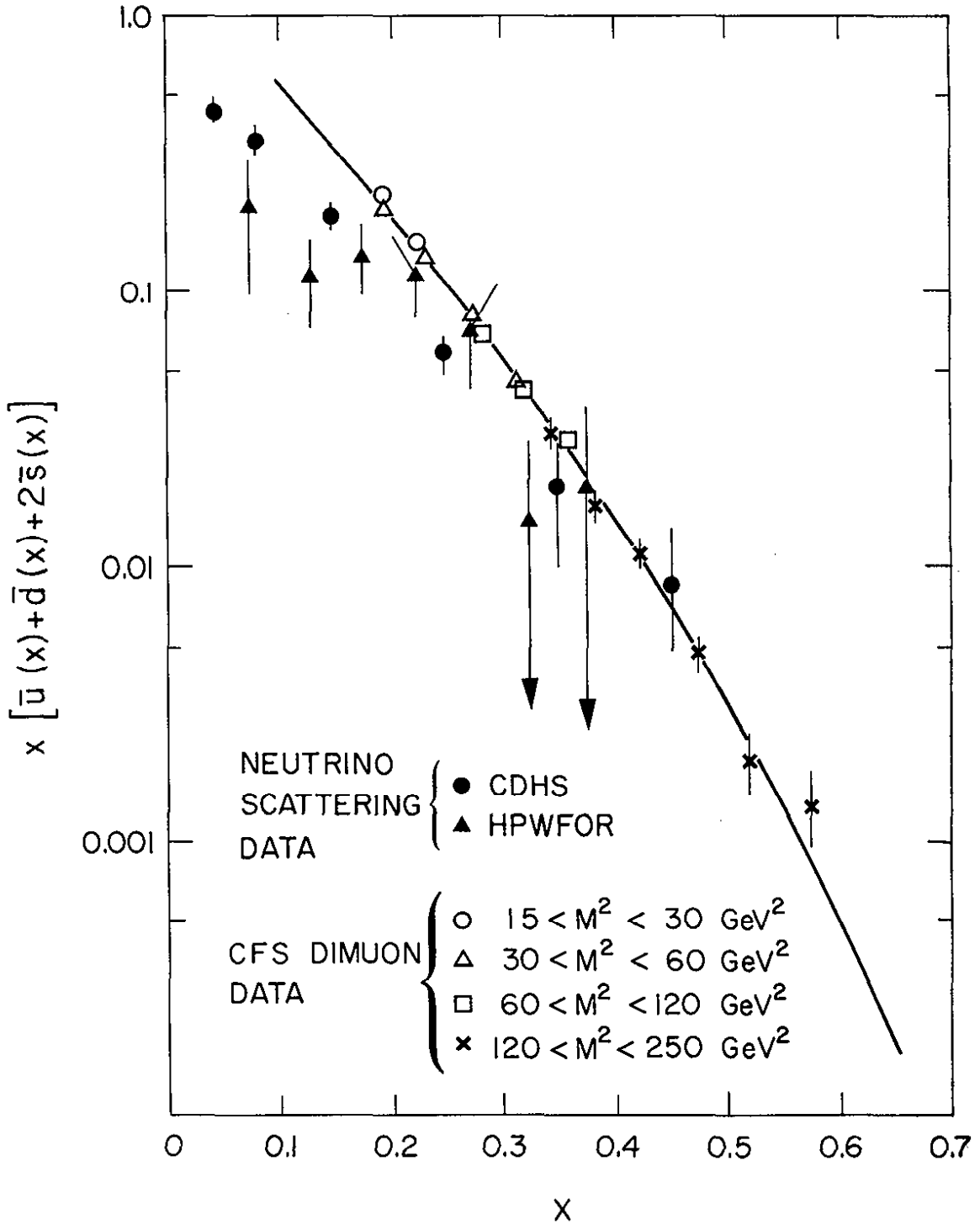
1.0
0.1
0.01
0.001
0
0.1
0.2
0.3
0.4
0.5
0.6
0.7
X
x [ū (x)+d̄ (x)+2s̄(x)]
NEUTRINO SCATTERING DATA
CDHS
HPWFOR
CFS DIMUON DATA
15 < M² < 30 GeV²
30 < M² < 60 GeV²
60 < M² < 120 GeV²
120 < M² < 250 GeV²

Fig. 26

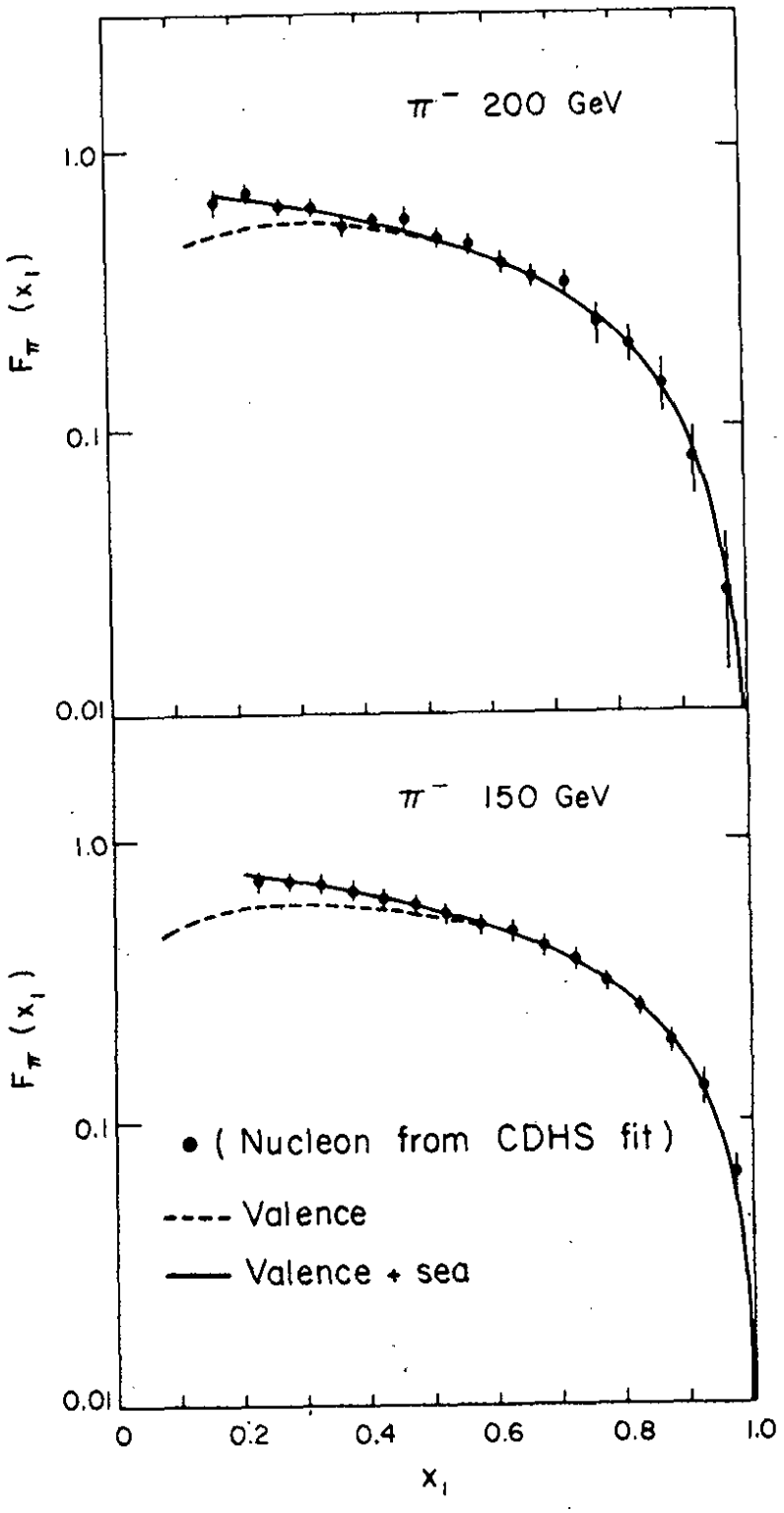
π⁻ 200 GeV
π⁻ 150 GeV
1.0
0.1
0.01
F_π (x_1)
• (Nucleon from CDHS fit)
---- Valence
—— Valence + sea
0
0.2
0.4
0.6
0.8
1.0
x_1

Fig. 27